Analysis of injection and recovery schemes for ERL based light source

DISSERTATION

zur Erlangung des akademischen Grades

doctor rerum naturalium

(Dr. rer. nat.)

im Fach Physik

eingereicht an der

Mathematisch-Naturwissenschaftlichen Fakultät I

Humboldt-Universität zu Berlin

von

Yuriy Petenev, M. Sc.

Präsident der Humboldt-Universität zu Berlin:

Prof. Dr. Jan-Hendrik Olbertz

Dekan der Mathematisch-Naturwissenschaftlichen Fakultät I:

Prof. Stefan Hecht PhD

Gutachter/in: 1. Prof. Aleksandr Matveenko

            2. PD. Dr. Atoosa Meseck

            3. Prof. Nikolay Vinokurov

Datum der Einreichung: 30.01.2014

Datum der Promotion: 14.05.2014

Abstract

A new generation of particle accelerators based on an Energy Recovery Linac (ERL) is a promising tool for a number of new applications. These include high brilliance light sources in a wide range of photon energies, electron cooling of ion beam and ERL-based electron-hadron colliders.

In January 2011 Helmholtz-Zentrum Berlin officially started the realization of the Berlin Energy Recovery Linac Project – BERLinPro. The goal of this compact ERL is to develop the accelerator physics and technology required to accelerate a high-current (100 mA) low emittance beam. The parameters are desired for future large scale facilities based on ERLs, e.g ERL-based synchrotron light sources. One of such large scale facilities is in the design phase at Helmholtz-Zentrum Berlin. This facility is called Femto-Science Factory (FSF). It is a GeV-scale multi-turn ERL-based light source. This light source will operate in the diffraction limited regime for X-rays and offer a short length of a light pulse in the femtosecond region. The average and peak brightness will be at least an order of magnitude higher than achievable from storage rings. In this work an overview of these two projects is given.

One potential weakness of the Energy Recovery Linacs is a regenerative form of BBU – transverse beam break up instability. This instability can limit a beam current. In this work the threshold current of the BBU instability was calculated for BERLinPro. The comparison of two linacs based on different types of superconducting cavities is made. Different methods of BBU suppression are investigated (e.g. the influence of solenoid, pseudo-reflector and quadruple triplets in the linac structure on the BBU threshold). Analytic solutions of the Twiss parameters are used to find the best optic in the linac with and without external focusing are presented.

Large scale ERL facilities can be realized on different schemes of beam acceleration. This dissertation compares a direct injection scheme with acceleration in a 6 GeV linac, a two-stage injection with acceleration in a 6 GeV linac and a multi-turn (3-turn) scheme with a two-stage injection and two main 1 GeV linacs. The key points of the comparison were total costs and BBU instability. Linac optic solutions are presented.

Keywords: energy recovery linac, synchrotron radiation, light source, beam breakup instability (BBU), threshold current, high order mode

Zusammenfassung

Neue Generation von Teilchenbeschleunigern, die auf Energierückgewinnung in einem linearen Beschleuniger basiert (eng. Energy Recovery Linac – ERL), ist eine vielversprechende Neuentwicklung für mehrere Anwendungen. Unter anderem sind das hochbrillante Lichtquellen im breiten Wellenlängenbereich, Elektronenkühlung von Ionenstrahlen, und ERL-basierte Elektronen-Hadronen Collider.

Helmholtz Zentrum Berlin für Materialien und Energie baut seit 2011 eine Testanlage Energy Recovery Linac Project – B*ERL*inPro. Das Ziel dieses Projektes ist den hohen Strom (100 mA) und hohe Brillanz von dem Elektronenstrahl in einem ERL zu demonstrieren. Die angestrebten Strahlparameter sind vergleichbar mit den Parametern von e.g. zukünftigen ERL-basierten Lichtquellen. Eine von solchen Anlagen ist Femto-Science Factory (FSF), die am HZB konzipiert wurde. FSF ist eine Lichtquelle in Röntgenbereich auf Basis von einem mehrumläufigen ERL mit zweistüfiger Injektion und Energie von einigen GeV. Die Quelle soll Diffraktionslimitiert sein und kurze (in Femtosekundenbereich) Lichtpulse erzeugen. Die durchschnittliche und spitzen- Brillanz soll mindesten eine Größenordnung höher liegen als die Brillanz der modernen Speicherring-basierten Lichtquellen. Ein Überblick von B*ERL*inPro und FSF ist gegeben in diese Dissertation.

Eine potentielle Schwäche von ERL besteht in Strahlinstabilitäten, insbesondere regenerative Beam Break Up (BBU). Die Instabilität kann den erreichbaren durchschnittlichen Strom in einem ERL begrenzen. Der Grenzstrom von der BBU für B*ERL*inPro ist berechnet in der Dissertation. Vergleich von zwei Linacs mit zwei verschiedenen supraleitenden Kavitätendesigns ist vorgestellt. Drei Methoden für Strahlstabilisierung (Einfluss von Strahlrotation mit einem Soleniod, Pseudoreflektor, und Tripleten von Quadrupolen in dem Linac auf den Grenzstrom) sind untersucht. Analytische Lösungen für die Twiss-Parameter wurden gefunden für die beste Linacoptik mit und ohne zusätzliche optische Elemente.

Zukünftige große ERLs können unterschiedliche Beschleunigungsschemen benutzen. Diese Dissertation vergleicht drei Schemas: unmittelbare Injektion in einen 6 GeV Linac; zweistufige Injektion in einen 6 GeV Linac; und zweistufige Injektion in einen mehrumläufigen (drei-umläufigen) Beschleuniger mit geteiltem Hauptlinac in zwei 1 GeV Linacs. Der Basis für den Vergleich ist die Vollkostenanalyse sowie erreichbarer Grenzstrom von den Instabilitäten. Optik für den Linacs in allen Schemas ist dargelegt.

Contents

1. Introduction

During the last half century synchrotron based light sources were rapidly developed and well established. One of the main reasons of such quick development is that all the other known light sources were coming to the limits in their wavelength. They could not generate short wave radiation (in a range of UV to X-Rays) with a competitive spectral flux. Originally, synchrotron light was a parasitic effect in ring based accelerators, which caused beam degradation and limited the final energy of electron positron colliders. At the beginning of 1960 synchrotron radiation was extracted from the bending magnets and studied. Such machines were named 1st generation light sources where this parasitic light was used in some other scientific fields.

The first storage ring commissioned as a synchrotron light source was Tantalus, at the Synchrotron Radiation Center in the university of Wisconsin–Madison, when first operation was in 1968 [1]. Later, two more generations of the light sources were developed for ring based machines, with multiple (tens) simultaneously available beamlines for the users. The synchrotron light became very useful for the scientific community in the various fields like biology, chemistry, material science, medicine etc. Nowadays, ring based light sources are reaching the limit of the beam properties of multi pass rings (such as the beam's emittance (size) and current). There are several novel projects like FLASH [2] at DESY or LCLS [3] at Stanford, which are Free Electron Lasers (FELs) and commonly known to be the 4th generation of the light sources. One other candidate to be a next generation light source is a machine with an Energy Recovery Linac (ERL) as a driver.

In ERL based machines, a beam is injected and accelerated in the main linac, then it can be used for some experiments. After the usage, the beam comes back to the linac with an RF phase shifted by 180 degrees, where it is decelerated and, therefore transfers the energy back to the cavities. Finally the beam can be dumped at a low energy, usually below 10 MeV, to save the energy and to reduce a radiation hazard. The simplest scheme is with one linac and one recirculation turn. It can be more complicated with multiple linear accelerators and recirculation turns. In this work different schemes of ERL based accelerator were studied.
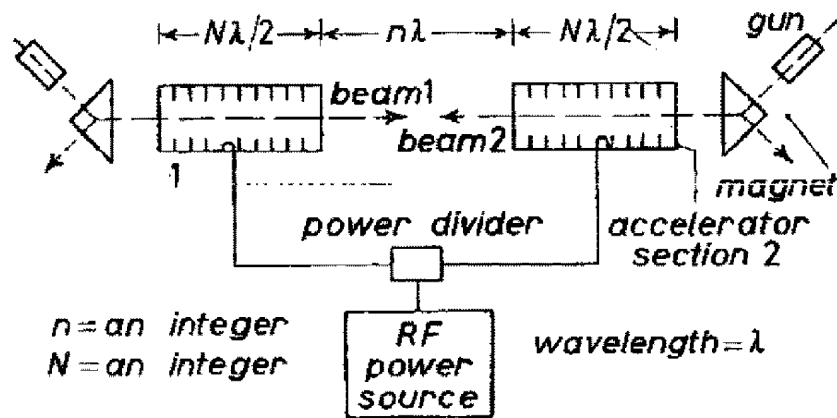
Figure 1.1: The first proposed scheme of ERL based e-e collider with two linacs.

Originally the idea of ERL based facilities came from Maury Tigner [4]. He proposed an ERL based electron-electron collider (see Fig. 1.1). The scheme consists of two similar guns and two similar linear accelerators located coaxially. The beams start simultaneously from both sides, accelerate, collide in the middle, decelerate in the opposite linac and, finally they are dumped. In the same paper he proposed a scheme with one injector and one linac (Fig. 1.2).

But at that time the superconducting radio frequency (SRF) technology was not developed well enough and, therefore, it couldn't be realized at that time. It required about 30-40 years of SRF development to achieve the feasible level for ERLs.
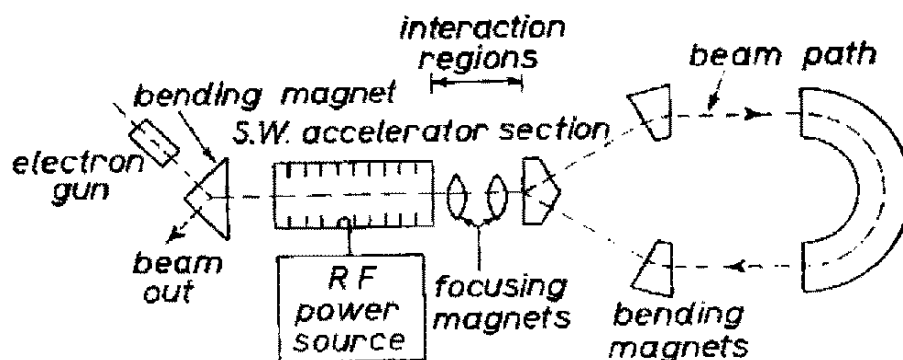

Figure 1.2: The first proposed scheme of ERL based e-e collider with one linac.

Nowadays, operating ERLs already exist (Fig. 1.3 presents a map with the existing and proposed ERLs), like FEL in Novosibirsk [5], which was the first multi-turn ERL based FEL, but normal conductive, or FEL at the Japan Atomic Energy Research Institute (JAERI) [6], or the most powerful in the world (at the moment) FEL based on SRF ERL at Thomas Jefferson National Accelerator Facility [7]. There are also a few existing small scale facilities (with energies below 500 MeV), like ALICE at Daresbury [8], or S-DALINAC in Darmstadt [9]. Some of the test projects are under construction, like cERL at KEK [10], test ERL at Brookhaven National Laboratory [11], test facility at CERN [12], IHEP ERL in Beijing [13], Peking University ERL test facility [14], B*ERL*inPro at Helmholtz-Zentrum Berlin (HZB) [15], etc. But all these projects and proposals are still relatively small with beam energies of hundreds MeVs. There is also a big number of proposed, let us call them, the large scale facilities with energy of some GeVs. There are proposed facilities with one turn, like ERL at Cornel University [16], or XFEL-O at KEK [17]. Also works are going on the multi-turn ERLs, like MARS in Novosibirsk [18] or FSF at HZB [19]. As one can see, there are a lot of projects of the ERL based light sources all over the world.

Figure 1.3: Existing and proposed facilities with an energy recovery linac for different applications.

ERLs, as drivers, are attractive not only for synchrotron light sources. They can be used for several different applications. For example, ERL can be a very good driver for electron-hadron colliders. There are several proposed facilities like LHeC at CERN, or eRHIC at BNL [20, 21] or MEIC at JLab [22]. Another very attractive application of ERL is Coherent Electron Cooling [23]. It seems that ERL can be the only one suitable driver for it according to [24]. There are some proposals for internal target experiments, for example, MESA at Mainz [25, 26].

These projects might be realized with different acceleration and recovery schemes. In this work the different schemes for ERL based light source, as part of studies for B*ERL*inPro and FSF projects, were compared.

1.1. BERLinPro

Helmholz-Zentrum Berlin has a project for the design and construction of the Berlin Energy Recovery Linac Project (B*ERL*inPro) [15, 27, 28]. The main goal of the project is to demonstrate the potential of superconducting energy recovery linacs for high average current and low emittance operation. The schematic layout of the facility is shown in Fig. 1.4. The main parameters of B*ERL*inPro are shown in Table 1.1.
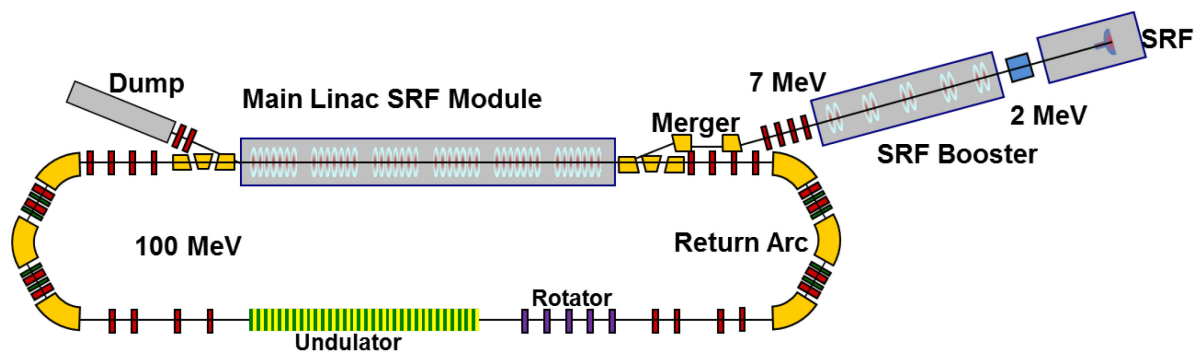
Figure 1.4: The basic scheme of 100 MeV B*ERL*inPro.

Originally the facility was planned to be built with a 100 MeV energy and 100 mA average current of an electron beam. But later, in order to guarantee the financial viability of the project, the beam energy was decreased to 50 MeV. What implied a shortening of the superconducting structures from 5 to 3 two-cell cavities in the booster and from 6 to 3 seven-cell cavities in the main linac. The new machine layout is shown in Fig. 1.5.

Table 1.1: The main parameters of BERLinPro

Parameter	Value
Max. beam energy	100/50 MeV
Average current up to	100 mA
Max. repetition rate	1.3 GHz
Emittance	< 1 mm mRad
Bunch length	< 2 ps
Injection energy	7 MeV

A beam is generated in a 1.3 GHz SRF photo injector and, after it passes a three cavity booster section and a dog-leg merger, it comes to the main linac with energy of 6 MeV. Then it accelerates to 50 MeV, recirculates, decelerates back in the main linac and dumps in a 600-kW beam dump. In the recirculation arc there is also some available space for future experiments which can demonstrate the potential of ERL based machines for a huge number of user applications.

Figure 1.5: The scheme of 50 MeV BERLinPro [15].

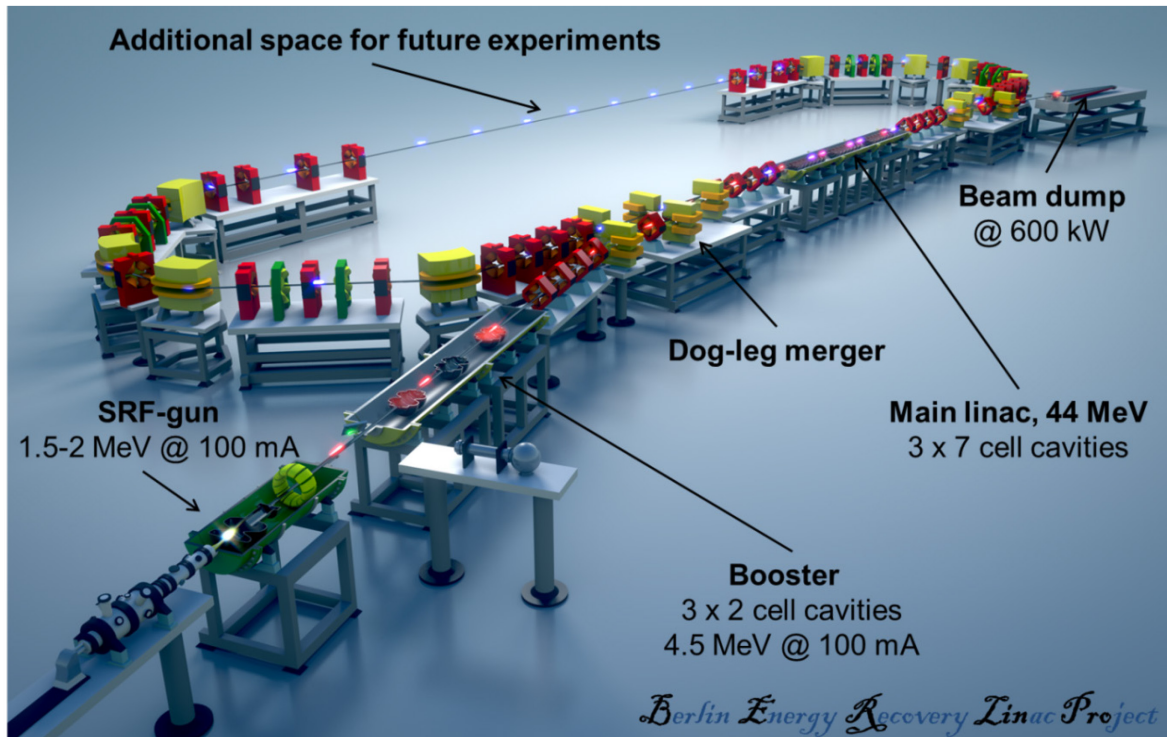In Chapter 2 will be discussed both versions of B*ERL*inPro and mostly the transverse Beam Breakup (BBU) instability in them. Since one of the main challenges of B*ERL*inPro is to achieve a stable recirculation of the beam without a beam breakup [15]. BBU threshold currents for a different main linacs based on three different types of cavities: TESLA-type, CEBAF-type and cavities, which will be developed for B*ERL*inPro, will be compared. A few methods of BBU instability suppression were applied for B*ERL*inPro. These methods include: optimization of the Twiss parameters of a beam in the main linac or, betatron phase advances adjustment in the recirculation turn or, insertion of a so-called pseudo-reflector or solenoid, which interchange the transverse x and y coordinates of the betatron motion, etc. The results are presented below.

Also, cavities which will be developed for B*ERL*inPro can be used for the future large scale ERL based light source, which is currently under development at HZB.

1.2. FSF

Our group at Helmholtz Zentrum Berlin is designing a new future multi-turn energy recovery linac based light source with a two stage injection and with a maximum energy of electron beam about 6 GeV. This future facility is named Femto-Science Factory (FSF) [19].

The problem of high brilliance SRF injectors is being intensively investigated as the injectors promise to deliver extremely low emittance bunches needed for the future linac-based light sources. An SRF injector with similar parameters to the B*ERL*inPro injector under development at HZB [29, 30] is considered. A beam is created in SRF gun with photo cathode (see Fig. 1.6). Then it passes a 100 MeV linac, which is used as a first cascade in the acceleration. And then, the beam is accelerated to 6 GeV after passing 3 times through each of two 1 GeV main linacs. In the achromatic arcs between the acceleration stages it is assumed to have undulators with 1000 periods in each and in the long straight section a long undulator with 5000 periods is assumed. After the beam was used it is decelerated back and goes to a dump.
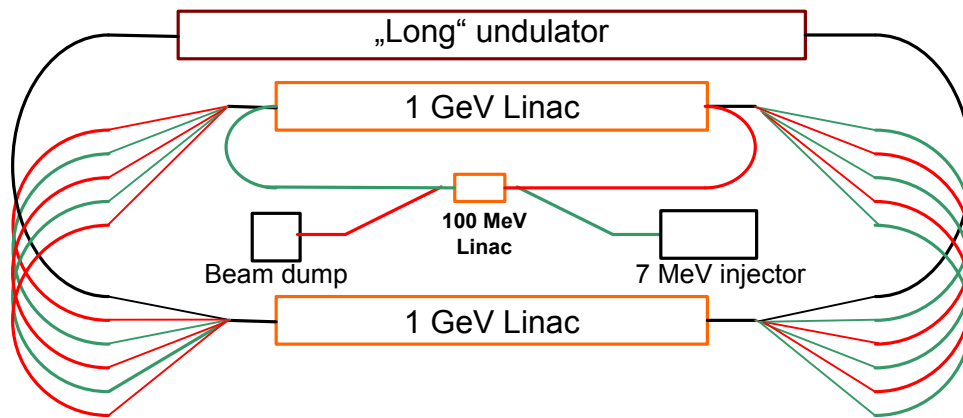
Figure 1.6: Principal layout of the multi-turn ERL with a cascade injection. The beam acceleration path is shown in green, deceleration path – in red.

The advantages and disadvantages of the two stage injection scheme with a split main linac will be discussed later in the next chapters. Now it should be noted, that the preinjection linac drastically improves the ratio between the initial and final energies on the first pass through the first 1 GeV linac. This improvement helps to make a reasonable focusing of the beam along the linac that improves the transverse beam break up instability of the facility. The scheme with a split linac allows separation of the beams in the arcs for different passes (e.g. the beam on decelerating pass will have different energy compared to what it had on the accelerating pass). This means they are transported in different vacuum chambers. In this way all beams on all passes are separated and, therefore, users can see only one energy of a beam per arc in undulators (if installed in arcs with 1, 2…5 GeV energy).
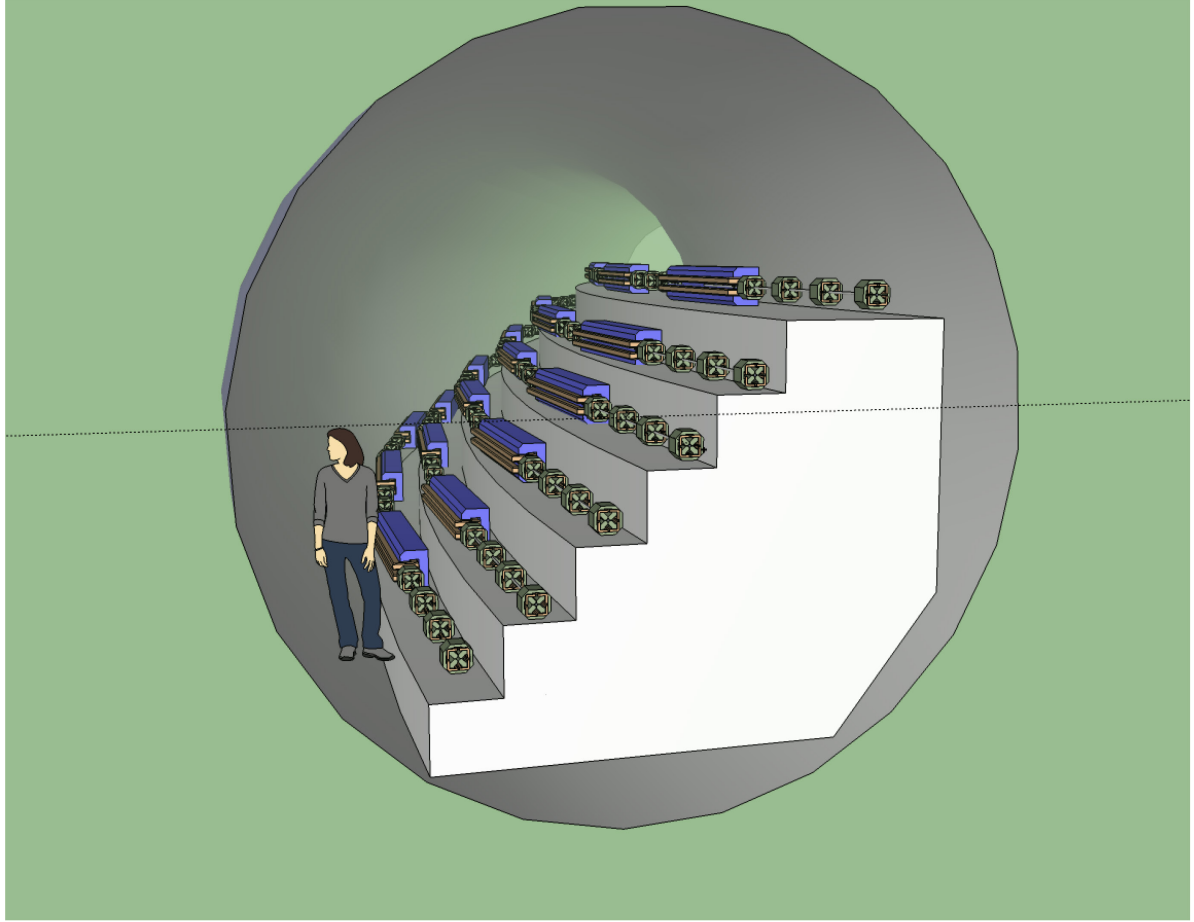
Figure 1.7: FSF arcs in a tunnel.

The design was optimised to achieve a proposed wavelength of 1 Å in a diffraction limited regime.

To reach such a wavelength [31], undulators require a period d=2 cm and K=0.8:

$$\lambda = \frac{d}{2\gamma^2}(1+\frac{K^2}{2}) \approx 1\mathring{A}, \tag{1.1}$$

for a 6 GeV beam.

Diffraction limited or spatially coherent regime reached when the transverse bunch size of a beam is smaller than σ (see Fig. 1.8) – the transverse "electron size" (size of single electron from the point of view of an observer of its light) in an undulator of length $L=N_p d$ and when the angular distribution of undulator radiation does not depends on the distribution of the particles in the beam, i.e. the angular spread is smaller than ψ – the radiation divergence angle for a single electron in an undulator. The ψ is given by [32]:

$$\psi = \sqrt{\frac{\lambda}{N_p d}} . \tag{1.2}$$
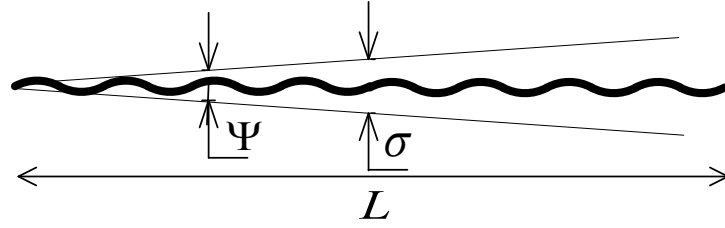
Figure 1.8: Source size of the undulator radiation.

The transverse electron size is given by:

$$\sigma \approx \frac{\sqrt{\lambda N_p d}}{2\pi} \approx 22 \, \mu m , \tag{1.3}$$

for an undulator with 1000 periods and $d = 2$ cm.

Therefore to work in diffraction limited regime a normalized emittance ε_n should be below:

$$\varepsilon_n \leq \frac{\gamma \sigma \psi}{2} = \gamma \frac{\lambda}{4\pi} \approx 0.1 \mu m . \tag{1.4}$$

FSF is a large scale facility which should fulfil the requirements of its high number of users. The typical needs of synchrotron radiation users can be divided into four groups:

a) Maximal average brilliance in diffraction limited regime – requires a low emittance;

b) Maximal peak brilliance – requires low emittance and short bunch;

c) Minimal bunch length – requires short bunch;

d) And the last one is the experiments with high bunch degradation (e.g. ERL with FEL, e-p collider, internal target experiments, etc.) on which we don't orient – requires large acceptance.

So, to achieve the record parameters which are above 3rd generation light sources it is planned to have two operation modes. The 1st mode will be optimized to provide a high brilliance beam. Another option is short bunch mode with a final beam minimal bunch length of around 10 fs.

The main design parameters of FSF are presented in Table 1.2.

Table 1.2: Main design parameters of FSF

Parameter	High brilliance mode	Short bunch mode
E, GeV	6	6
<I>, mA	20	5
Q, pC	15	4
τ, fs	200-1000	~10
<B>, ph/s/mm^2/mrad^2/0.1%	$8 \cdot 10^{22}$	$\sim 4 \cdot 10^{21}$
B$_{peak}$, ph/s/mm^2/mrad^2/0.1%	10^{26}	$\sim 10^{26}$
Accelerating gradient, MV/m	17	
Energy gain per linac, GeV	1	
f, GHz	1.3	

So for the high brilliance mode it is proposed to have an average beam current I about 20 mA. The spectral brilliance of undulator radiation is given by [32]:

$$B(\omega) = \frac{\dot{N}_{ph}(\omega)}{4\pi^2 \sigma_x \sigma_{x'} \sigma_y \sigma_{y'} \dfrac{d\omega}{\omega}} . \tag{1.5}$$

So the maximum average brilliance can be written in a diffraction limited regime as:

$$<B(\omega)>_{max} = \frac{<\dot{N}_{ph}(\omega)>}{\dfrac{\lambda^2}{4} \dfrac{d\omega}{\omega}} = 5 \cdot 10^{23} \frac{ph}{s \cdot 0.1\% \cdot mm^2 \cdot mrad^2}, \tag{1.6}$$

where the average photon flux is given by:

$$<\dot{N}_{ph}> = \pi \alpha N_p \frac{d\omega}{\omega} \frac{I_{av}}{e} A(K), \tag{1.7}$$

with $A(K)$:

$$A(K) = \frac{K^2 [JJ]}{1 + 0.5K^2} \tag{1.8}$$

and

$$[JJ] = \left[J_{\frac{1}{2}(k-1)}\left(\frac{K^2}{4 + 2K^2}\right) - J_{\frac{1}{2}(k+1)}\left(\frac{K^2}{4 + 2K^2}\right) \right]^2, \tag{1.9}$$

where J is the Bessel function and $\alpha \sim 1/137$ is a fine-structure constant. The estimation in (1.6) was done for $K = 0.8$, $N = 1000$ and $I = 20$ mA. Estimated value of an average brilliance is higher than for the 3rd generation light sources (see Fig. 1.9).
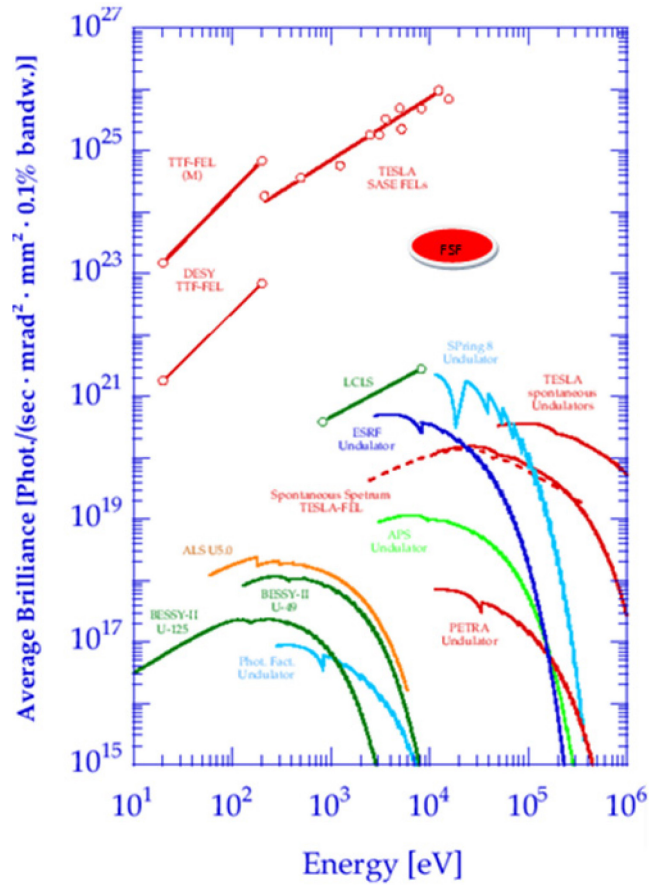
Figure 1.9: Average brilliance of synchrotron light sources [33].

Bunch compression is required to achieve high peak brilliance. The compression is subtle as not to spoil the emittance. The compression limit is set by the initial longitudinal emittance of the beam and by the effects of coherent and incoherent synchrotron radiation. With an average current of 20 mA, longitudinal size of 200 fs and peak current of 30 A one can likewise estimate the peak brilliance B_p.

$$ B_p = \dot{N}_{ph} \frac{4/\lambda^2}{d\omega/\omega} \approx 7 \cdot 10^{26} \frac{ph}{s \cdot 0.1\% \cdot mm^2 \cdot mrad^2} \, . \tag{1.10} $$

A comparison between peak brilliance of 3rd generation light sources, Free Electron Lasers and FSF is presented in Fig. 1.10.
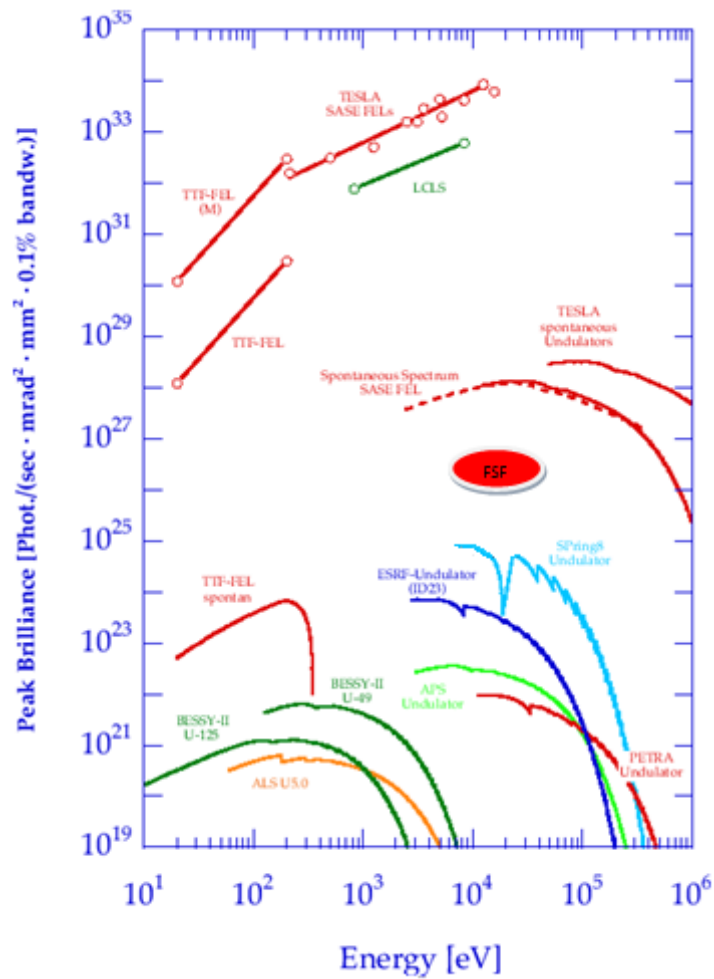
Figure 1.10: Peak brilliance of synchrotron light sources [33].

Let's proceed with an optic in the arcs. Arcs are assumed to be similar and each arc consists of 6 30°-bending sections and 5 undulators with 1000 periods in between of them (Fig. 1.11). The bending section (Fig. 1.12) consists of 4 identical triple-bends with 4 quadrupoles on sides to match the following element (undulator or spreader). Each bending section in the 3-6 GeV arcs was optimized to suppress the emittance growth due to coherent and incoherent synchrotron radiations (CSR and ISR).
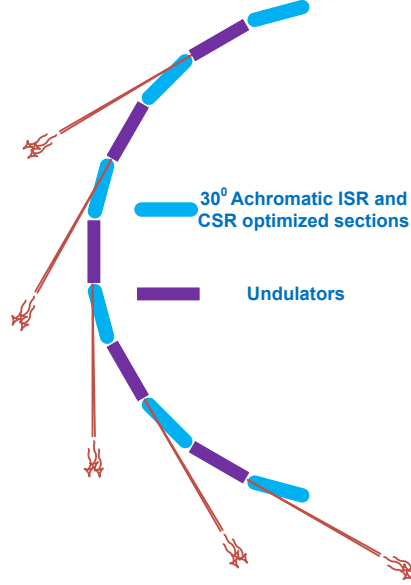
Figure 1.11: Arc of FSF.

One of the main features of the arc design is that each triple bend has an anti-dipole magnet in the middle in order to achieve a zero R_{56} at reasonable strengths of quadrupoles. The betatron phase advance Q_x of each triple-bend section equals to 3/4 to cancel out the influence of CSR to the emittance [34]. The emittance growth due to incoherent synchrotron radiation can be written as [e.g. 35]:

$$\Delta\varepsilon_x = \frac{2}{3}r_e C_q \gamma^5 I_5 ,\tag{1.11}$$

where r_e is the classic radius of an electron, γ is the Lorentz factor of the beam,

$$C_q = \frac{55}{32\sqrt{3}}\frac{\hbar}{mc} = 3.84\cdot10^{-13}\ \text{m}\tag{1.12}$$

is a quantum constant and radiation integral I_5 is given by:

$$I_5 = \int\frac{H}{\rho^3}ds ,\tag{1.13}$$

where ρ is the bending radius of dipoles and H is the Courant-Snyder parameter:

$$H = \gamma\eta^2 + 2\alpha\eta\eta' + \beta\eta'^2 ,\tag{1.14}$$

which depends on the dispersion η, its derivative and on the Twiss parameters of the beam. Therefore, in order to suppress the emittance growth due to ISR, the Twiss parameters of the beam were optimized to minimize the radiation integral I_5.
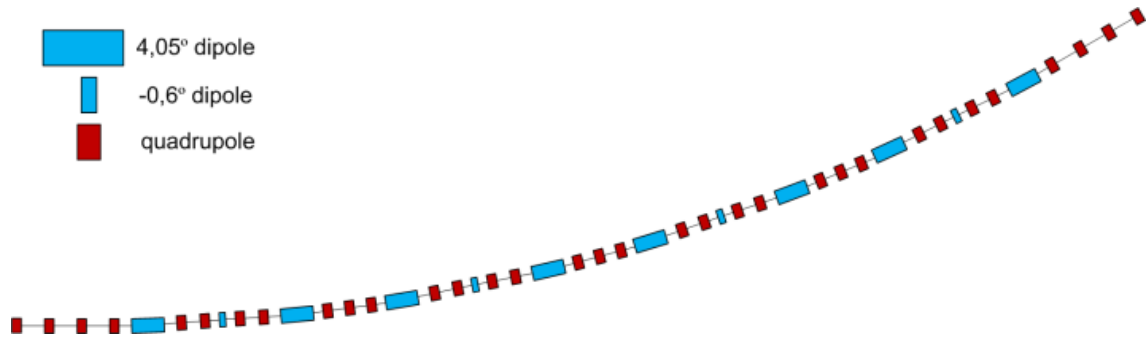
Figure 1.12: 30^0 bending section of the FSF arc.

Another very important part of the accelerator layout is the spreader/recombiner sections. The layout of the spreader after the second main 1 GeV linac is identical to the recombiner at the entrance to this linac and presented in the Fig. 1.13. The second pair of spreaders and recombiners for the first 1 GeV linac is identical, but without the 6 GeV beam line, which goes to the long undulator section. All spreader lines are isochronous.

One of the limiting factor for the spreader design is the contribution to the radiation integral I_5, which characterizes the transversal emittance growth due to incoherent synchrotron radiation. Relatively high value of the horizontal β-function (50-100 m) from the linac section limits the bending angle of the separating dipoles (which represents η'). Quadrupoles are necessary to minimize the contributions of other dipoles to I_5, which in combination with isochronous and reasonable β-functions conditions requires a large number of them. Also a compact design is advantage for the installation footprint.

The difficulties (which grow with the number of the beam energies to be separated) originate from the conditions on the β-functions (low I_5 contradicts with „natural" β-functions out of the linacs) and dispersion (low I_5 contradicts with the beam lines separation). To reduce the distances required for separation of the beams it was assumed to couple coordinates in the vertical plane. For this a magnet like a Lambertson separation septum [e.g. 36] for 4, 5, and 6 GeV beam lines (green in Fig. 1.13) is used. The coupling in the spreader makes the analysis and optimization of the spreader/recombiner section to be really complicated.

Figure 1.13: Spreader section after the second 1 GeV linac.

2. Mode excitation by electron beam and BBU instability

In the superconducting cavities the electromagnetic fields might be expressed as sums of transverse magnetic (TM) and transverse electric (TE) modes. For TM modes there is a longitudinal electric field presented and a magnetic field could be ever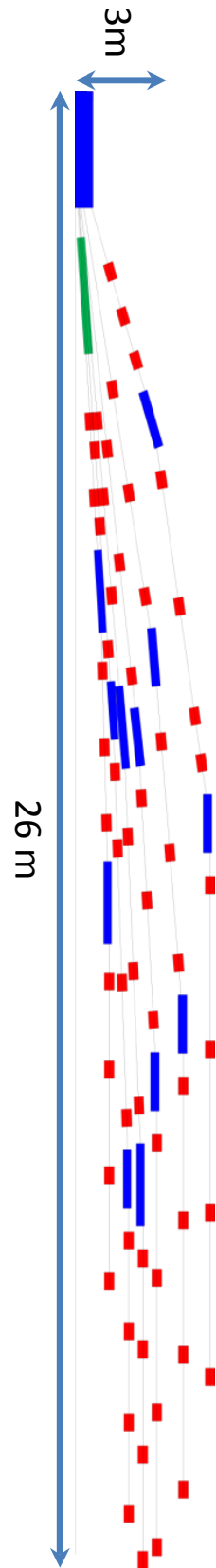ywhere perpendicularly to the longitudinal axis. For TE modes the situation is conversed with an existing longitudinal magnetic field and with electrical field transverse to it everywhere. When a charge passes through a cavity it excites modes and induces fields which provide a retarding force. Some of the modes could be excited quite strong and lead to beam instabilities and finally to a beam loss.

At the beginning of this chapter formulas for the excitations of high order modes (HOMs) (as example for monopole and dipole modes) will be derived. When it is not specially linked then all the ideas in §2.1 and §2.2 are from [37]. One of these instabilities due to dipole modes – Beam Break Up instability will be discussed in the following paragraphs.

Different types of BBU instabilities will be discussed, such as single bunch BBU caused by short-range wakefields and two types of multi-bunch instabilities caused by long-range wakefields. As it will be shown later, one of the most problematic instabilities for the energy recovery linac based machines is a regenerative form of a transverse BBU. All types of BBU have a similar nature – they are caused by interaction of a beam with high order modes, but all of them are very different from each other. At the beginning single bunch BBU will be discussed, and then it will be continued with multi-bunch instabilities.

On one hand, some of the modes (eg. quadrupole modes) can lead to beam degradation that means the losses of luminosity for colliders or what is more important for us – the losses of brightness for synchrotron light sources. On the other hand, the excited modes give addition power dissipation in the cavity walls that increases the cryogenic losses.

At the end of this Chapter the modelling of the BBU instability for B*ERL*inPro and the methods of BBU suppression will be discussed.

2.1. Monopole mode excitation

Modes of a cavity are independent from each other and form a complete orthogonal system and, therefore we can study the effects of the modes excitation individually for each mode. The final result will be given by a sum of all modes. Therefore let's start with monopole modes.

First of all let's determine the voltage induced by a point charge, moving on a cavity axis. To do that the following facts will be used: first of all is that the energy in the system of a cavity and a charge is conserved, and the second that all fields excited by the charge may be added as superposition to any fields already existing in the cavity.

Let's start with analysis of charges moving on axis. In this case only monopole TM modes can be excited because all other modes do not have any longitudinal electric field on the axis. Let the voltage, induced by the charge in one mode of the cavity be:

$$\widetilde{V}_q = V_q e^{i\alpha} e^{-i\omega_n t},$$
(2.1)

where V_q is the magnitude of the complex quantity $\widetilde{V}_q$ and therefore is always positive, α is the phase between the charge and $\widetilde{V_q}$ and ω_n is the eigenfrequency of the mode.

One can continue with a postulate that the induced voltage also interacts with the charge itself. So, the effective voltage acting on the charge can be written as some fraction f of the total voltage:

$$\widetilde{V}_{eff} = f\widetilde{V}_q.$$
(2.2)

To find the change in the voltage it is assumed that the cavity has no losses and it has been already excited to the voltage $\widetilde{V}_c$:

$$\widetilde{V}_c = V_c e^{i\varphi} e^{-i\omega_n t},$$
(2.3)

where the phase φ is an arbitrary angle at the time of passage and V_c is a positive real quantity.

Therefore, the initial stored energy in the cavity is given by:

$$U_i = \frac{V_c^2}{\omega_n \dfrac{R_a}{Q_0}},$$
(2.4)

where R_a is the shunt impedance of the mode and Q_0 is the unloaded quality factor. The final voltage, after the charge has passed the cavity, is given by the superposition:

$$U_f = \frac{\left|V_c e^{i\varphi} + V_q e^{i\alpha}\right|^2}{\omega_n \dfrac{R_a}{Q_0}}.$$
(2.5)

The energy change in the cavity is:

$$\Delta U_c = U_f - U_i = \frac{2V_c V_q \cos(\varphi - \alpha) + V_q^2}{\omega_n \dfrac{R_a}{Q_0}}. \tag{2.6}$$

The charge has also changed its energy:

$$\Delta U_q = q(V_c \cos\varphi + fV_q \cos\alpha). \tag{2.7}$$

And, as it was said earlier, the energy of the whole system – charge-cavity is conserved and, therefore, one has:

$$\Delta U_c + \Delta U_q = 0, \tag{2.8}$$

that gives:

$$-q(V_c \cos\varphi + fV_q \cos\alpha) = \frac{2V_c V_q \cos(\varphi - \alpha) + V_q^2}{\omega_n \dfrac{R_a}{Q_0}}, \tag{2.9}$$

Now the superposition principle can be used. It requires $V_q \sim q$ and in Eq. 2.9 one can equate the terms with the same powers of q:

$$-qV_c \cos\varphi = \frac{2V_c V_q \cos(\varphi - \alpha)}{\omega_n \dfrac{R_a}{Q_0}}, \tag{2.10}$$

$$-qfV_q \cos\alpha = \frac{V_q^2}{\omega_n \dfrac{R_a}{Q_0}}, \tag{2.11}$$

Since the phase φ is arbitrary, Eq. 2.10 can be true if α is 2π times an integer if $q < 0$, and π times an odd integer if $q > 0$. Therefore one find that:

$$\widetilde{V}_q = \mp \frac{\omega_n R_a}{2Q_0} |q| e^{-i\omega_n t} \tag{2.12}$$

and with Eqs. 2.2 and 2.12:

$$\widetilde{V}_{eff} = \frac{\widetilde{V}_q}{2}. \tag{2.13}$$

The quantity

$$k_n \equiv \frac{\omega_n R_a}{4Q_0} \tag{2.14}$$

is called a mode loss factor. It should be noted that the shunt impedance depends only on the geometry of the cavity and, therefore the loss factor as well. Using 2.4, one can find that:

$$k_n = \frac{V_c^2}{4U}.$$

(2.15)

The Eq. 2.12 is given for point charge moving thought the lossless cavity. If it is required to include the losses, then the Eq. 2.12 still applies if the charge exits the cavity before the fields decayed substantially. The decay time is typically few microseconds or even longer ($Q \gg 1$) when the transit time of the charges is of the order of nanoseconds.

2.2. Dipole mode excitation

In the previous chapter the effect of monopole mode excitation in a cavity was studied. A monopole mode was excited by a charge moving on axis. It should be noted, that for all other modes the longitudinal electric field vanishes on axis. However, in a real accelerator bunches of charges perform some transverse oscillations about the design beam trajectory and therefore the other modes can be excited. In this chapter, using the same approach as in the previous chapter, excitation of dipole modes was studied.

Let's start with a definition of a dipole loss factor k_d, which is quite similar to the monopole mode loss factor (2.15). A force from a dipole mode on a charge increases linearly with a distance from the cavity axis therefore one need to choose a suitable reference distance. Let's define V_a as an accelerating voltage on the distance a – the beam pipe radius. So, now a loss factor can be defined as:

$$k_d = \frac{V_a^2}{4U}.$$

(2.16)

Now again, let a charge q to travel through a previously excited cavity with a stored energy of:

$$U_i = \frac{V_a^2}{4k_d}.$$

(2.17)

And after the passage its energy might be written as:

$$U_f = \frac{\left|V_a e^{i\varphi} + V_q e^{i\alpha}\right|^2}{4k_d}.$$

(2.18)

The phases φ and α have the same meanings as in the problem for monopole modes. V_q is the charge-induced voltage at the beam pipe radius.

The energy change of the charge moving at the distance ρ off the cavity axis is given by:

$$\Delta U_q = q(V_c \cos\varphi + fV_q \cos\alpha)\frac{\rho}{a}. \qquad (2.19)$$

It should be noted that in Eq. 2.19 the field linearity in dependence on the offset from axis ρ was taken into account. As in the previous chapter, due to the energy conservation, now the energy change in the cavity and the energy gained by the charge can be equated. Again the superposition principle that $(V_q \sim q)$ can be used, that gives:

$$a = 2\pi k, \text{ for integer } k \text{ and } q<0, \qquad (2.20)$$

$$a = \pi l, \text{ for odd integer } l \text{ and } q>0. \qquad (2.21)$$

And one found:

$$\tilde{V}_q = \mp 2k_d |q| \frac{\rho}{a} e^{-i\omega_n t}, \qquad (2.22)$$

where $\rho \leq a$.

Due to the linear field variation with the distance from the axis the quantity V_ρ/ρ is constant, where V_ρ is the voltage at the distance ρ off axis. Therefore, the shunt impedance of a dipole mode can be defined as:

$$\left(\frac{R}{Q}\right)_d = \frac{V_a^2}{\left(\frac{\omega_n}{c}\right)^2 a^2 P_c}, \qquad (2.23)$$

where P_c is the power, dissipated in the cavity walls. It should be noted that the defined shunt impedance is given in ohms (it is important for modeling). Now one can find the dipole loss factor:

$$k_d = a^2 \left(\frac{\omega_n}{c}\right)^2 \frac{\omega_n}{4} \frac{R_d}{Q_0}, \qquad (2.24)$$

where Q_0 is the unloaded quality factor of the mode.

Dipole modes deflect a beam. And if they are strongly excited it could lead to a beam instability and finally to a beam loss. Especially this parasitic effect leads to so called beam break up instability in machines with energy recovery. This type of the instability will be discussed in the next sections.

2.3. Single bunch Beam Break Up

As it was discussed in the previous paragraphs the excited high order modes can be a reason for instabilities in Linear Accelerators. In this paragraph a single bunch BBU caused by short-range wakefields (for more details see e.g. [38, 39]) will be discussed. To illustrate the effect of this type of instability a two-particle model (shown in Fig. 2.1) for a bunch will be used. In this model it is assumed that the bunch consists of two ultrarelativistic macroparticles and each of them contains a half of the particles $N/2$ of the whole bunch. We assume the case of a smooth approximation that the head particle performs simple betatron oscillations with a frequency ω_β, which is independent of s, and, therefore:

$$x_h(s) = \tilde{x}_h \cos(k_\beta s),$$ (2.25)

where $k_\beta = \omega_\beta/c$ is the betatron wave number.
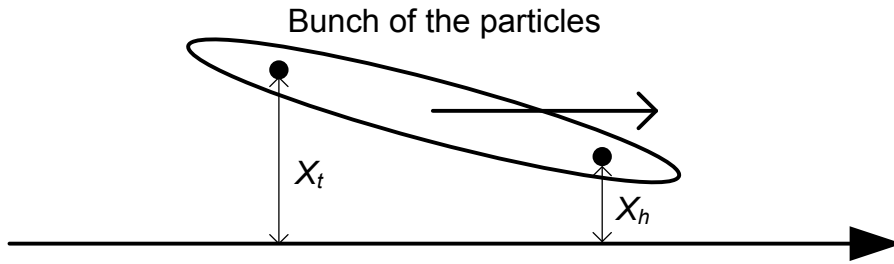
Figure 2.1: Two macroparticles model for single bunch BBU.

If the transverse wakefields are not induced by the head particle, then the tail particle would just follow the head.

When the wakefields are induced, the tail particle sees the deflecting wake field at the distance $-\sigma_z$ behind and one can write the equation of motion for it, as:

$$x_t'' + k_\beta x_t = \frac{N r_e W_\perp(2\sigma_z)}{2\gamma L} x_h(s),$$ (2.26)

where r_e is the classical radius of an electron, σ_z is the beam size, γ is the relativistic factor corresponding to a beam energy and L is the length of the cavity period, $W_\perp \sim 2\ cm^{-2}$ is the transverse wake function taken at the distance $2\sigma_z$ behind the head particle. The solution of the Eq. 2.26 is given by:

$$x_t(s) = \widetilde{x}_h \left(\cos(k_\beta s) + \frac{N r_e W_\perp(2\sigma_z)}{4 k_\beta \gamma L} s \sin(k_\beta s) \right), \tag{2.27}$$

where the first term describes just the betatron oscillations and the second term is the reaction to the wakefield left by the head particle.

Let's continue with an introduction of a dimensionless, so called, instability growth parameter which is given by the ration of two amplitudes of the tail and the head:

$$\tau = \frac{\widetilde{x}_t}{\widetilde{x}_h} = \sqrt{1 + \left(\frac{N r_e W_\perp(2\sigma_z)}{4 k_\beta \gamma L} L_{acc} \right)^2}, \tag{2.28}$$

where L_{acc} is the total length of the linac. Usually 1 in the square root in Eq. 2.28 is neglected because it is assumed that there is instability with a high growth parameter $\gg 1$.

Equation (2.28) was derived for the case without acceleration in the linac. As it was noted in [38], acceleration can be included by just replacing the factor L_{acc}/γ for its integral counterpart $\int_0^{L_{acc}} \frac{ds}{\gamma(s)} = \frac{L_{acc}}{\gamma_f} ln \frac{\gamma_f}{\gamma_i}$, where $\gamma_{i,\,(f)}$ is the initial (final) relativistic factor.

If we use now the parameters of the FSF beam presented in the Tab. 1.2, we get that the most unstable is the preinjection linac with a growth parameter $\tau \sim 1 + 2 \cdot 10^{-6}$, that means that the tail is almost following to the head. Therefore, one can conclude that single bunch BBU is not a problem for the FSF facility. In the next paragraph another type of BBU instability – multi-bunch BBU in machines with energy recovery linac will be discussed.

2.4. Multi-bunch Beam Break Up instability

As it was shown in the previous chapter the single bunch BBU does not strongly influences the bunch of the FSF. In this chapter another type of instability will be discussed – multi-bunch BBU. It also has two forms – a cumulative and the most important for us a regenerative form of BBU instability.

The cumulative BBU occurs when there is no electromagnetic coupling between cavities but the dipole mode is excited in each cavity of the linac. The bunch is deflected in the first cavities by a dipole mode and excites the later cavities due to the off-axis position of the beam in the following cavities. The deflection grows with each cavity. Cumulative BBU is important for the facilities with a long linac.

Another form – so-called regenerative BBU occurs, when there is a strong electromagnetic coupling between the accelerating cavities. In this case the deflecting mode is like one mode in a multi-cell structure, when it moves synchronous with a beam, the beam get unstable. The excitation of the mode from the beam is carried electromagnetically from one cell to the next in the linac structure. The bunch is deflected in the first cavities and then it excites the later cavities or it excites the same cavity after recirculation so that the deviation is carried by the beam. This excitation grows with each bunch and, if the energy transfer to the cavity is greater than the ohmic losses of the cavity, then the instability develops.

This type of BBU instability can limit a beam current in the machines with energy recovery when the excitation is transferred by a bunch to the same mode on the recovery pass through the linac. Regenerative type of instability will be discussed in the next paragraphs.

2.4.1. Introduction to Regenerative Beam Break Up instability

One potential weakness of the ERLs is a regenerative form of transverse BBU instability, which may severely limit a beam current. The actuality of this problem was recognized in early experiments with the recirculating SRF accelerators at Stanford [40] and Illinois [41], where the average threshold current of this instability was about a few microamperes. In the works of Rand and Smith in [42] dipole high order modes were identified as a driver of this instability. In late 80's the detailed theoretical model and simulation programs had been developed [43, 44]. Nowadays the interest to this problem was renewed. The requirements for more detailed theory and simulation programs [45-47] are given by the needs of high current (~100 mA) ERLs.

Let's first briefly explain the fundamentals of the BBU instability. If an electron bunch passes through an accelerating cavity it interacts with dipole modes (e.g. TM_{110}) in the cavity (Fig. 2.2). First, it exchanges energy with the mode; second, it is deflected by the electromagnetic field of the mode. After recirculation the deflected bunch interacts with the same mode in the cavity again and transfers the energy. If the net energy transfer from the beam to the mode is larger than the energy loss due to the mode damping then the beam becomes unstable.
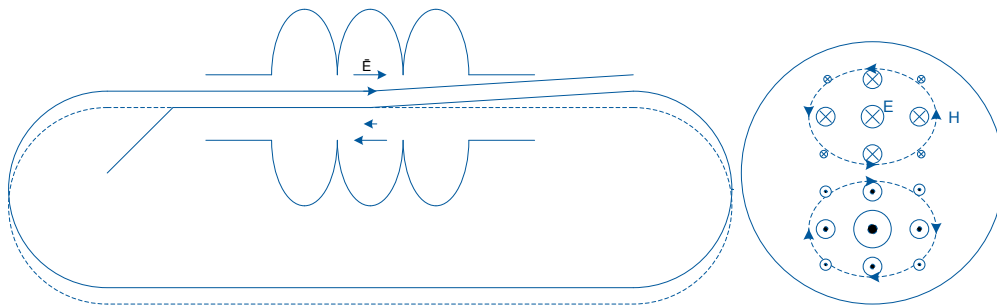
Figure 2.2: Mechanism of BBU instability. On the left side schematically presented a layout of an ERL and trajectory kick due to a dipole mode. On the right side the fields in the transversal plane in this mode are presented.

Let's start with a simple model of a single pass machine with one cavity and with one dipole mode in it. The length of the cavity is neglected and it is assumed that the mode gives a point like kick (so-called thin element approximation). Due to the fact, that the magnetic field of the mode is constant, one can assume that the bunch is one particle with the charge q. So, at the first pass:

$$\begin{cases} x_1 = 0 \\ x_1' = -\dfrac{eV_a}{\omega a p}\sin(\varphi) \end{cases}, \tag{2.29}$$

where x_1 is the coordinate (it is assumed that a beam moves on the axis on the 1-st pass and, therefore, there is no energy change) and x_1' is the kick angle, φ is the phase and p is the momentum of the bunch. After the pass through a recirculating ring with a transfer matrix $M = (m)_{ij}$, the bunch will come with an offset.

$$x_2 = m_{12}x_1'. \tag{2.30}$$

The energy deposited by the bunch in the mode can be written as:

$$\Delta U_2 = -q \frac{V_a}{a} \cos(\varphi + \omega T_r) m_{12} x_1'. \tag{2.31}$$

Ohmic losses in the cavity were discussed earlier (Eq. 2.23) and can be expressed as:

$$P_c = \frac{V_a^2}{\left(\dfrac{\omega}{c}\right)^2 a^2 \left(\dfrac{R}{Q}\right)_d Q}. \tag{2.32}$$

The threshold value is reached, when the ohmic losses and the average power deposited by individual bunches are equal:

$$< \Delta U_2 > f_b - P_c = 0. \tag{2.33}$$

The averaging over the phase of the mode φ is done. This is possible due to assumption that the beams are moving with the frequency of the main acceleration mode, which is not a multiple to the frequency of the dipole mode therefore, the phase of the dipole mode at the beam passes is a random value normally distributed at $[0; 2\pi]$. The frequency f_b at the threshold current is given by:

$$f_b = I_{th} / q. \tag{2.34}$$

And now Eq. 2.33 leads to the final equation for the threshold current:

$$I_{th} = - \frac{2pc^2}{e\omega \left(\dfrac{R}{Q}\right)_d Q m_{12} \sin(\omega T_r)}. \tag{2.35}$$

From Eq. 2.35 one can see that the threshold current is proportional to the beams energy. It means that the most problematic cavities are where a beam has a lower energy. The threshold current is inversely proportional to:
- the impedance and the quality factor of the mode which should be minimized on a cavity design stage;
- the m_{12} matrix element, which for the case of a single mode and one cavity can be written as $\sqrt{\beta_1 \beta_2} \sin \mu$, where $\beta_{1,2}$ – is a Twiss parameter of a beam on the 1st and 2nd passes correspondingly, should be minimized to achieve the highest threshold current. The betatrone phase advance μ is additional optimization parameter.

It is required to know the phase of the mode φ, when the HOM frequency is equal to a harmonic number of the bunch repetition rate ($M/N \cdot f_b$, with integer M, N). In this resonant case the presented model does not provide the right solution. One has to calculate the phase

using some other method or some simulation program. It should be noted that the resonance cases should be avoided on the design stage by a proper choice of the beam frequency and of the cavity parameters. Also, Eq. 2.35 is true only for the case when the term $m_{12}\sin(\omega T_r) < 0$. This case perfectly agrees with simulation results as it was presented in [48]. Eq. 2.35 gives beams stability for the opposite case, when $m_{12}\sin(\omega T_r) > 0$, but the simulation results show that the beam can be unstable with a high threshold current. This discrepancy caused by the assumption that the voltage induced by the beam on the second pass is very small compared to the HOM voltage, which fails at high bunch charges. In this case a more complicated theory is required. Such a theory was well described by G. Hoffstaetter and I. Bazarov in [45]. In the next paragraph the ideas are briefly summarized.

2.4.2. Regenerative BBU instability theory

In [45] the more general formulas for the BBU threshold current were derived. In principle authors used another approach to the same problem. In this part the main aspects of this paper are reviewed.

A simple model of one cavity and one dipole mode is assumed. If a mode is excited then a beam gets a transverse kick and after a recirculation it comes back to the cavity with an offset, and transfers the energy to the mode. If the energy of the mode increases, then the following bunches will experience the stronger kick that leads to the further energy grow of the mode and there is instability.

To describe this effect let's start at a point of time t', when the charge $I(t')dt'$ with an offset $x(t')$ passes through the cavity on its deceleration loop and excites the HOM. The following particles on acceleration will see the transverse kick, which can be written as:

$$\Delta p_x(t) = \frac{e}{c}W(t-t')x(t')I(t')dt',\qquad(2.36)$$

where $W(\tau)$ is the wake function which describes the transverse force at the time τ after the mode was excited.

An effective change of the transverse voltage of the HOM is given by:

$$\Delta V(t) = \frac{c}{e}\Delta p_x(t).\qquad(2.37)$$

Now it can be assumed that all bunches are injected on the cavity axis and, therefore, they do not excite the mode on the first pass during acceleration. The effective transverse voltage determines which kick the bunch sees and which position it will have after the recirculation

time T_r. The transfer matrix element $T_{12} = m_{12}/p$ maps the transverse momentum $p_x(t)$ to the offset:

$$x(t + T_r) = T_{12} p_x(t) .$$ (2.38)

Using (2.36) an integral equation for the effective voltage of the mode can be written as:

$$V(t) = \int_{-\infty}^{t} W(t - t') I(t') T_{12} \frac{e}{c} V(t' - T_r) dt' .$$ (2.39)

To find the solution of this equation one can assume now that the current is a train of short bunches like the Diracs's-delta functions with an intervals t_b (see Fig. 2.3), so the current on the second deceleration pass is given by:

$$I(t) = I_0 t_b \sum_{m=-\infty}^{+\infty} \delta_D(t - T_r - m t_b) .$$ (2.40)
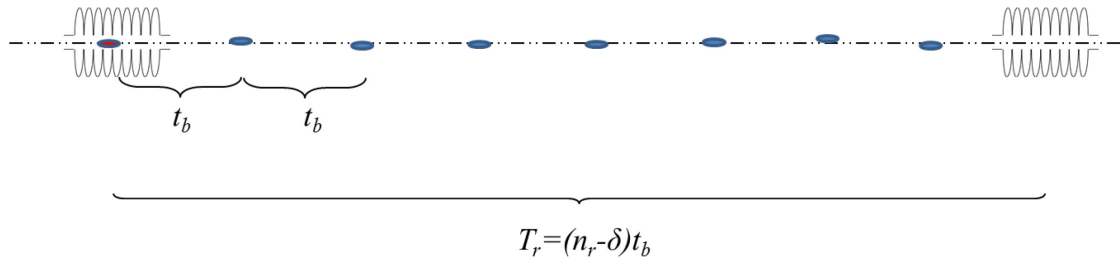
Figure 2.3: Picture of time scales in the ERL.

The time t_b is proportional with some integer coefficient to an RF circulation time t_0, which is inverse proportional to the main RF frequency ω_0:

$$t_0 = \frac{2\pi}{\omega_0} .$$ (2.41)

Now the recirculation time T_r can be written as:

$$T_r = (n_r - \delta) t_b .$$ (2.42)

For an ERL δt_b is given by:

$$\delta t_b = (n + \frac{1}{2}) t_0 ,$$ (2.43)

where n is integer.

Now, using (2.39) one can rewrite the effective voltage of the HOM at the time between some bunches $t \in [nt_b+t_r, (n+1)t_b+t_r]$ as:

$$V(t) = I_0 t_b T_{12} \frac{e}{c} \sum_{m=-\infty}^{n} W(t-T_r-mt_b)V(mt_b) . \qquad (2.44)$$

Let's proceed at the time when the bunch passes through the cavity on the deceleration at the time $t=nt_b+t_r$:

$$V(nt_b+T_r) = I_0 t_b T_{12} \frac{e}{c} \sum_{m=0}^{\infty} W(mt_b)V((n-m)t_b) . \qquad (2.45)$$

As it was discussed §2.1 and §2.2, the voltage can be written as:

$$V(t) = V_0 e^{-i\omega t} . \qquad (2.46)$$

where a positive imaginary part of frequency ω indicates instability. Now (2.46) can be used in (2.45), that leads to the following equation:

$$\frac{1}{I_0} = t_b T_{12} \frac{e}{c} e^{i\omega t_r} \sum_{m=0}^{\infty} W(mt_b) e^{i\omega m t_b} . \qquad (2.47)$$

The threshold current I_{th} is the smallest real value of the current I_0 which corresponds to the real ω. In [45] authors used a Laplace transformation and wrote the dispersion relation as:

$$\frac{1}{I_0} = t_b T_{12} \frac{e}{c} e^{i\omega n_r t_b} \sum_{n=0}^{\infty} W([n+\delta]t_b) e^{i\omega n t_b} . \qquad (2.48)$$

The sum in the dispersion relation (2.48) can be obtained in the far field approximation for the wakes. When the wake function can be written as:

$$W(\tau) = \left(\frac{R}{Q}\right)_\lambda \frac{\omega_\lambda^2}{2c} e^{-(\omega_\lambda/2Q_\lambda)\tau} \sin \omega_\lambda \tau . \qquad (2.49)$$

The summation can be made as a geometric progression if $Im(\omega) > (-\omega_\lambda/2Q_\lambda)$ and gives:

$$\begin{aligned}
w(\delta) &= \sum_{n=0}^{\infty} W([n+\delta]t_b) e^{i\omega n t_b} \\
&= \left(\frac{R}{Q}\right)_\lambda \frac{\omega_\lambda^2}{4c} e^{-i\omega\delta t_b} \frac{e^{i\omega^+(\delta-1)t_b} \sin(\omega_\lambda \delta t_b) - e^{i\omega^+\delta t_b} \sin(\omega_\lambda[\delta-1]t_b)}{\cos\omega^+ t_b - \cos\omega_\lambda t_b} ,
\end{aligned} \qquad (2.50)$$

where $\omega_\lambda^\pm = \omega_\lambda \pm i \frac{\omega_\lambda}{2Q_\lambda}$ and $\omega^+ = \omega + i \frac{\omega_\lambda}{2Q_\lambda}$. Therefore, the equation for the current (2.48) becomes:

$$I_0 = \frac{2}{KT_{12}} e^{-i\omega n_r t_b} \frac{e^{\frac{\omega_\lambda}{2Q_\lambda}\delta t_b}[\cos(\omega^+ t_b) - \cos(\omega_\lambda t_b)]}{e^{-i\omega^+ t_b}\sin(\omega_\lambda \delta t_b) - \sin([\delta-1]\omega_\lambda t_b)}, \qquad (2.51)$$

where $K = et_b\left(\dfrac{R}{Q}\right)_\lambda \dfrac{\omega_\lambda^2}{2c^2}$.

And now, for the case with energy recovery, when δ=1/2:

$$I_0 = \frac{1}{KT_{12}} e^{-i\omega t_r} \frac{\cos(\omega^+ t_b) - \cos(\omega_\lambda t_b)}{\cos(\omega^+ t_b/2)\sin(\omega_\lambda t_b/2)}. \qquad (2.52)$$

For a positive current I_0 the values ω which corresponds to this value in the dispersion relation in principle will be a complex numbers. If the current is small then the imaginary parts of all of them are negative and the beam motion is stable. But when the current is increased then at some point one of them will become real. This point indicates the threshold current (see Fig. 2.4). So, the threshold current is the smallest real current I_0 for which there is a real ω which satisfies the dispersion relation.
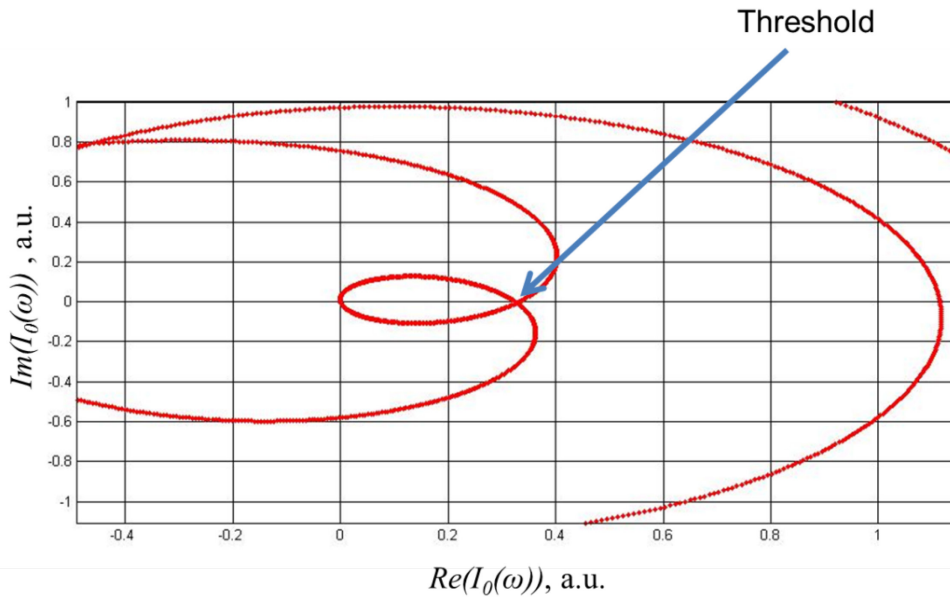

Figure 2.4: Dependence of $I_0(\omega)$ in the complex plain in arbitrary units. The threshold point is indicated.

It should be noted that (2.52) can be simplified to (2.35) in the case of a single mode and one pass. Linearization and approximation that the HOM decay $\frac{\omega_\lambda}{2Q_\lambda}t_b \ll 1$ is negligible in comparison to the bunch spacing t_b is required.

In the case of multiple recirculation turns and multiple HOMs in the cavities the solution can be found by the same approach as for a single mode and single recirculation case. One just has to introduce additional indexes for the numbering of the modes and of the recirculation turns. After that it should be carefully summarized and result will be found. Here I would like to show the equation for a multi-pass ERL with one cavity and one mode in it, which was derived in [47]:

$$I_b \approx I_0 \frac{\lambdabar^2}{QL_{eff}\sqrt{\sum\limits_{m=1}^{2N-1}\sum\limits_{n=m+1}^{2N}\frac{\beta_m\beta_n}{\gamma_m\gamma_n}}}, \qquad (2.53)$$

where I_0- Alfven current, Q is the quality factor of HOM, $\lambdabar = \lambda/2\pi$, λ is the wavelength corresponding to the resonant frequency of the TM_{110} mode, γ_m is the relativistic factor at the m-th pass through the cavity, β_m – is the Twiss parameter, L_{eff} – is the effective length of the cavity. This expression shows that it is preferable to have low β-functions at low energies. It also indicates the limitation for the number of passes.

For a modeling people have already developed computing codes, for example, TDBBU code developed at JLAB [49], MATBBU [50], the tracking code "bi" [51], GBBU code [52] and etc. All of the codes have the same theoretical base. In the modeling GBBU code was used.

2.4.3. Regenerative BBU instability in a cavity with a quadrupole mode

Instability of a beam in the field of a quadrupole mode of an accelerating cavity differs in the mechanism from the BBU in the field of a dipole mode.

Fig. 2.5 shows schematically the field distribution in a quadrupole mode. XY cross-section of a pillbox cavity, E_z and $B_\perp$ field lines, and force on the electron beam are shown. The effect of the mode on the beam is, therefore, focusing in y and defocusing in x direction similar to a stationary quadrupole field but time dependent.
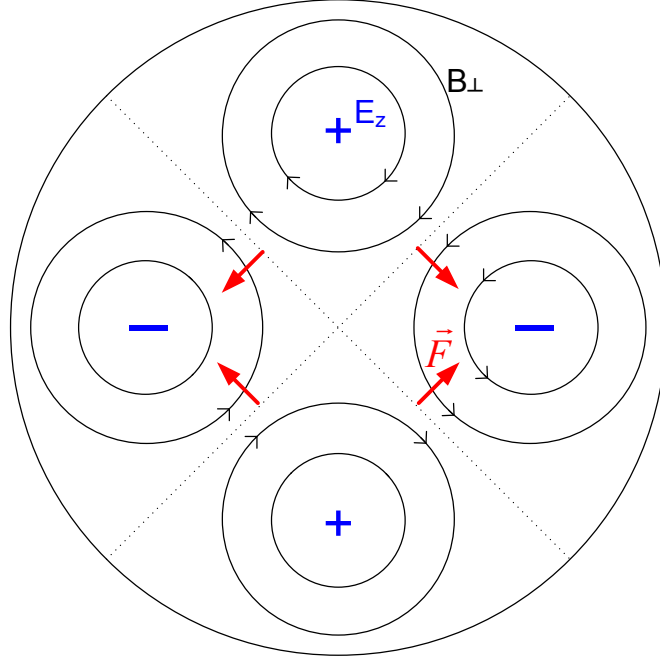
Figure 2.5: Field distribution in a quadrupole mode. XY cross-section of a pillbox cavity is schematically shown. E_z and $B\perp$ field lines, and force on the electron beam are shown.

It can be seen from Fig. 2.5 that only in the case of a round on-axis beam energy transfer to the mode is zero. Elliptical beam excites the mode. If the instability develops, the beam is lost due to an over focusing by the mode. In comparison to the interaction with a dipole mode, axially symmetrical beam does not excite a dipole mode and the mode deflects the beam.

Further, this argument will be reconsidered analytically. For simplicity let us consider a TM_{220} mode in a rectangular cavity. The electric field of the mode near the center is given by:

$$E_z = \frac{V}{l}\frac{y^2 - x^2}{a^2}\cos(\omega t + \varphi). \tag{2.54}$$

Magnetic field is calculated from Maxwell's equation:

$$\mathrm{rot}\vec{E} = -\frac{1}{c}\frac{\partial \vec{B}}{\partial t}, \tag{2.55}$$

which gives:

$$B_x = -\frac{2Vyc}{\omega l a^2}\sin(\omega t + \varphi), \tag{2.56}$$

$$B_y = -\frac{2Vxc}{\omega l a^2}\sin(\omega t + \varphi). \tag{2.57}$$

For an electron with the coordinates (x_1, y_1) coming to the cavity at $t = 0$ one can calculate the deflection angles:

$$\delta x' = -\frac{eB_y l}{pc} = \frac{2eVx_1}{\omega p a^2}\sin(\varphi),$$ (2.58)

$$\delta y' = \frac{eB_x l}{pc} = -\frac{2eVy_1}{\omega p a^2}\sin(\varphi),$$ (2.59)

In linear approximation the electron comes to the cavity after recirculation with addition to the coordinates:

$$\begin{cases} \delta x = m_{12}\delta x' \\ \delta y = m_{34}\delta y'. \end{cases}$$ (2.60)

As it is mentioned above, elliptical beam excites the mode. Therefore, the difference of the energies transferred to the mode with and without taking into account additional electron offset can be calculated.

$$\Delta U = q\Delta E_z l = q\frac{V}{a^2}\cos(\omega t + \varphi)((y_2 + \delta y)^2 - (x_2 + \delta x)^2 - y_2^2 + x_2^2) \approx$$
$$\approx 2q\frac{V}{a^2}(y_2\delta y - x_2\delta x)\cos(\omega t + \varphi) = -4q\frac{V^2 e}{\omega p a^4}(m_{12}x_1 x_2 + m_{34}y_1 y_2)\cos(\omega t + \varphi)\sin\varphi$$ (2.61)

After averaging over initial phase (it is assumed that there is no resonance between the quadrupole mode and the beam, therefore, all values of φ are equiprobable) one can get:

$$\Delta U = 2q\frac{V^2 e}{\omega p a^4}(m_{12}x_1 x_2 + m_{34}y_1 y_2)\sin(\omega T).$$ (2.62)

Averaging over the particles in the beam gives:

$$\Delta U = \frac{qV^2 e}{2\omega p a^4}(\varepsilon_{1x}\beta_{1x}\beta_{2x}\sin(2\mu_x) + \varepsilon_{1y}\beta_{1y}\beta_{2y}\sin(2\mu_y))\sin(\omega T),$$ (2.63)

If this energy is larger than the energy lost in the cavity, the beam is unstable. The threshold current for the instability is therefore given by:

$$\Delta U\frac{I_{th,q}}{q} = P = \frac{V^2 c^4}{(R/Q)_q Q_q a^4 \omega^4},$$ (2.64)

which gives the equation for the threshold current:

$$I_{th,q} = \frac{2pc^4}{eR_q\omega^3(\varepsilon_{1x}\beta_{1x}\beta_{2x}\sin(2\mu_x) + \varepsilon_{1y}\beta_{1y}\beta_{2y}\sin(2\mu_y))\sin(\omega T)},$$

(2.65)

where $R_q = (R/Q)_q Q_q$ is the HOM impedance in Ohm.

We compare this result with the threshold current for a dipole mode (see Eq. 2.35) assuming round beam with equal horizontal and vertical emittances. Quadrupole modes are important for the BBU analysis if:

$$R_q \sim R_d \frac{c^2}{8\omega^2\varepsilon\beta} \sim 500R_d,$$

(2.66)

for the estimation we took $\varepsilon = 5\cdot10^{-3}$ mm·mrad, $\beta = 10$ m and $\omega = 2\pi\cdot3$ GHz.

For the new design of BERLinPro cavities it was reported [e.g. 53, 54] that there can be quadrupole modes with a shifted electromagnetic centrum from the cavity axis (see Fig. 2.6).

In the case of a cavity with a mode, which centrum is shifted for coordinates (x_0, y_0), the electric field of the mode can be written as:

$$E_z = \frac{V}{l}\frac{(y-y_0)^2 - (x-x_0)^2}{a^2}\cos(\omega t + \varphi).$$

(2.67)

And now, using the same approach described above, the equation of the threshold current can be derived:

$$I_{th,q} = \frac{2pc^4}{eR_q\omega^3(\varepsilon_{1x}\beta_{1x}\beta_{2x}\sin(2\mu_x) + \varepsilon_{1y}\beta_{1y}\beta_{2y}\sin(2\mu_y) + x_0^2\sqrt{\beta_{1x}\beta_{2x}}\sin\mu_x + y_0^2\sqrt{\beta_{1y}\beta_{2y}}\sin\mu_y))\sin(\omega T)}.$$

(2.68)

When the offset of the mode is greater than the beam size, then such shifted modes can be a reason for the instability and modelling of BBU instability is required with such modes.
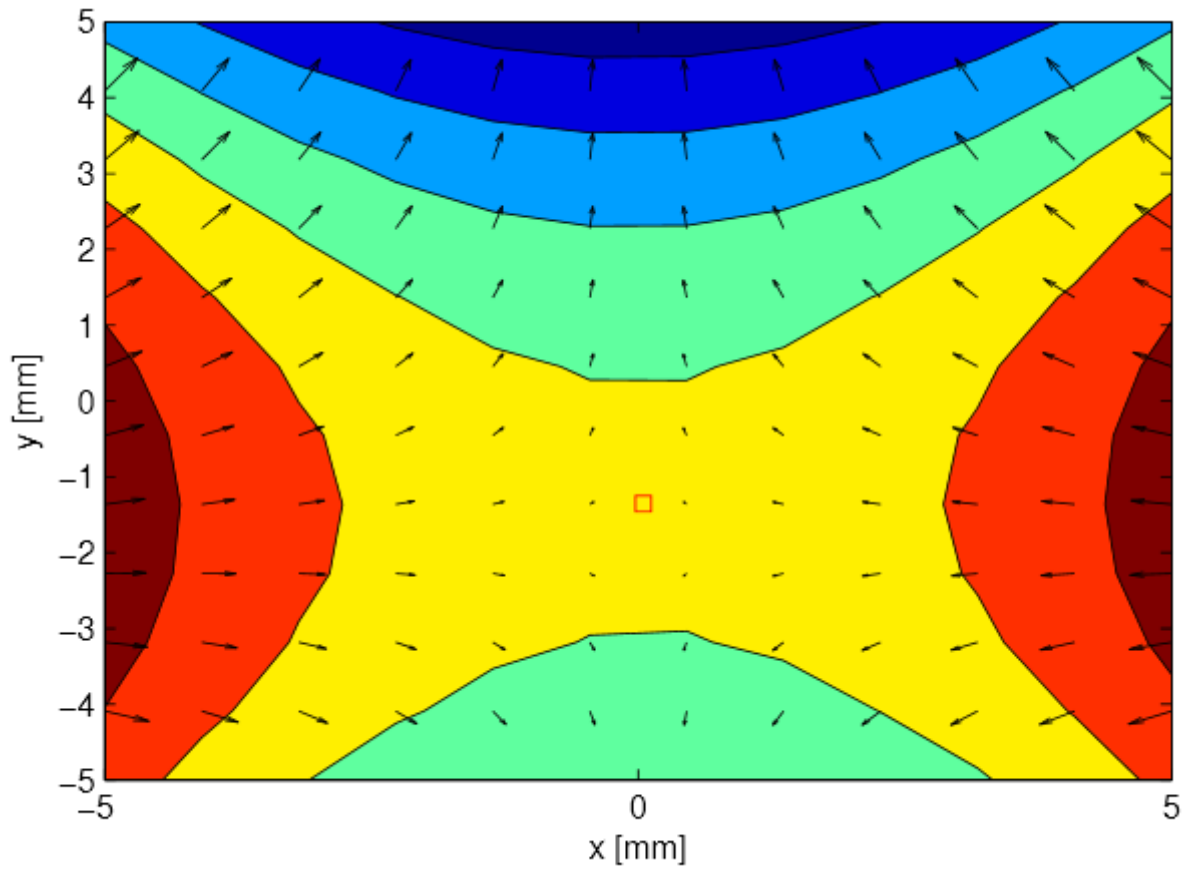
Figure 2.6: Field distribution in a quadrupole mode with a shifted electromagnetic center. XY cross-section of a pillbox cavity is schematically shown. E_z and B field lines, and force on the electron beam are shown [54].

2.5. Modelling of BBU instability for BERLinPro

In this part the modelling of BBU instability for B*ERL*inPro is discussed. In the modelling GBBU program was used. The results include the modelling for both schemes of B*ERL*inPro –with 100 MeV and with 50 MeV maximum beam energy. In the modelling two types of the cavities for the main linac were used – the TESLA [55] and the CEBAF type geometries [56]. The main goal was to develop some methods to increase the BBU threshold current of B*ERL*inPro and to compare the results of the BBU modelling for different cavity models.

In the next chapters first of all the focusing effects of RF fields in the linear accelerators will be discussed. Then the influence of different focusing models for the beam break up instability will be analyzed. Then it will be continued with a comparison of the 2 different types of cavities. Later methods of BBU suppression will be analyzed.

2.5.1. The focusing effects of radio-frequency fields in linear accelerators

In this paragraph the focusing effects of RF fields in linear accelerators will be discussed. Let's start with an equation of motion (2.69) for an ultra-relativistic ($v\sim c$) charged particle in the transverse RF fields in a cylindrically symmetric, spatially periodic RF cavity.

$$\frac{dp_r}{dt} = e\left(E_r + \frac{1}{c}\left[\vec{v}\times\vec{B}\right]_r \right),\qquad(2.69)$$

where E_r and B_φ are the components of the field which are solutions of the Maxwell equations and for the on-axis field $E_z(z,t)$ in the paraxial approximation one has:

$$
\begin{aligned}
div\vec{E} &= 0 \Rightarrow E_r = -\frac{r}{2}\frac{\partial E_z}{\partial z},\\
rot\vec{B} &= \frac{1}{c}\frac{\partial \vec{E}}{\partial t} \Rightarrow B_\varphi = \frac{r}{2c}\frac{\partial E_z}{\partial t}.
\end{aligned}
\qquad(2.70)
$$

And now, substituting the fields one can get:

$$\frac{d\gamma m\dot{r}}{dt} = -\frac{er}{2}\left(\frac{\partial E_z}{\partial z} + \frac{v}{c^2}\frac{\partial E_z}{\partial t} \right) \approx -\frac{er}{2}\frac{dE_z}{dz}.\qquad(2.71)$$

After differentiation and changing independent variable to *z* the equation of radial motion gets the form:

$$r'' + \left(\frac{\gamma'}{\gamma}\right) r' + \frac{\gamma''}{2\gamma} r = 0, \qquad (2.72)$$

where $\gamma' = \dfrac{eE_z}{mc^2}$.

Serafini and Rosenzweig [57] used the following approach to describe the focusing in an accelerating cavity. The average focusing over one cell is calculated and included in the equation of motion. They come to an equation of particle trajectories in the form:

$$r'' + \left(\frac{\tilde{\gamma}}{\gamma}\right) r' + \frac{1}{8\cos^2(\varphi)} \left(\frac{\tilde{\gamma}}{\gamma}\right)^2 r = 0, \qquad (2.73)$$

where $\tilde{\gamma}$ is the average value over the cell, φ is the phase of the accelerating field with respect to the phase of the particle, $\varphi=0$ means maximum acceleration.

The solution of the equation (2.73) is given by the following matrix (2.74), which is implemented in Elegant program [58] (RFCA element):

$$\begin{pmatrix} \cos(\alpha) - \sqrt{2}\sin(\alpha)\sin(\varphi) & \dfrac{\sqrt{8}\gamma_0 L \sin(\alpha)}{\Delta\gamma_{max}} \\ -\dfrac{(2\sin^2\varphi + 1)\Delta\gamma_{max}}{\sqrt{8}} \dfrac{\sin(\alpha)}{L\gamma_1} & \left(\cos(\alpha) + \sqrt{2}\sin(\alpha)\sin(\varphi)\right)\dfrac{\gamma_0}{\gamma_1} \end{pmatrix}, \quad (2.74)$$

where $\alpha = \dfrac{\ln\left(\gamma_1/\gamma_0\right)}{\sqrt{8}\sin(\varphi)}$, $\gamma_{1(0)}$ is the final(initial) normalized energy of the particle, L – the length of the cavity.

2.5.2. The focusing in the modelling

There are three possibilities to choose the focusing model in the GBBU program:

1. Method "Unity". The program assumes that the cavity focusing matrix is a unity matrix. We can provide our own matrices as separate "matrix" elements;

2. Method "Simple". The code assumes uniform acceleration. Although, there is no external focusing in this case, the matrix is not equal to unity and depends on the cavity and beam parameters, and can be written as:

$$\begin{pmatrix} 1 & \dfrac{L\gamma_0}{\Delta\gamma_{max}}\ln(\dfrac{\gamma_1}{\gamma_0}) \\ 0 & \dfrac{\gamma_0}{\gamma_1} \end{pmatrix}; \qquad (2.74^*)$$

3. And the 3-rd opportunity is to provide the real field distribution in a file.

To compare the threshold currents for the CEBAF and TESLA type linacs the method "Unity" and Elegant program were used to calculate the transport matrices of the linac parts. Elegant program calculate the matrix from the beginning of line to any point of the beam line.
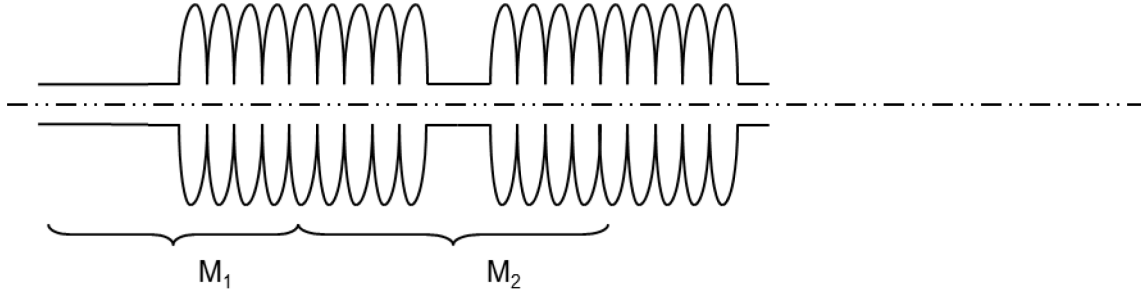
Figure 2.7: Linac and its matrices.

Let us analyse an example of linac which consists of N cavities and has $N+1$ drifts at the beginning, end and between the cavities. The GBBU program calculates the matrices as shown in Fig. 2.7. M_1 – is the matrix from the beginning of the linac to the middle of the 1st cavity and M_2 – is the matrix from the middle of the 1st cavity to the middle of the 2nd cavity and so on. So the last matrix M_{N+1} – is the matrix from the middle of the last cavity to the end of the linac.

The matrices on deceleration are also necessary. There are two ways to get them:

1. To use the Elegant program again, like it was done for acceleration;
2. To use the matrices which we already have and transform them using the procedure described below.

Consider some optical structure with the transport matrix M.

$$\begin{pmatrix} x_1 \\ x_1' \end{pmatrix} = M \begin{pmatrix} x_0 \\ x_0' \end{pmatrix}. \tag{2.75}$$

If we want to "transport" the beam back and to found the matrix (M') of this inverse structure, we should inverse the sign of the angle x′: analytically it is equivalent to the multiplying the x′ on the reflection matrix J.

$$\begin{pmatrix} x_1 \\ -x_1' \end{pmatrix} = \begin{pmatrix} 1 & 0 \\ 0 & -1 \end{pmatrix} \begin{pmatrix} x_1 \\ x_1' \end{pmatrix} = J \begin{pmatrix} x_1 \\ x_1' \end{pmatrix}. \tag{2.76}$$

The next obvious equation helps to find the M′:

$$M'J\begin{pmatrix} x_1 \\ x_1' \end{pmatrix} = M'JM\begin{pmatrix} x_0 \\ x_0' \end{pmatrix} = J\begin{pmatrix} x_0 \\ x_0' \end{pmatrix}. \qquad (2.77)$$

So, this method can be used to derive the matrices on the deceleration:

$$M_{k+1}^{decc} = JM_{N+1-k}^{-1}J^{-1}, k = 0,.., N . \qquad (2.78)$$

2.5.3. The TESLA and the CEBAF type 100 MeV linacs

The TESLA 9 cell cavity, with ~1.038 m length and accelerating gradient E ~16 MeV/m was assumed. So, the TESLA type linac requires 6 TESLA cavities to accelerate the beam up to 100 MeV (5 MeV beam from the injector).

As a base for a new HOM-damped design of the cavities suitable for high current operation 5-cell CEBAF-type geometry was taken. The parameters of the cavity relevant for the BBU modeling were calculated at JLab and provided to HZB [56]. We assume the same average accelerating gradient in the cavity (16 MeV/m). The CEBAF type linac requires 11 cavities to accelerate the beam up to 100 MeV.

The frequency of the main accelerating mode of the CEBAF cavities is 1.5 GHz. Therefore, for the comparison of the two linacs to be "fair", the CEBAF cavity geometry was scaled to make the frequency of the accelerating monopole mode equal to such a frequency of the TESLA cavities (from 1.5 to 1.3 GHz). The frequencies of all other modes are scaled correspondingly. It should be noted, that the values of R/Q used in the modeling program GBBU are defined according to the equation (2.23). In this definition R/Q for dipole modes are in Ohm and not in Ohm/m^2 as in modeling programs like CST MWS [59] or MAFIA [60]. The additional conversion factor $(\omega_n / c)^2$ is frequency dependent. This factor was taken into account during the conversion of R/Q for both TESLA and CEBAF type cavities:

$$R_{d_n}[\Omega] = \frac{1}{\left(\dfrac{\omega_n}{c}\right)^2} r_{d_n}[\frac{\Omega}{m^2}]. \qquad (2.77)$$

The strongest modes for the two cavity types are listed in the Tables 2.1, 2.2. Calculated parameters of the modes for the CEBAF-type cavities are given. The external Q variation due to manufacturing accuracy is reported [55] to be quite large. We take calculated R/Q and (as an example) Q's of one of the TESLA-type cavities measured in HoBiCaT [61]. One can see that the difference of $(R/Q)Q$ for the strongest modes is about a factor of 6 higher for TESLA cavities. So, the threshold current in CEBAF-type linac is expected to be about this factor

higher. The difference in the number of cavities in the linacs is under consideration. This difference leads to additional interplay between the cavities.

Table 2.1: The strongest modes in CEBAF- type cavities

f, GHz	R/Q, Ohm	Q	R, Ohm
Modes perpendicular to FPC			
1.8235	43.10	3460	149125
1.8631	48.04	10420	500608
1.8846	8.96	36787	329459
Modes in FPC direction			
1.8245	43.76	4013	175621
1.8640	45.15	13868	626122
1.8853	8.69	50742	440849

Table 2.2: The strongest modes in TESLA - type cavities

f, GHz	R/Q, Ohm	Q	R, Ohm
Both polarizations have nearly equal parameters			
1.713	86	40000	3440000
1.739	118	32000	3776000
1.865	42	21000	882000
1.873	58	27000	1566000
2.578	90	19000	1710000

At the start, it was taken into account 22 strongest modes (11 of each polarization) in each of 11 CEBAF-type cavities and 11 strongest modes (5 of each polarization plus one whose pair is weak) in each of 6 TESLA-type cavities. Analysis of the results showed that the threshold current is defined by several strongest modes.

Threshold current depends on the length of the recirculation loop (through $\sin(\omega T_r)$ in the Eq. 2.35). The recirculation time of the beam is a half integer of the period of the fundamental mode (1.3 GHz). The length of the loop was taken to be 226.5·λ for CEBAF

type and 216.5·λ for TESLA-type linac. This length is additional optimization parameter which changes the interaction of different modes.

First of all the modelling results compared for different focusing models in GBBU program, which were discussed in the previous paragraph. For 100 MeV B*ERL*inPro based on 6 TESLA type cavities different models of the cavities were provided to GBBU program:

a) Real fields measured in a cavity provided from file;

b) Method "unity", model of a cavity given by Serafini and Rozenzweig (SRS model) and calculated in Elegant;

c) Method "simple", the code assumes uniform acceleration. Although, there is no external focusing in this case, the matrix is not equal to unity and depends on the initial beam energy and on the field gradient in the cavity;

d) Method "unity", model of the cavity calculated in Elegant for the case when the focusing effects are switched off.

Recirculator optics was assumed to be flexible. First the revolution matrix (from the end of the linac after acceleration to the beginning of the linac before the deceleration) is set to have equal betatron phase advances in x and y planes and scanned over the phase advance. The optics was assumed to be symmetrical with the β-function at the beginning of the recirculation turn (β_0) and at the end (β_1) equal to 30 m and α-function $\alpha_0=\alpha_1=0$. The frequency spread of the dipole modes due to fabrication accuracy is of the order of 1-10 MHz [55, 62]. HOM has a width of the resonance curve:

$$\Delta f \sim \frac{f}{Q}. \qquad\qquad (2.78)$$

For a typical quality factor $Q \sim 10^4$ the width of the mode is about $\Delta f \sim 2 \cdot 10^5$ Hz. If the mode frequencies overlap, threshold current can decrease drastically, therefore the overlapping should be generally avoided. In the results presented in Figs. 2.8-9 this is done artificially by a fixed distance (1 MHz step) between the modes in different cavities.

The results of the modelling for different cavity models presented in Fig. 2.8.
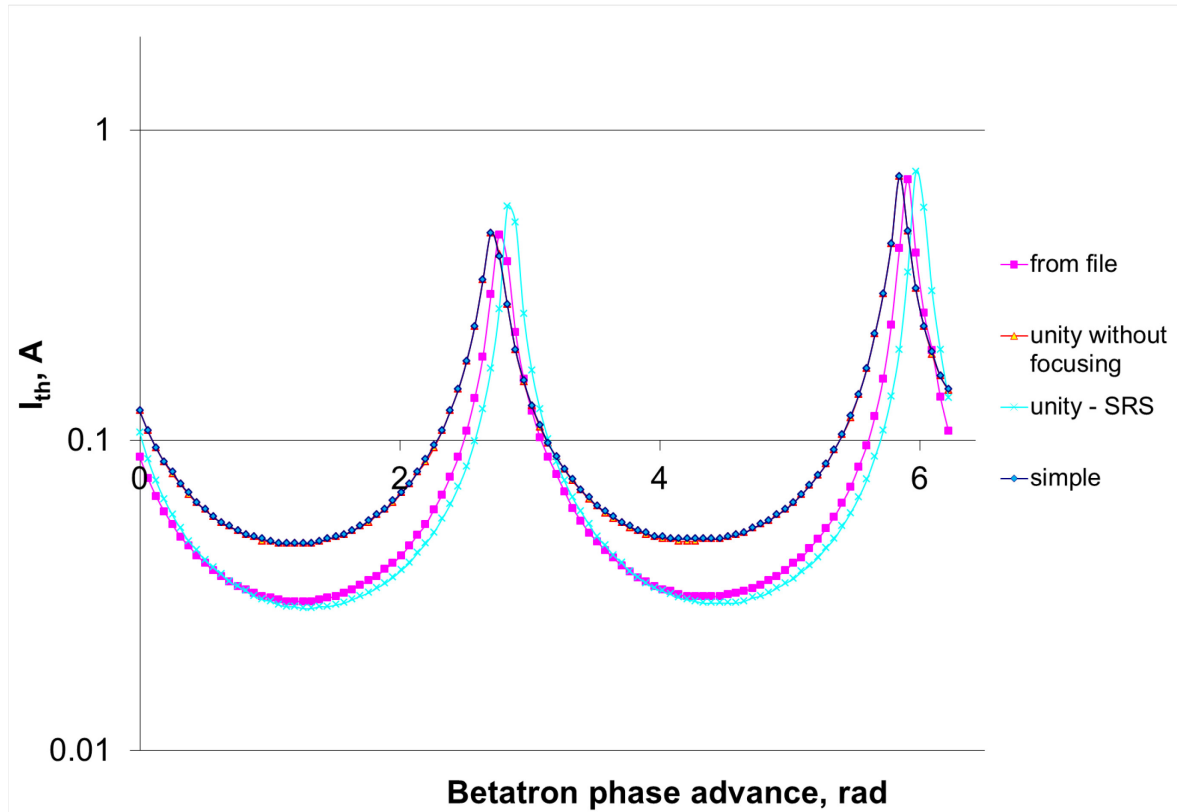
Figure 2.8: Threshold current for 100 MeV B*ERL*inPro based on TESLA type cavities, comparison of the different cavity models.

As one can see from Fig. 2.8 the results when the fields were provided in a file and for SRS model are in a good agreement, but slightly different. That means that SRS model is quite close to the reality. On the other hand, another pair of methods – "unity" and "simple" gives the same results, as it was expected. The results differ in the minimums of the threshold currents by the factor of about 1.5 when the maximums are comparable.

With the second experiment the TESLA and the CEBAF types of cavities were compared. The results of the modeling are presented in Fig. 2.9. Method "unity" was used in GBBU program. Transport matrices of the linac structure were calculated by Elegant program and focusing effects in cavities were included in this modeling for both cavity types. Recirculator optics again was assumed to be flexible and symmetrical with the β-function at the beginning (β_0) and at the end (β_1) equal to 30 m and α-function $\alpha_0 = \alpha_1 = 0$ for both types of cavities.

In accordance with the analytical prediction, the threshold current for CEBAF-type linac is factor 2÷10 higher, than for the TESLA-type linac.
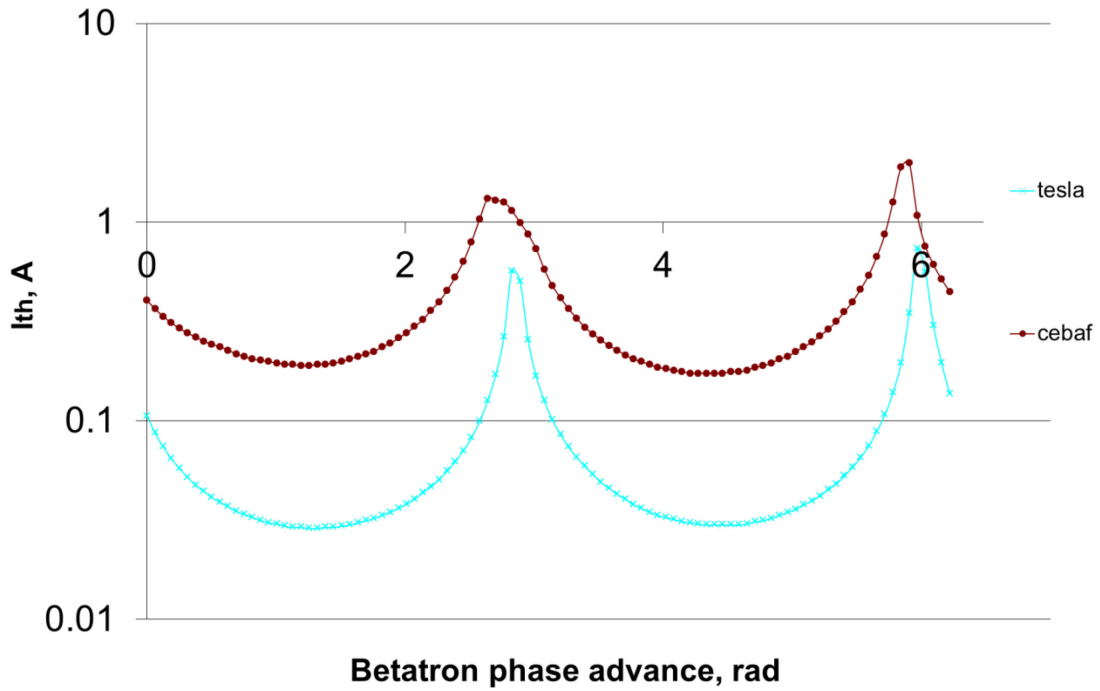
Figure 2.9: Comparison of the threshold currents for TESLA and CEBAF type linacs for 100 MeV B*ERL*inPro. Method "unity" was used in GBBU program and matrices of the cavities were provided from Elegant assuming Serafini-Rosenzweig model.

In the Fig. 2.9 one can see that for the linac, based on CEBAF-type cavities, for all betatron phases the threshold currents varies from about 0.2 to 1.9 A and higher than 0.1 A required for the B*ERL*inPro. When for the TESLA type linac most of the phases give the results below requirement with the lowest current about 30 mA. But there are exist phases when the threshold current is higher than 100 mA.

Optimization of the length of the recirculation loop and modeling with the random distribution of the HOM frequencies will be discussed in the next chapters.

2.5.4. Frequencies overlapping

In this paragraph more attention is paid to frequencies overlapping. If the frequency differences between two modes in some cavities are smaller than the width of the mode *Δf* (2.78), then the HOMs of these cavities start to interact with each other and the threshold current decreases. As an example, the TESLA type linac in 100 MeV B*ERL*inPro was used.

Let's assume:

$$f_i = f + df_i, \qquad\qquad (2.79)$$

where f_i is the frequency of a HOM in the ith cavity, addition to the frequency due to fabrication accuracy df_i has Gaussian distribution – $\Phi_{0,\sigma}{}^2$ and $i = 1..6$ – is the number of the cavity, $\sigma = 1\text{-}10$ MHz.

Let's find a probability P, when any pair of frequencies overlap in the interval:

$$\left|f_n - f_m\right| < \Delta f .$$
(2.80)

This probability P is the same for the value

$$\left|x\right| = \left|df_n - df_m\right| < \Delta f ,$$
(2.81)

because f is a constant.

The value x has Gaussian distribution $\Phi_{0,2\sigma}{}^2$ due to the fact that if two independent values $X_1 \in \Phi_{\mu 1,\sigma 1}{}^2$ and $X_2 \in \Phi_{\mu 2,\sigma 2}{}^2$ then $X_1 + X_2 \in \Phi_{\mu 1 + \mu 2, \sigma 1}{}^2{}_{+ \sigma 2}{}^2$ (see e.g. [63]).

And now the probability P_0 for fixed n,m may be found as:

$$P_0 = F\!\left(0, 2\sigma^2, \Delta f\right) - F\!\left(0, 2\sigma^2, -\Delta f\right) = 2F\!\left(0, 2\sigma^2, \Delta f\right) - 1 ,$$
(2.82)

where

$$F(\mu, \sigma^2, z) = \frac{1}{\sigma\sqrt{2\pi}} \int_{-\infty}^{z} e^{-\frac{(t-\mu)^2}{2\sigma^2}} \, dt .$$
(2.83)

Now let's find a probability that at least one pair overlap. Here the Bernoulli's scheme is used:

$$P = \sum_{k=1}^{n} C_n^k P_0^k (1 - P_0)^{n-k} = 1 - C_n^0 P_0^0 (1 - P_0)^{n-0} = 1 - (1 - P_0)^n ,$$
(2.84)

where $n = C_6^2$ – the number of pairs

Let's calculate the probability P for TESLA cavity for the mode with the highest Q ($R/Q = 86$ Ohm, $Q = 40000$, $f = 1.7 \cdot 10^9$ Hz, $\Delta f = 42$ kHz) and the lowest ($R/Q = 82$ Ohm, $Q = 5400$, $f = 2.58 \cdot 10^9$, $\Delta f = 477$ kHz). For the first mode the probability equals 0.224 and for the second 0.956, for $\sigma = 1$ MHz.

To study the effect of overlapping, BERLinPro based on the TESLA cavities was modelled with randomly distributed frequencies of the HOMs. The maximum threshold current from Fig. 2.9 was chosen $I_{th} = 0.566$ A. For the betatrone phase which corresponds to this current value, the series of simulations were carried out using randomly generated additions to the HOMs frequencies assuming Gaussian distribution with $\sigma = 1$ and 10 MHz.

To generate the additions with a Gaussian distribution a Box-Muller transform [64] was used. With this method a random number with a Gaussian normal distribution (zero expectation ($\mu = 0$), unit variance ($\sigma = 1$)) can be generated by generating a pair of independent random numbers (let us call them U_1 and U_2), which are uniformly distributed in the interval (0, 1]. The variable

$$Z = \sqrt{-2\ln U_1}\,\cos(2\pi U_2) \tag{2.85}$$

is an independent random variable with a normal distribution of standard deviation 1. And the value

$$X = \mu + \sigma Z \tag{2.86}$$

has a normal distribution with an expectation μ and variance σ.

In Fig. 2.10 the results of the modelling are presented.

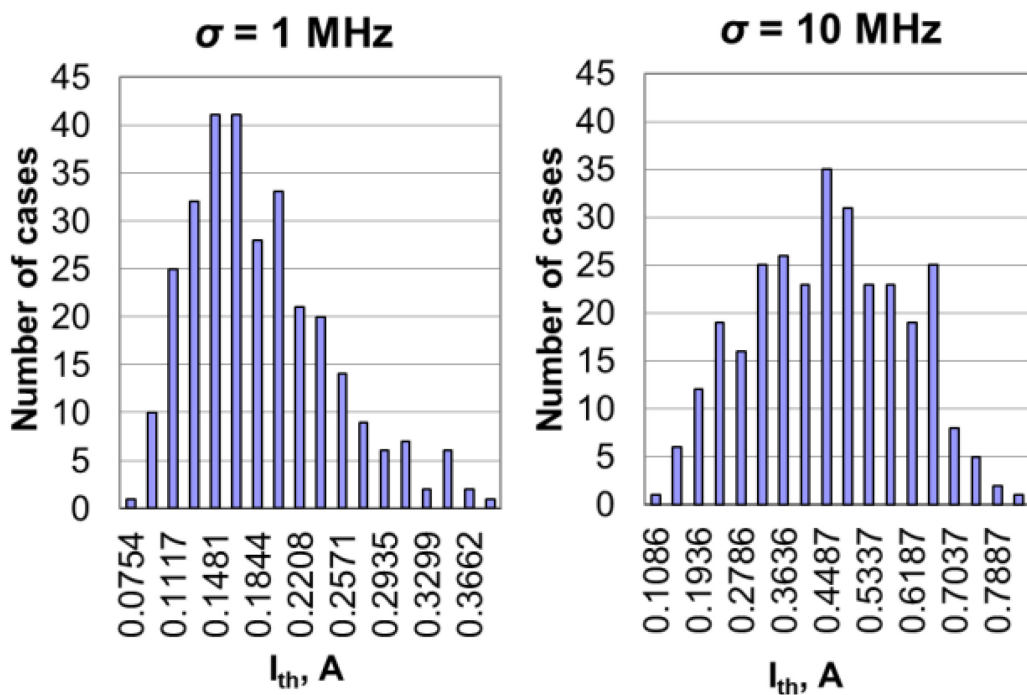Figure 2.10: Results of BBU modeling for TESLA type linac with a frequency spread of the modes between different cavities of $\sigma = 1$ and 10 MHz.

As you can see, for $\sigma = 1$ MHz all values of the threshold currents are below the initial value of 0.566 A (when the frequencies were ordered with a step of 1 MHz). The average value is about 0.18 A that is higher than 0.1 A required for BERLinPro. For $\sigma = 10$ MHz the

average threshold current is about 0.42 A and there are exist values higher than 0.566 A. This means that overlapping of the frequencies of the modes is important for BBU.

Let analyse the worst case from the Fig. 2.10 for $\sigma = 1$ MHz. In this case the threshold current is 0.075 A. It should be noted, that only one or a small number of strongest modes defines the threshold current. By deleting the modes from the cavity parameters in the modelling it was found that in our case it is the only one defining mode. This is the mode with $f_0 = 1.739$ GHz and $Q = 32000$ (see Table 2.2). Deviations of the frequencies of this mode for different cavities are presented in Table 2.3.

Table 2.3: The strongest modes in TESLA - type cavities

Cavity	1	2	3	4	5	6
df, kHz	-815	-475	-649	472	-577	-827

The width of the mode f_0/Q is about 54 kHz. For the first and sixth cavities frequency difference is 12 kHz that is below the width of the mode.

First of all to see if the problem is there, let's change this difference to be more than f_0/Q, for example exchange only df_6 to -900 kHz. After this exchange, the modelling shows the threshold current of 0.135 that is almost double of the value which was before. So we can conclude now that the problem was in the 1st and 6th cavities.

On the other hand, let's assume that it is possible somehow to recombine the cavities inside the linac. The idea is that the most problematic for BBU stability are the cavities where a beam has the lowest energies (first and last) and less problematic are the cavities in the middle. In our case, there is a problem in the 1st and 6th cavities. Let's put them into the middle of the linac in the way (2-3-1-6-4-5). The modelling gives a new threshold current of 0.14 A. That is a double value from the original.

In reality it seems to be impossible to change the order of the cavities in the linac without changing the parameters of the cavities. Therefore, one has to think about the problem of overlapping in advance. It can be good to know the exact parameters of the HOMs in the cavities before building the facility. But it seems to be impossible because they can be changed during the process of assembling the cryomodule.

2.5.5. Initial Twiss parameters for a linac with external focusing

In this paragraph the way how to find the best initial Twiss parameters of a beam for a facility which consist of two parts with a focusing in between of them is under discussion. A good example of such facility is 100 MeV B*ERL*inPro (or preinjection linac for a high scale facility). In our case, for the focusing in between of the cryomodules, a triplet of quadrupoles is assumed. The role of this triplet is to change the sign of the Twiss parameter α of the beam. Let us find the initial injection Twiss parameters which will give the same threshold currents defined by Eq. 2.53 for the entrance and for the middle of the linac. A model of a linac with one dipole HOM is assumed. This one mode was located at different positions in the linac. Matrix $M = m_{ij}$ is the transfer matrix of the 1st cryomodule and can be found using the model of the cavity described in §2.5.1, Eq. 2.74 or the matrix elements can be taken directly from Elegant. Also it is assumed that there are symmetrical β-functions on acceleration and deceleration in the linac.

Therefore the beta function can be transferred through the 1st cryomodule as (see e.g. [65]):

$$\beta_1 = \frac{\gamma_1}{\gamma_0}(\beta_0 m_{11}^2 - 2\alpha_0 m_{11} m_{12} + \frac{1+\alpha_0^2}{\beta_0} m_{12}^2). \qquad (2.87)$$

As it was already said the role of the triplet is to change the sign of alpha, therefore it can be assumed that at the entrance to the second cryomodule the beam will have β_1 and $-\alpha_1$. The triplet should be calculated to achieve it. So the beta function at the end of the linac can be found as:

$$\beta_2 = \frac{\gamma_2}{\gamma_1}(\beta_1 t_{11}^2 + 2\alpha_1 t_{11} t_{12} + \frac{1+\alpha_1^2}{\beta_1} t_{12}^2). \qquad (2.88)$$

where t_{11} and t_{12} are the transport elements of the second cryomodule.
The minimum of the β_2 is reached, when

$$\alpha_1 = -\frac{\beta_1}{L} t_{11}, \qquad (2.89)$$

that gives

$$\beta_2 = \frac{\gamma_2}{\gamma_1} \frac{t_{12}^2}{\beta_1}. \qquad (2.90)$$

Now let's proceed (using Eq. 2.53) with an equation which gives the same threshold currents for the middle and the beginning (end) of the linac:

$$\sqrt{\frac{\beta_0 \beta_2}{\gamma_0 \gamma_2}} = \frac{\beta_1}{\gamma_1} . \tag{2.91}$$

Using Eqs. 2.90 and 2.91 the initial beta-function can be found as:

$$\beta_0 = \frac{\gamma_0}{\gamma_1} \frac{\beta_1^3}{t_{12}^2} . \tag{2.92}$$

And now from Eq. 2.87 one can get:

$$\beta_1 = \frac{\gamma_1}{\gamma_0} \left(\frac{\gamma_0}{\gamma_1} \frac{\beta_1^3}{t_{12}^2} m_{11}^2 - 2\alpha_0 m_{11} m_{12} + \frac{1+\alpha_0^2}{\beta_1^3} \frac{\gamma_1}{\gamma_0} t_{12}^2 m_{12}^2 \right) . \tag{2.93}$$

The minimization over α_0 gives:

$$\alpha_0 = \frac{m_{11}}{m_{12}} \frac{\gamma_0}{\gamma_1} \frac{\beta_1^3}{t_{11}^2} . \tag{2.94}$$

The corresponding beta-functions at the entrance, in the middle and at the end of the linac are therefore:

$$\beta_0 = \sqrt{\frac{\gamma_1}{\gamma_0} \frac{m_{12}^3}{t_{12}}} , \tag{2.95}$$

$$\beta_1 = \sqrt{\frac{\gamma_1}{\gamma_0} t_{12} m_{12}} , \tag{2.96}$$

$$\beta_2 = \sqrt{\frac{\gamma_0 \gamma_2^2}{\gamma_1^3} \frac{t_{12}^3}{m_{12}}} . \tag{2.97}$$

And, using (2.92) in (2.90) the required initial parameter alpha can be found as:

$$\alpha_0 = m_{11} \sqrt{\frac{\gamma_1}{\gamma_0} \frac{m_{12}}{t_{12}}} . \tag{2.98}$$

Using Elegant program one can calculate the matrix elements of the cryomodules: $m_{11}= -0.259$, $m_{12}= 1.082$ m. and $t_{12}= 2.712$ m. And finally the initial parameters are: $\alpha_0 = -0.44$ and $\beta_0 = 1.84$ m. It should be noted that the initial parameters we found are at the entrance to the cavity but not to the cryomodule (where it is about 1 m of a free drift for the separation of cold and warm parts (see [15, §2.5.2.3]), therefore it should be transferred back. The final optic is presented in Fig. 2.11.

It should be noted that in GBBU program the HOMs are assumed to be in the middles of the cavities. In the model it was not taken into account. But it will be done in the next chapter for the facilities without additional focusing in the linac.

The value of the threshold current can be estimated combining Eqs. 2.35 and 2.53:

$$I_{th} = \frac{2c}{e\omega\left(\dfrac{R}{Q}\right)_d Q} \frac{1}{\sqrt{\dfrac{\beta_0\beta_1}{E_0 E_1}}} , \qquad (2.99)$$

for the estimations we used the mode with $(R/Q)_d \cdot Q = 6 \cdot 10^5$ Ω, $\omega = 2\pi \cdot 2 \cdot 10^9$ Hz and optic presented in Fig. 2.11. The threshold currents for the middle of the first, second and third cavity, reaches the values of 1.36, 1.74 and 1.18 A correspondingly. As we said before our goal was to have the same values of the threshold currents for all cavities in the linac. But in our model we assumed the same values for the first and the last cavity of the cryomodule in fact we got it comparable but the value in the middle of the cryomodule is higher, one can see this already from Fig. 2.11.
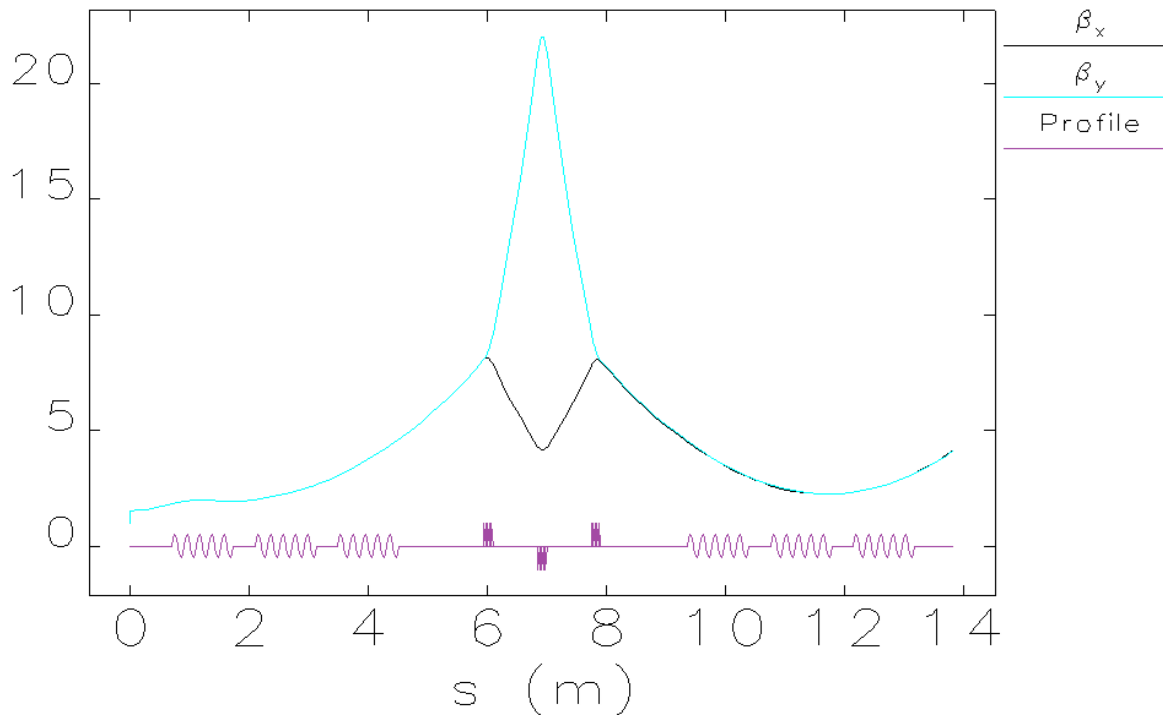
Figure 2.11: Optics of a 100 MeV B*ERL*inPro linac, optimized for BBU.

Now let's proceed with a modeling of the instability. As it was already said the optics for deceleration is given from right to left in Fig. 2.11. So the transfer matrix of the recirculation turn can be written in a common form as (see e.g. [65]):

$$M = \begin{pmatrix} \cos(\mu) + \alpha_2 \sin(\mu) & \beta_2 \sin(\mu) \\ \dfrac{2\alpha_2 \cos(\mu) - (1-\alpha_2^2)\sin(\mu)}{\beta_2} & \cos(\mu) + \alpha_2 \sin(\mu) \end{pmatrix}. \quad (2.100)$$

As one can see from Eq. 2.100 there is still available one more parameter to vary – it is the betatrone phase μ. So, we set the revolution matrix to have a different betatron phase advances in x and y planes and scanned over the phase advances (30x30). The results of this modeling are presented in Fig. 2.12. The maximum threshold value is about 930 mA and the minimum is 170 mA.

Figure 2.12: The results of 2D phase scan.

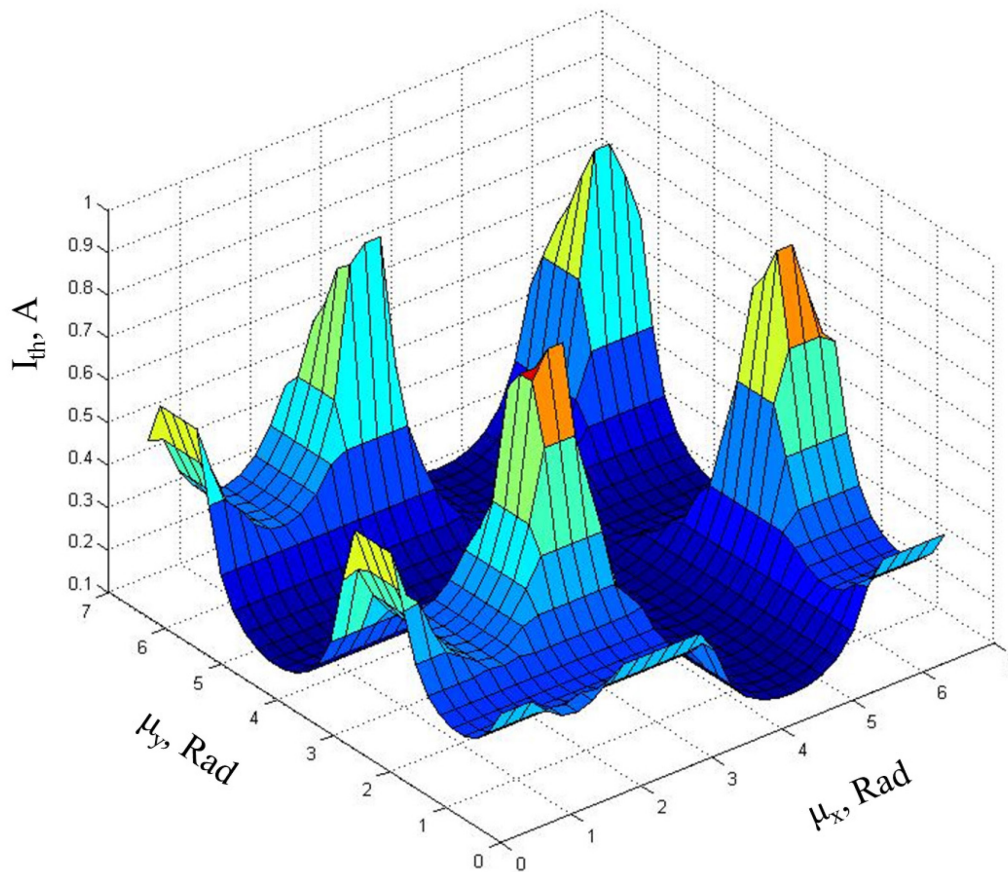One more way to increase the threshold current is to change the length of the recirculation pass. The phases corresponding to the maximum value of the current from Fig. 2.12 were chosen and the length of the recirculation pass was varied. Originally the length of 188.5λ was taken. The results of the modeling are presented in Fig. 2.13. The threshold current varies from 650 to 930 mA. Occasionally, the length, which was taken at the beginning, gives the highest current. Also one can see that the threshold current varies from maximum to minimum when the length changes roughly around ±λ.

So change of the pass length can vary the threshold current for about 300 mA. But unfortunately this method seems impractical, since the mode parameters are not known exactly before the assembling of the linac. And building of a turn with a variable pass length for at least ±20 cm is complicates the facility layout and increases its costs.
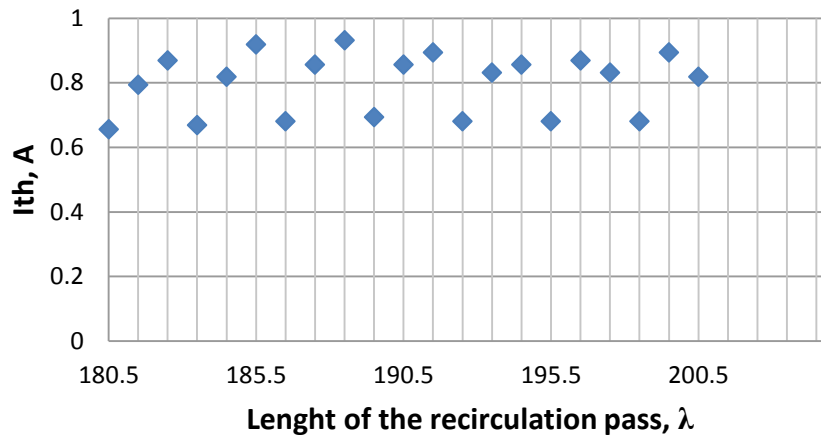
Figure 2.13: Dependence of the threshold current to the length of the recirculation pass.

One of the methods to suppress BBU is to mix the x and y planes of motion. To do this a pseudo-reflector (rotator) or 90^{0}-solenoid can be used in the long drift between two arcs of the main ring [48]. To calculate the influence of these elements on BBU the matrix of the recirculation optics was divided in two parts and put the matrix M_{sol} for solenoid or M_{pr} for pseudo-reflector.

To divide the effects of focusing and rotation of the solenoid let's transform [31, p.59]:

$$M_{sol} = M_f M_{rot} M_f, \qquad (2.101)$$

where M_f contains the focusing of the solenoid and M_{rot} – matrix of 90^{0}- the rotation.

$$M_{rot} = \begin{pmatrix} 0 & 0 & 1 & 0 \\ 0 & 0 & 0 & 1 \\ -1 & 0 & 0 & 0 \\ 0 & -1 & 0 & 0 \end{pmatrix}. \tag{2.102}$$

When the role of pseudo-reflector is to exchange x and y coordinates:

$$M_{PR} = \begin{pmatrix} 0 & 0 & 1 & 0 \\ 0 & 0 & 0 & 1 \\ 1 & 0 & 0 & 0 \\ 0 & 1 & 0 & 0 \end{pmatrix}. \tag{2.103}$$

Figure 2.14 shows the results of BBU modeling for BERLinPro based on TESLA cavities. Pseudo-reflector, solenoid or unity matrix is used. The same betatron phase advances for the x and y coordinates of the beam were used, that is in principle a diagonal scan at the Fig. 2.12 for the unity matrix.
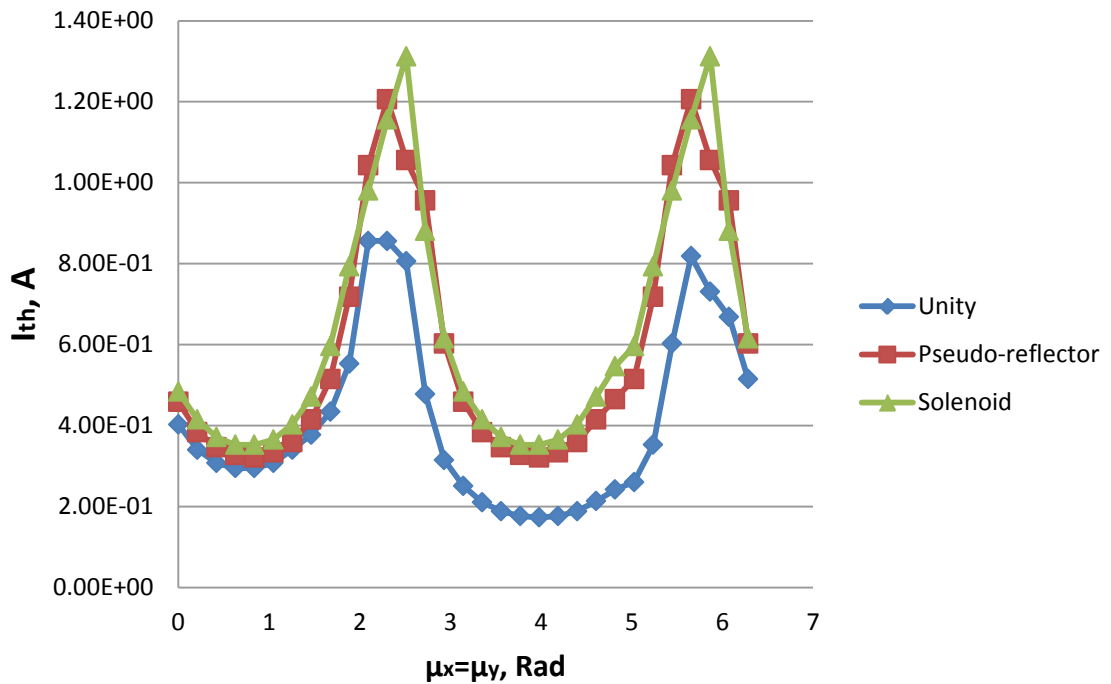

Figure 2.14: The results of BBU modeling for 100 MeV B*ERL*inPro based on TESLA cavities with rotator and solenoid. Unity shows the results when there is no coupling between *x* and *y* motions.

As you can see solenoid is more effective for BBU suppression but to rotate a 100 MeV beam for 90^0 it requires quite strong field:

$$(BL)_{sol} = 2B\rho \frac{\pi}{2} \sim 1\,T \cdot m\,,$$

(2.104)

where $(B\rho)$ is the momentum of central trajectory.

2.5.6. Initial Twiss parameters for a linac without external focusing

In this part the design of optics for machines which have no additional focusing in the linac (or this focusing is known) and have one recirculation turn. An example of such machine is BERLinPro without addition focusing in it (50 or 100 MeV). Here the optic on deceleration pass is assumed to be symmetrical to the optic on acceleration pass, what automatically gives the same threshold currents for cavities located symmetrically to the middle of the linac. So, let us find optic solution which gives the highest threshold current. Since there is no additional focusing in the linac except for RF, the elements m_{ij} of the transfer matrix of the linac are known. Elegant was used to find them. The β-function at the end of the linac is given by (2.87) and can be minimized over α_0:

$$\beta_1 = \frac{\gamma_1}{\gamma_0} \frac{m_{12}^2}{\beta_0}, \alpha_0 = \frac{m_{11}}{m_{12}} \beta_0\,.$$

(2.105)

With this solution one can find that the square root in the denominator of Eq. (2.53) does not depends on the initial Twiss parameters, but only on the m_{12} matrix element and initial energy:

$$\sqrt{\frac{\beta_0 \beta_1}{\gamma_0 \gamma_1}} = \frac{m_{12}}{\gamma_0}\,.$$

(2.106)

Now we still have one free parameter to vary. To achieve the highest threshold in the middle of the linac let us minimize the beta-function there, which can be found by introducing t_{ij} as the matrix elements of the first half of the linac:

$$\beta_{1/2} = \frac{\gamma_{1/2}}{\gamma_0} (\beta_0 (t_{11} - \frac{m_{11}}{m_{12}} t_{12})^2 + \frac{t_{12}^2}{\beta_0})\,.$$

(2.107)

And, after the minimization one can get:

$$\beta_0 = \frac{1}{\left| \dfrac{t_{11}}{t_{12}} - \dfrac{m_{11}}{m_{12}} \right|}.$$

(2.108)

It should be noted that in GBBU program we use for the modeling, HOMs are assumed to be in the middle of the cavities, therefore one should take the elements of the transfer matrix in the following way: m_{12} is the element from the middle of the first to the middle of the third cavity and t_{12} is the matrix element from the middle of the first to the middle of the second cavity.

For 50 MeV BERLinPro based on 7-cell cavities (final design) one can find the matrix elements using Elegant program: t_{11} = 0.578, t_{12} = 0.866, m_{11} = 0.286, m_{12} = 1.315, what gives β_0 = 2.23 m and α_0 = 0.48 for the middle of the 1st cavity. Now one can easily find the Twiss parameters of the beam at the beginning of the cavity: β_0^* = 2.36 m and α_0^* = -0.42. Optic corresponding to this solution is presented in Fig. 2.15:
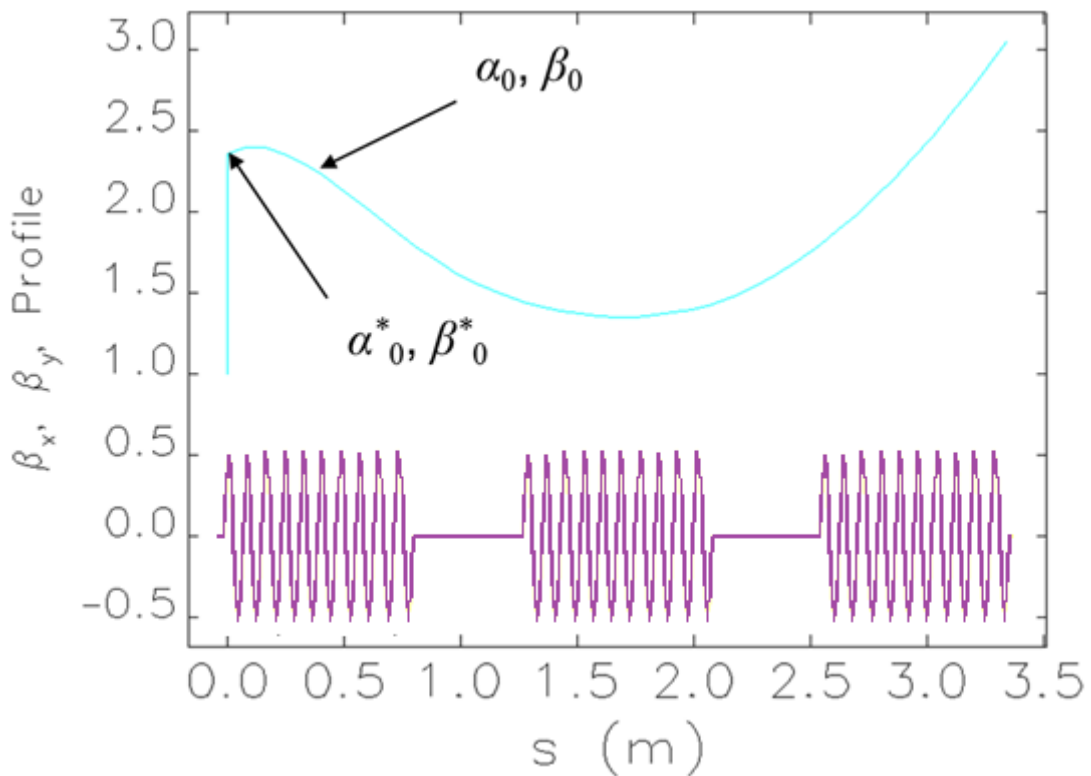

Figure 2.15: Optimum optic solution for 50 MeV BERLinPro.

The threshold current can be found using Eq. 2.99. For a mode with $R_d = 6 \cdot 10^5 \Omega$, $\omega = 2\pi \cdot 2 \cdot 10^9$ Hz one can find that the threshold current is about 0.9 A for the first/third and about 1.8 A for the middle of the linac. The Eq. 2.99 gives the smallest value of the threshold current because in this equation the betatron phase advance was chosen to have the largest elements of the transfer matrix of the recirculation turn $\sin(\mu) = 1$ and $\sin(\omega T) = 1$.

Therefore, to compare this estimation results with simulations one have to find the minimum threshold current by varying the betatron phases and the length of the recirculation pass. First of all one mode (with the same parameters we used for the estimation) was set in the first and in the second cavities independently. Then it was scanned over the phase advances two times and the smallest values of the threshold currents were found for both cavities. After that one can choose the transfer matrices corresponding to these values and vary the length of the recirculation pass. So finally it was found $I_{th1} = 0.806$ A and $I_{th2} = 2.14$ A for the 1st (3rd) and 2nd cavities correspondingly. This is in a good agreement with estimations.

For the standard optic of BERLinPro (Fig. 2.16), the beam has Twiss parameters at the end of the 3rd cavity: $\beta_x = 3.01$ m and $\alpha_x = -2.267$, $\beta_y = 0.689$ m and $\alpha_y = 0.011$.
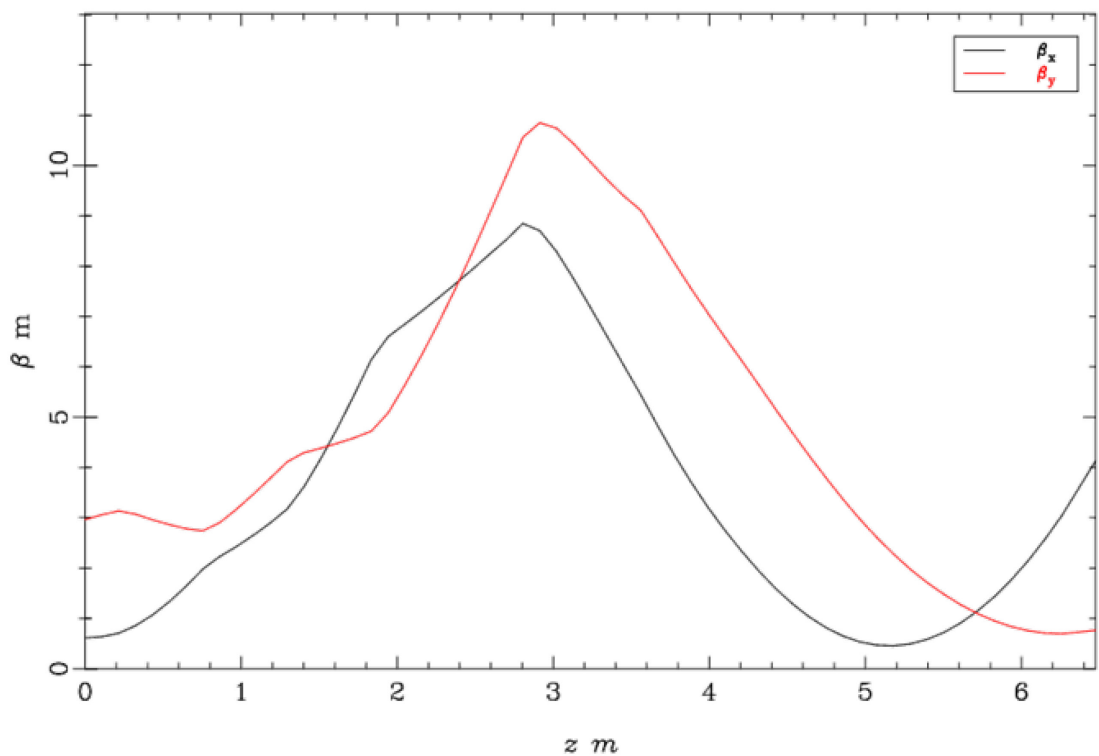
Figure 2.16: Standard optic design of the 50 MeV BERLinPro linac. The middle of the 1st cavity is at 3.15 m.

So after the same procedure which was described above (but now the same mode was used for x and y polarisations simultaneously, because of not symmetric optic), one can find $I_{th1} = 0.559$ A and $I_{th2} = 0.497$ A. What 30% less for the 1st cavity and about 75% less for the middle cavity than in the theoretical case. And in total the threshold current changed for about 40% and instability now develops in the second cavity. So in the theoretical solution one can have the worst cavity in the middle which can have factor 2.5 higher $(R/Q)Q$ of the HOM.

3. Injection schemes

In this chapter different acceleration schemes for an Energy Recovery Linac based light source are discussed. It is assumed that all schemes have the same injector and dump as B*ERL*inPro. The first scheme (direct injection scheme) consists of one main linac with direct injection at 7 MeV. The second scheme differs from the first one that it has a preinjection linac. This makes lower the high-to-low energy ratio in the main linac. This improves transverse optic in the linac and therefore, the BBU instability. Another advantage of having a preinjection linac is that the preinjection arcs can be used for longitudinal bunch compression [66] (additional compression stage) on acceleration, to reduce the energy spread during deceleration by decompression, and to compensate for the average energy loss of the beam due to radiation. The third scheme which is proposed for the FSF has the same preinjector but it is a multi-turn scheme with 6 passes on acceleration/deceleration and with a split main linac. The split main linac allows having different arcs for each beam energy on acceleration and deceleration.

3.1. Direct injection scheme

In this part the simplest layout of an ERL based LS is under discussion. In this scheme the beam after an injector section goes directly to the main linac (see Fig. 3.1), where it is accelerated up to 6 GeV of energy and then it is used for the experiments. After the recirculation turn the beam is decelerated back in the main linac and dumped.
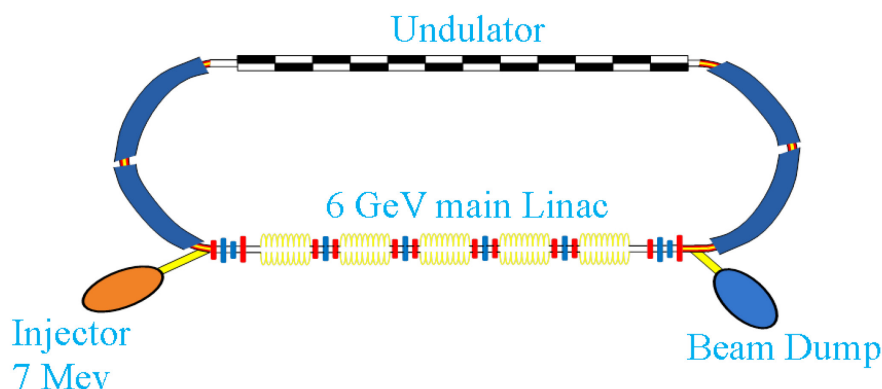

Figure 3.1: Layout of direct injection scheme.

The linac is planned to be based on the B*ERL*inPro 7-cell cavities. To reach 6 GeV in the linac 464 cavities were taken with an accelerating gradient *G* about 16.02 MeV/m and distributed over 58 cryomodules. The cryomodule is schematically presented in Fig. 3.2, where λ=0.2306 m is the wavelength of the accelerating mode.
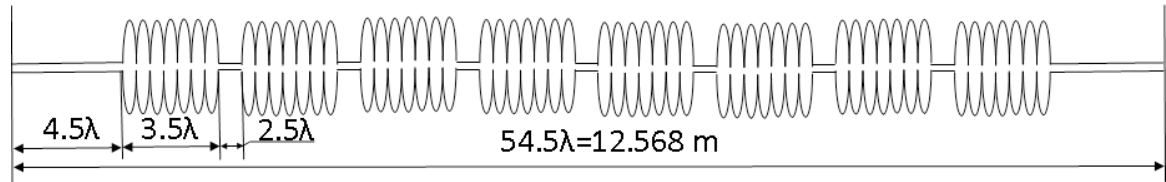

Figure 3.2: The scheme of FSF cryomodule.

Triplets of quadrupoles are planned to be in between the cryomodules in the linac. The full length of the linac is then about 800 m. The strengths of the quadrupoles were optimized in such a way that the BBU instability will develop similarly (with the same threshold current) for all the cavities in the linac. In this case the highest threshold current can be achieved. As one can see from Eq. 2.53 the threshold current is higher when the coefficient $\beta_1\beta_2/\gamma_1\gamma_2$ is minimized. Here $\beta_{1,2}$ – the beta function, $\gamma_{1,2}$ – the Lorentz factor on the acceleration and deceleration passes correspondingly. It should be noted, that as in §2.5.5 this equation will be used to find the best optic solution. It is assumed that optimization procedure described below gives the best results for the most sets of the cavities. However, there could be some unique set of the HOMs parameters when there will exist a better optic solution. The effect of frequencies overlapping, which was discussed in §2.5.4, is not taken into account. The most dangerous for the BBU stability are the cavities where the beam has the lowest energies. These cavities are located at the beginning when a beam passes them on acceleration and at the end of the linac on deceleration stage. Therefore, the initial Twiss parameters before the linac were optimized to minimize the beta functions in the first cryomodule. In this cryomodule the energy is changed from 7 to 110 MeV. And an RF focusing still affects the beam in the first cavities.

To estimate the optimum values of the initial Twiss parameters Serafini-Rosenzweig model of the cavity (Eq. 2.74) was used. It was assumed that the cryomodule is one long cavity with an effective gradient given by:

$$G_{eff} = G\frac{8L_{cav}}{L_{cryo}},$$ (3.1)

where L_{cav} is the length of the cavity and L_{cryo} the length of the crymodule.

The beta function can be transferred through the 1st cryomodule as:

$$\beta_1 = \frac{\gamma_1}{\gamma_0}(\beta_0 m_{11}^2 - 2\alpha_0 m_{11}m_{12} + \frac{1+\alpha_0^2}{\beta_0}m_{12}^2),$$ (3.2)

where $m_{11} = \cos(\alpha) - \sqrt{2}\sin(\alpha)$, $m_{12} = \frac{\sqrt{8}E_0\sin(\alpha)}{G_{eff}}$ – the coefficients of the transfer matrix

of the cryomodule and $\alpha = \frac{1}{\sqrt{8}}\ln\left(E_1 \middle/ E_0\right)$, $E_{1(0)}$ is the final(initial) normalized energy of the

particle. Now we just have to minimize β_1 in Eq. 3.2 over initial α_0:

$$\frac{\partial \beta_1}{\partial \alpha_0} = \frac{\gamma_1}{\gamma_0}(-2m_{11}m_{12} + \frac{2\alpha_0}{\beta_0}m_{12}^2) = 0.$$ (3.3)

And finally one can find that:

$$\alpha_0 = \frac{m_{11}}{m_{12}}\beta_0.$$ (3.4)

We also want to keep constant the value of β/γ:

$$\frac{\beta_0}{\gamma_0} = \frac{\beta_1}{\gamma_1}.$$ (3.5)

The solution is given by:

$$\begin{cases} \beta_0 = m_{12} \sim 2m \\ \alpha_0 = m_{11} \sim -0.61 \\ \beta_1 = \frac{\gamma_1}{\gamma_0}m_{12} \sim 31m \end{cases}.$$ (3.6)

Modelling in Elegant program shows similar results but our model is not ideal, because it was assumed one long cavity instead of 8 short with drifts in between. Therefore, the initial Twiss parameters of the beam were adjusted to get the smaller value of the β_1. The difference in optic given by the theoretic results from (3.6) and after an optimization with Elegant is presented in Fig. 3.3. The black curve (β_x) shows dependence of the beta-function for the theoretical and the blue one (β_y) for the initial parameters optimized by elegant.
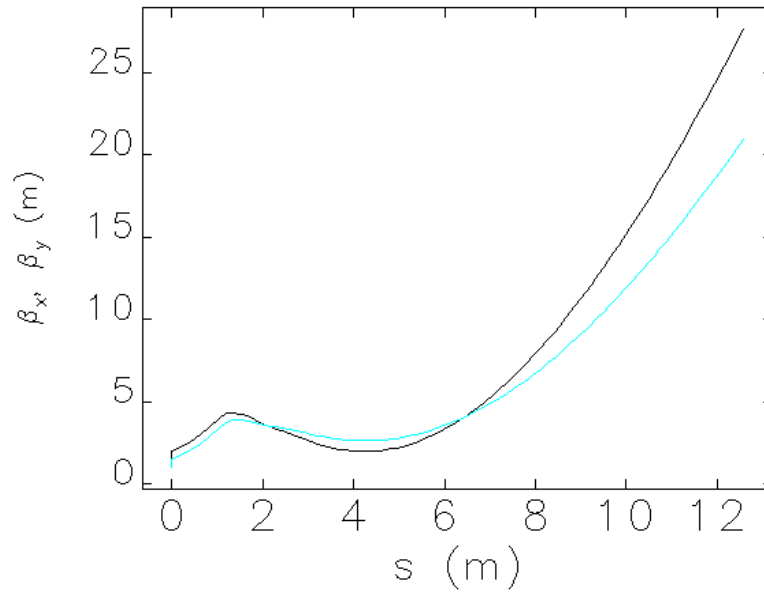
Figure 3.3: Beta-functions in the first cryomodule.

Later on the higher energies the RF focusing can be neglected. Therefore, one can use the model of cavity as a free drift but with acceleration. In Fig. 3.4 the dependence of (m_{12}/L) is shown for different cavities. On the x axis the number of the cavity is shown and on the y axis one can see how the matrix element, which is responsible for RF focusing, differs from the length of the cavity L. The results show that they quite fast reach each other and for the last cavity of the first cryomodule this coefficient is about 0.95.
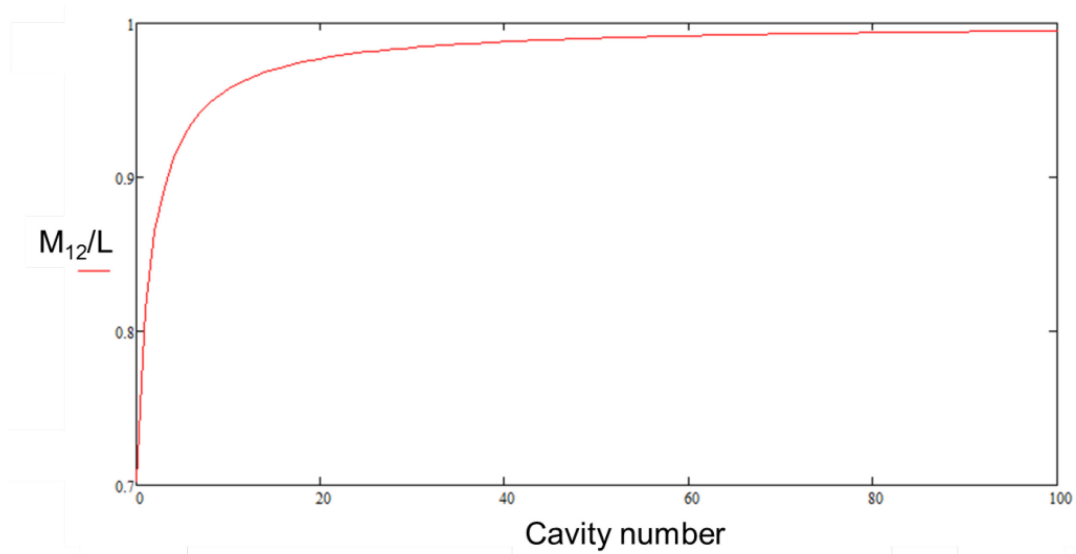
Figure 3.4: Difference of M_{12} matrix element from length of the cavity for different cavities.

So our goal is to keep constant the values of β/γ, the preferable theoretically for the BBU stability optics should look then like it is shown in Fig. 3.5. The red line shows the values with a constant $\beta/\gamma \sim 0.1$ m, and the values below this line will give a higher threshold current. Therefore, the values below this line are acceptable for us and we can use that fact that the beta function changes as a "parabola" in a free drift with acceleration.
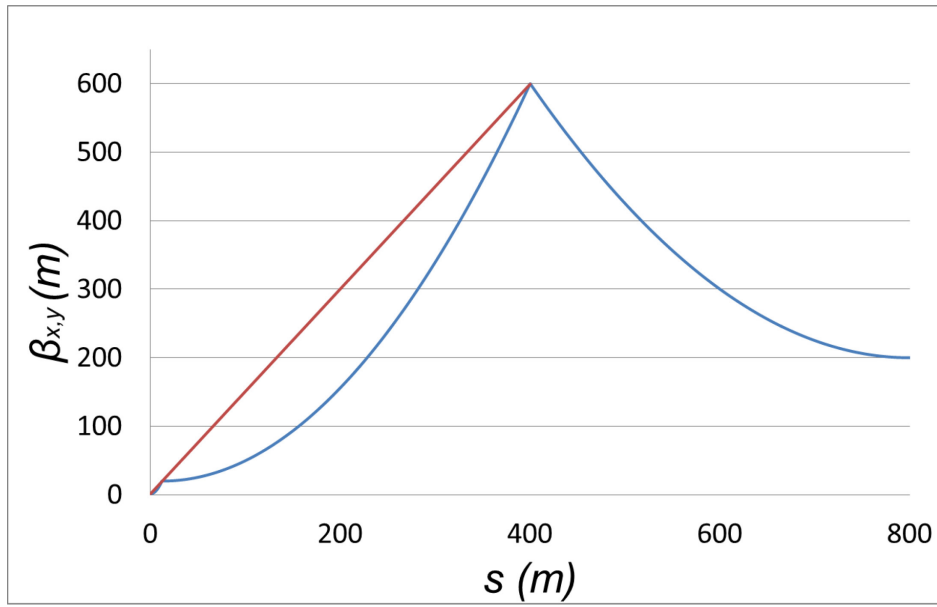
Figure 3.5: Theoretical optics solution for the direct injection scheme

In the linac the optic is assumed to have mirror symmetry at the middle. Optic for deceleration is then shown from right to left in Fig. 3.6.
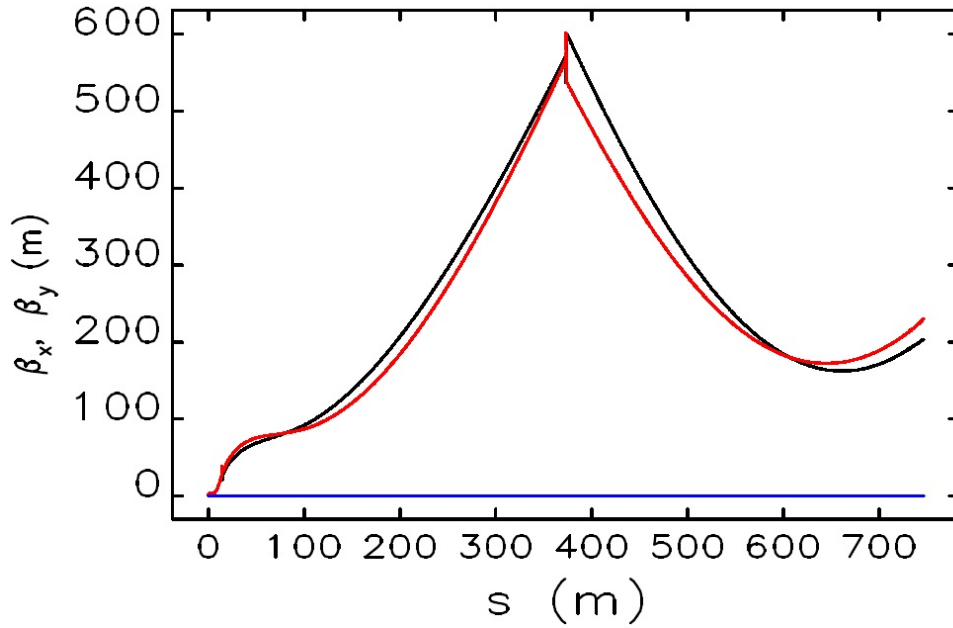
Figure 3.6: Optics design of the main 6 GeV linac for the direct injection scheme.

Optics of the beginning of the linac (zoomed from Fig. 3.6) is presented in Fig. 3.7. From this figure one can see the strong focusing in the first cryomodule.
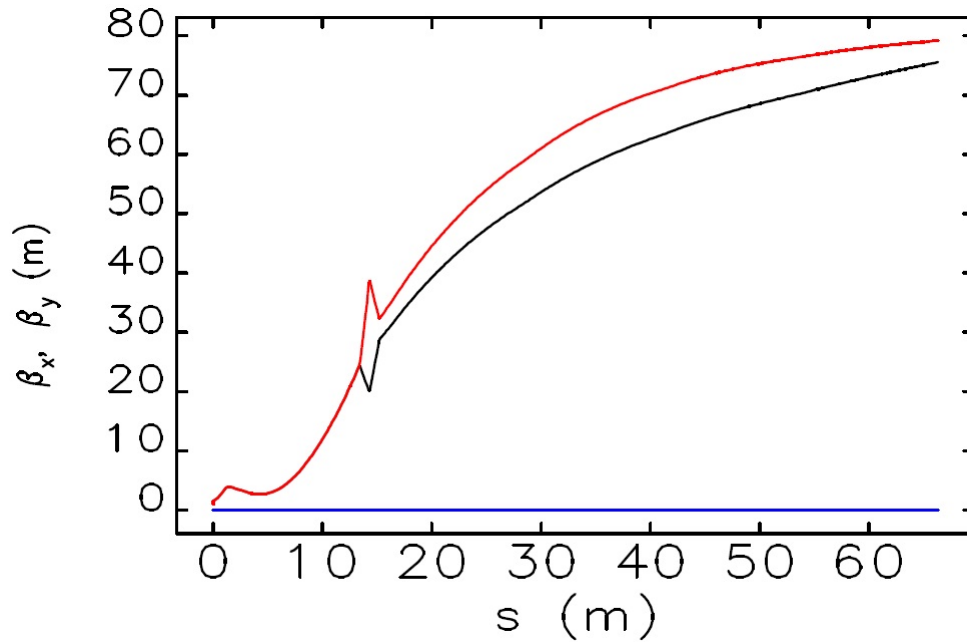
Figure 3.7: Beginning of the main 6 GeV linac for the direct injection scheme.

It should be noted that only 5 triplets were used. These triplets are located between first and second, between 8th and 9th cryomodules and in the middle of the linac. As it was said above, optics has mirror symmetry, therefore, there are two more triplets at the second half of the linac. The length of the linac is then about 750 m.

The main disadvantage of this scheme is the high ratio between the injection energy E_{in}=7 MeV and the final energy E_{fin}=6 GeV:

$$\frac{E_{in}}{E_{fin}} \sim 850 . \tag{3.7}$$

This complicates the transverse focusing in the main linac, because the triplets which focus a beam at the beginning of the linac will not affect the beam at the same position on the deceleration stage. For a given optics in Fig. 3.6 one can estimate the value of the threshold current using (2.35): $I_{th} = \frac{10^{-6}}{4\pi} \frac{E}{\beta} \sim 400 \, mA$ for the middle point of the linac. For the estimations we took a mode with $(R/Q)_d \cdot Q$=6·10^5 Ω, ω=2π·2·10^9 Hz.

3.2. Two stage injection scheme

In this part an improved scheme of the ERL based light source is discussed. The layout of this scheme is presented in Fig. 3.8.
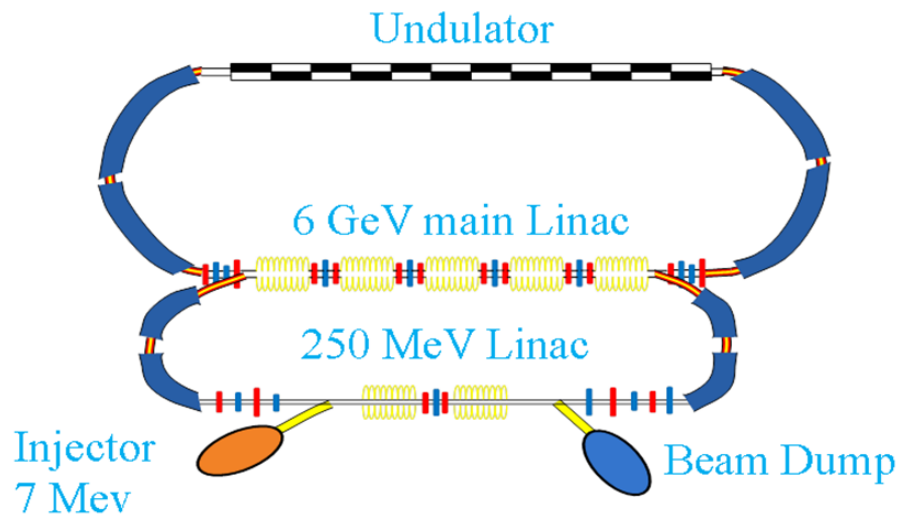
Figure 3.8: Two stage injection scheme.

The main improvement is that now a beam after an injector goes to a short linac (preinjector), where it is accelerated up to 250 MeV, then it passes the first arc and comes to

the main linac where it is accelerated up to 6 GeV. After that it might be used as a light source. After the beam was used it goes back on the deceleration phase. Our goal again will be to find the optimum optic solution for the beam break up stability in the both linacs. But first let us discuss the instability in the preinjection linac.

3.2.1. Preinjector

For the preinjection linac it is suggested to use two cryomodules with a triplet of quadrupole magnets in between, like it was discussed in §2.5.5. To find the optimum initial Twiss conditions one can use the solution given by Eqs. (2.95) and (2.98). The role of the triplet is to change the sign of the Twiss parameter α of the beam. So it has to be optimized in a proper way. Using Elegant program one can find the matrix elements of the cryomodules: m_{11} = -0.835, m_{12} = 1.62 m. and t_{12} = 7.261 m. And finally the initial Twiss parameters are: α_0 = -1.421 and β_0 = 2.757 m. As it was mentioned above, the role of the triplet of quadrupole magnets is to change the sign of the alpha-function. It should be noted, that the initial parameters we found are at the entrance to the cavity but not to the cryomodule (where it is about 1 m of a free drift Fig. 3.2), therefore they should be transformed back for this distance. The final optic is presented in Fig. 3.9.
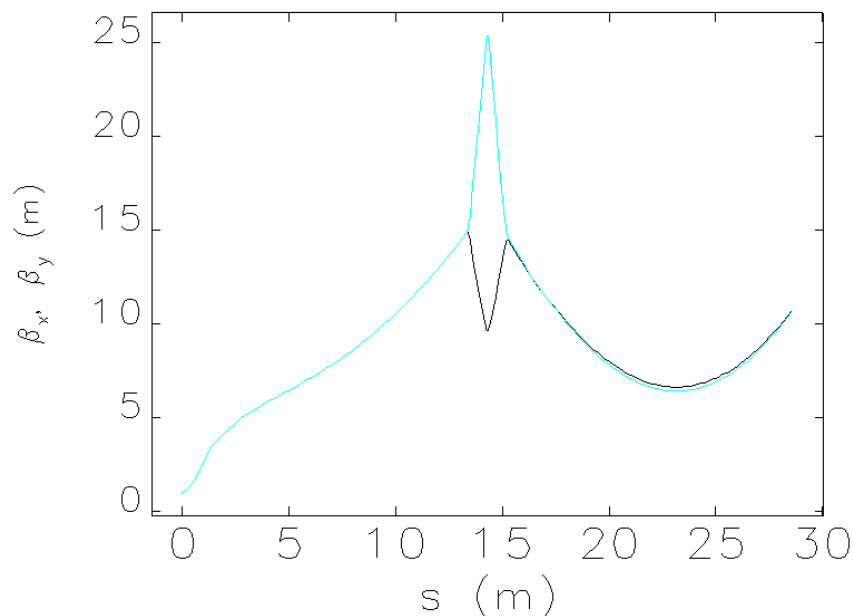
Figure 3.9: Optics design of the preinjection linac.

The estimated value of the threshold current for a mode with $(R/Q)_d \cdot Q = 6 \cdot 10^5$ Ω, $\omega = 2\pi \cdot 2 \cdot 10^9$ Hz located in the first and the last cavities is 1.64 A, when the value in the middle of cryomodule is higher – about 2.5 A. In the next part we discuss the optics in the main linac.

3.2.2. Main linac

The main difference for the optic design between layouts with direct injection and with a preinjector is that in the scheme with two stage injection the initial energy in the main linac is 250 MeV instead of 7 in the scheme with a direct injection. Therefore, it strongly improves the optics. The quadrupole magnets which focus the beam on the low energies (>250 MeV) will also focus the beam on the high energies (<6 GeV). And on such high energies as we already discussed the cavity is like a free drift with acceleration, so RF focusing can be neglected. Therefore, the optic was calculated in the following way: for the first half of the linac the triplets between the cryomodules were adjusted in such a way that the beam will go like in a free drift with initial/final beta-functions about the length of the cryomodule (Fig. 3.10). The role of the triplets is to change the sign of the alpha-function, so it should be calculated for this purpose. The second part assumed to be symmetrical to have the same optics on the deceleration, which is given from right to left in Fig. 3.10. In this optics design there are different thresholds for different cavities in the linac. For the first and last cavity estimations give the threshold current about 4 A and 35 A for the cavity in the middle of the linac for the mode with $(R/Q)_d \cdot Q = 6 \cdot 10^5$ Ω, $\omega = 2\pi \cdot 2 \cdot 10^9$ Hz.
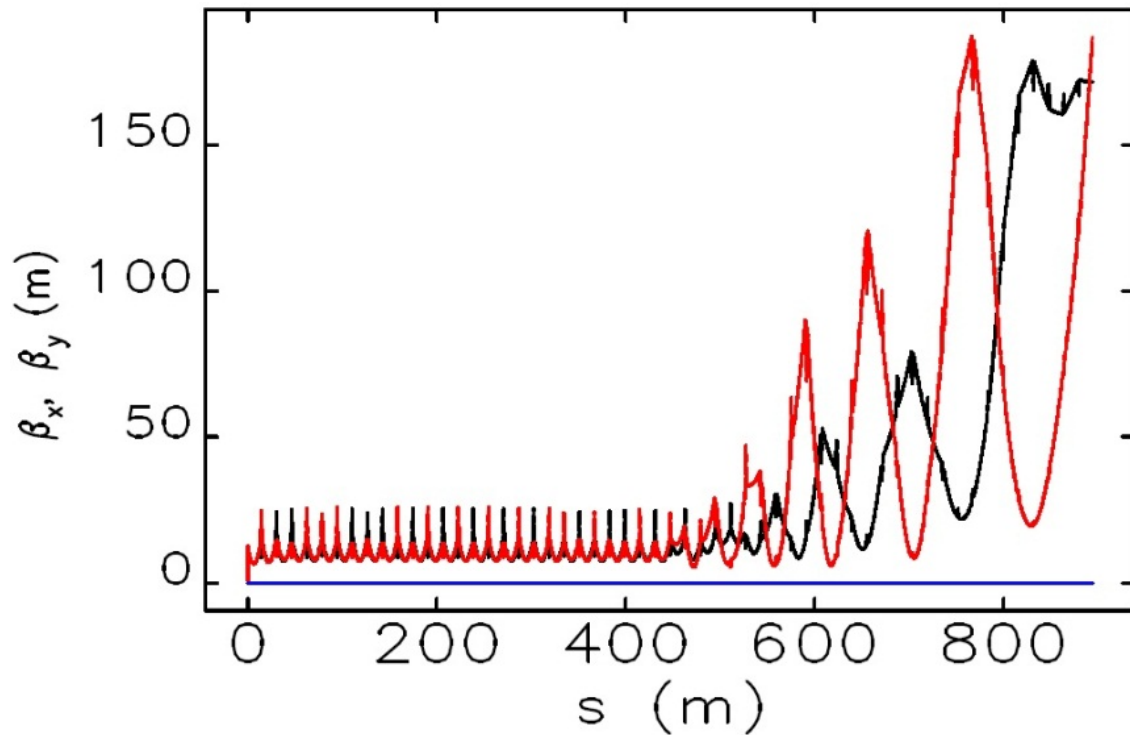
Figure 3.10: Optics design of the main 6 GeV linac for two stage injection scheme.

3.3. FSF

In this part different acceleration patterns for FSF and linac optic designs for them are discussed. The main questions discussed here is: "which energy gains should be the in the linacs and what is the best optic solution for them for better BBU stability?"

3.3.1. The 1st proposed scheme

The very first proposed scheme of FSF is presented in Fig. 1.6. In this scheme a beam accelerated in the preinjection linac up to 100 MeV and there are 1 GeV energy gains in both main linacs on the each pass.

The linac is planned to be based on the B*ERL*inPro 7-cell cavities. To reach 1 GeV in the linac we took 72 cavities and distributed them over 9 cryomodules. The cryomodule is schematically presented in Fig. 3.2.

Triplets of quadrupoles are planned to be in between the cryomodules in the linac. The full length of the linac is then about 140 m. Optics for all three passes through the first 1 GeV linac is presented in Fig. 3.11. It will be discussed below that BBU instability will develop in

the 1st linac. Therefore, the strengths of the quadrupoles were optimized to have the minimum of the beta functions on the 1st pass through the 1st linac.
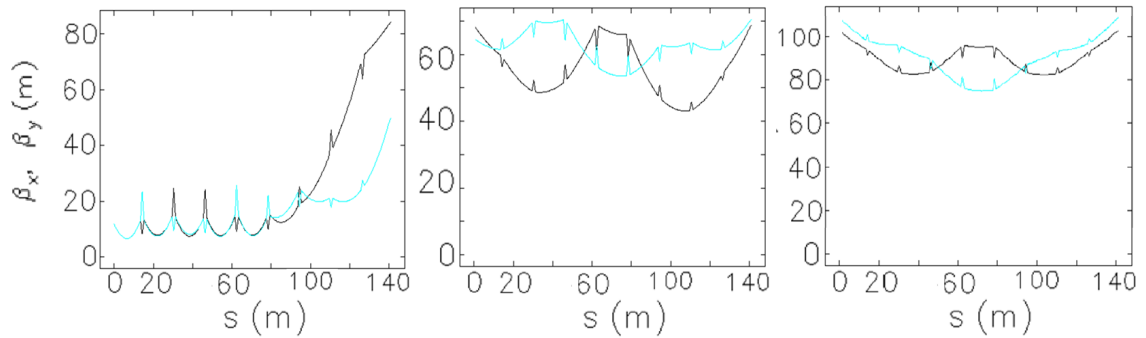
Figure 3.11: Optics design of the first 1 GeV linac. 3 passes with 1, 3 and 5 GeV beam energy after the pass from left to right correspondingly.

Also the optics was designed for the second 1 GeV Linac and it is presented in Fig. 3.12.
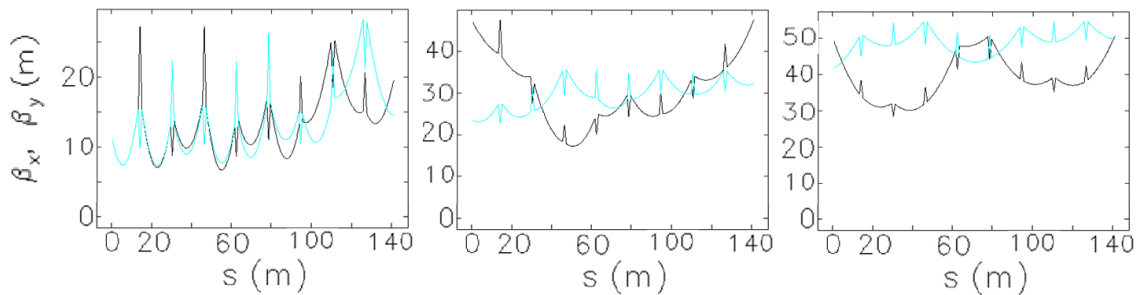
Figure 3.12: Optics design of the second 1 GeV linac. 3 passes with 2, 4 and 6 GeV beam energy after the pass from left to right correspondingly.

In both linacs the optic is assumed to have mirror symmetry at the middle of the 5-th cryomodule. Optic for deceleration is shown from right to left in Figs. 3.11-12.

Optics in the preinjector is the same as for 100 MeV BERLinPro (Fig. 2.11).

For optic, presented in Figs. 3.11-12, the threshold current can be estimated using Eq. 2.97 and the typical parameters of the mode we used before: $(R/Q)_d \cdot Q = 6 \cdot 10^5$ Ω, $\omega = 2\pi \cdot 2 \cdot 10^9$ Hz. The instability will develop in the first/last cavities in the first linac 1 GeV linac with a threshold current of about 0.88 A. The estimated value of the threshold current for the second linac is higher – about 3.73 A. And in the preinjector this value is about 1.26 A. As you can see, the value of the threshold current in the second 1 GeV linac is about 4

times higher. Let's change the energy gains in the main linacs to decrease this difference. This should increase the threshold current of the facility.

3.3.2. Different acceleration pattern

In this paragraph an improvement of the first proposed scheme of FSF is under discussion. The first scheme had 100 MeV preinjection and then two 1 GeV linacs (Fig. 1.6). The new improved scheme is presented in Fig. 3.13.
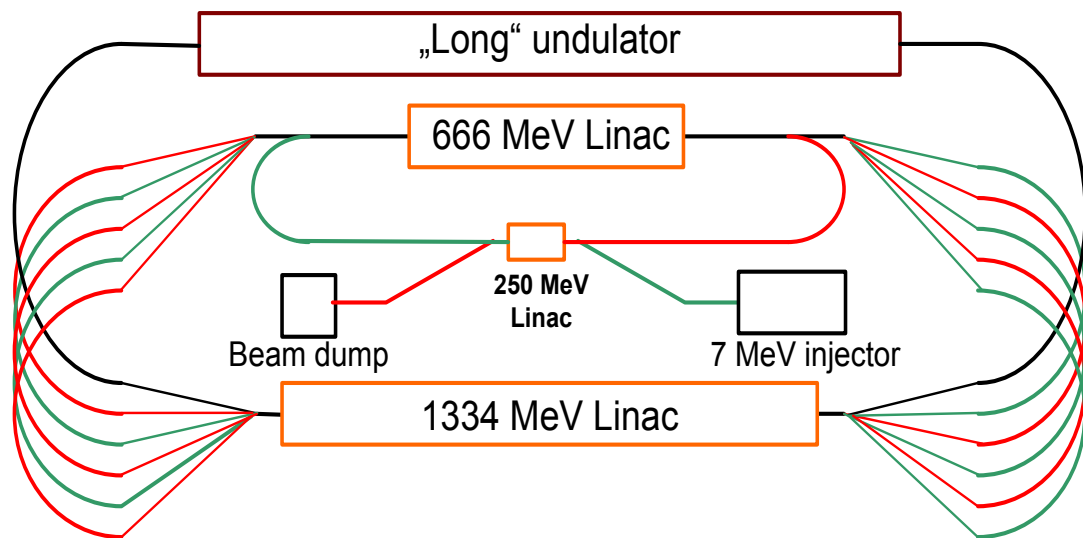
Figure 3.13: The improved acceleration scheme of FSF.

The main motivation of this improvement is BBU instability. The new scheme gives roughly 1.7 times better threshold current for the 1st cavity in the 1st linac, where the instability develops in the first scheme. The energy gain in the preinjector was also increased up to 250 MeV, so now it is like described in §3.2.1.

The easiest way to see the reason of rebalancing of the energies in the two main linacs is to analyse Eq. 2.53, especially the square root in the denominator. Let's find a balance between the energy gains in two main linacs to have equal threshold currents for them. To do that, a model with linacs, when a focusing from a triplets is neglected for the second and the third passes, will be analysed. In this model with the injection energy of about 250 MeV the transverse focusing inside the cavities can be neglected. So, it is assumed that the beta functions of a beam at the exit and at the entrance to the linac are about the length of the linac for the second and the third passes and for the end of the linacs at the first pass. But it is about the length of the one cryomodule at the entrance to the 1st linac at the first pass.

Let's introduce G as a gradient of the cavities in MeV/m, $L= 2000$ [MeV] $/G$ is a length of the cavity structure, required to accelerate to the final energy of 2 GeV, x is the length of the first linac and, therefore, $L-x$ is the length of the 2-nd. Now one can find energies $\gamma_{1(2),n}$ for each pass and as we assumed before $\beta_{1,1(6)} = \beta_{2,1(6)} \sim 12.57$ m and $\beta_{1,n} = x$ or $\beta_{2,n} = L-x$ for the first and the second linac respectively and for n=2..5.

Let's proceed with the following equation:

$$\sqrt{\sum_{m=1}^{2N-1}\sum_{n=m+1}^{2N}\frac{\beta_{1,n}\beta_{1,m}}{\gamma_{1m}(x)\gamma_{1n}(x)}} = \sqrt{\sum_{m=1}^{2N-1}\sum_{n=m+1}^{2N}\frac{\beta_{2,n}\beta_{2,m}}{\gamma_{2m}(x)\gamma_{2n}(x)}} \, , \qquad (3.8)$$

when the threshold currents have the same values for the 1st and last cavities in both linacs. This equation can be solved numerically and gives the result that $x \sim L/3$ with injection energy – $\gamma_{1,1} = 480$. With this result one can get the energy gains in the first and second main linacs to be 666 and 1334 MeV correspondingly.

Let's continue with a modeling of the linac optics in Elegant program. Optics for all three passes through the first 666 MeV linac is presented in Fig. 3.14.
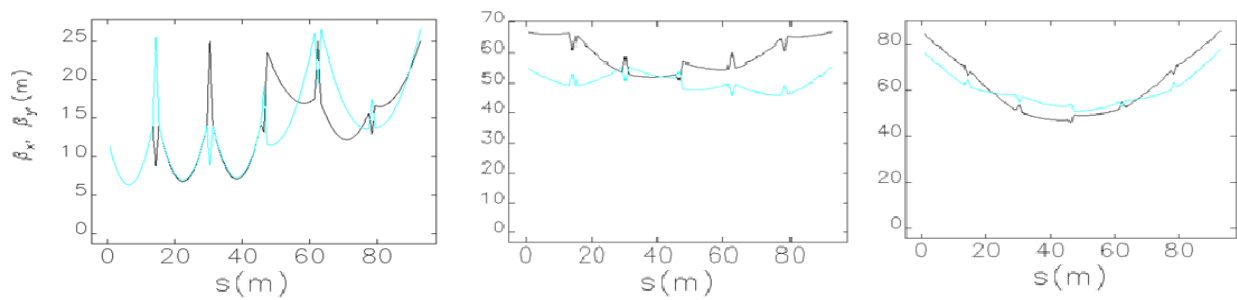
Figure 3.14: Optics design of the first 666 MeV linac. 3 passes with 250, 2250 and 4250 MeV beam injection energy from left to right correspondingly.

Also the optics was calculated for the second 1334 MeV linac and it is presented in Fig. 3.15.
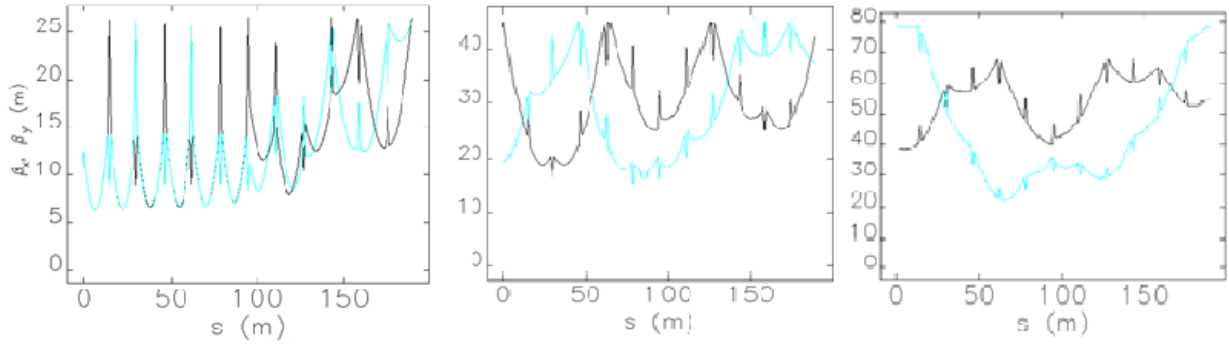
Figure 3.15: Optics design of the second 1334 MeV linac. 3 passes with 916, 2916 and 4916 MeV beam injection energy from left to right correspondingly.

To estimate the values of the threshold currents the same approach as usual can be used (Eq. 2.99 and a mode with $(R/Q)_d \cdot Q = 6 \cdot 10^5$ Ω, $\omega = 2\pi \cdot 2 \cdot 10^9$ Hz). And for the first linac the threshold current is improved and it is about 1.46 A, when for the second it is 3.58 A and slightly decreased. So, the value of threshold current for the 1st main linac was improved. It was also slightly decreased for the 2nd linac and for the preinjection linac its value about 1.64 A. But this scheme has a more complicated spreader, because the energies of the beam in the spreader are: …4250, 4916, 6250, which closer than in the first scheme: 4250 and 5250… Therefore, this scheme seems impractical for us. In the next paragraph let's go back for the scheme with the same energy gains in the main linacs, but with thoughts to connect energies of a beam on different passes to fix the spreader design.

3.3.3. Scalable scheme with preinjector and 3 passes

In this part an upgrade of the acceleration scheme of the FSF is presented. In this scheme the acceleration in the preinjector and in two main linacs is assumed to be scalable. The final energy of a beam $E_{fin} = (E_0 + E_{preinj})(1 + 2Nk) = 6$ GeV, where $E_0 = 10$ MeV is the energy after booster, E_{preinj} is the energy gain in the preinjector, N is the number of passes during acceleration and constant $k = 4$. Therefore, one has $E_{preinj} = 230$ MeV and $E_{linac} = 960$ MeV. So the main scheme of FSF is now looks like it is presented in Fig. 3.16.
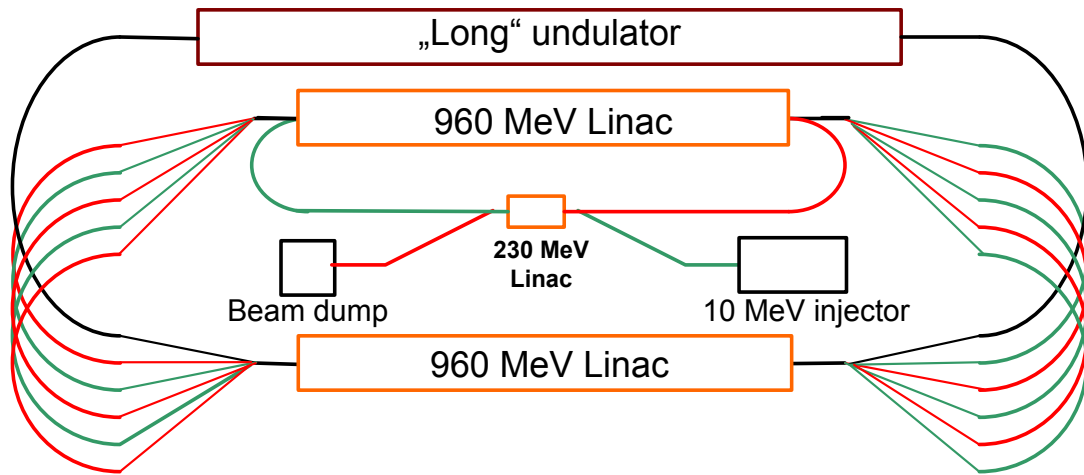
Figure 3.16: Layout of scalable scheme of FSF.

This change for the scalable facility was made because of the spreader design. A design of the spreader for 6 arcs is complicated and if the energy is changed due to unforeseen circumstances (e.g. one of the linacs could not achieve the design energy) we could simultaneously change the field gradients of cavities in a proportional way everywhere to use the same spreader.

Optics in the preinjection linac was optimized to achieve the same threshold currents in all cavities of the linac (Fig. 3.17) as it is described in a part about preinjector for the two stage injection scheme (§3.2.1). Only one difference that now it is a 230 MeV linac.
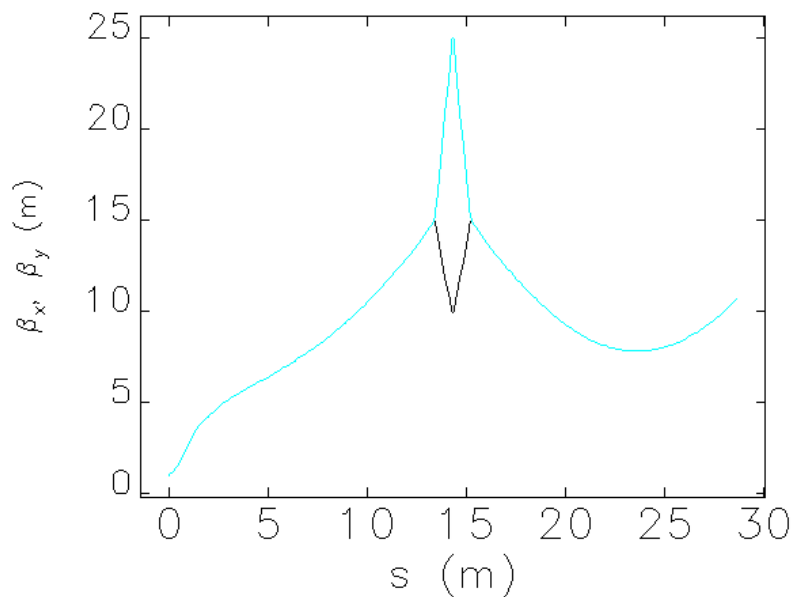
Figure 3.17: Optics in the preinjection linac of scalable FSF.

The strengths of the quadrupoles were optimized to have the minimum of the beta functions on the 1st pass. Optic for the 3 passes through the first and the second main linacs is presented in Figs.3.18-19. In both linacs, the optic is assumed to have mirror symmetry at the middle of the 5-th cryomodule.
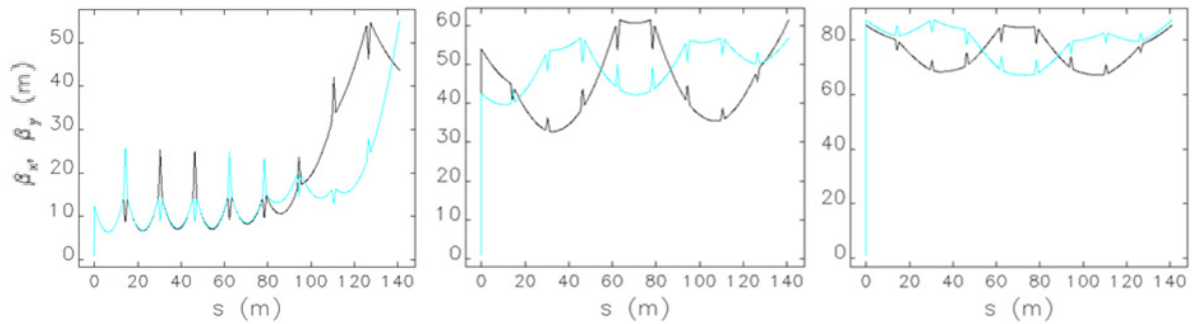
Figure 3.18: Optics design of the first 0.96 GeV linac of scalable scheme of FSF. 3 passes on acceleration are presented from left to right.

The threshold currents for the optics presented in Figs. 8, 9 can be estimated as usual, using Eq. 2.99 and for a mode which we always used ($(R/Q)_d \cdot Q = 6 \cdot 10^5$ Ω, $\omega = 2\pi \cdot 2 \cdot 10^9$ Hz) one could get for the beginning of the first linac $I_{th} = 0.73$ A and for the second $I_{th} = 2.34$ A, when for the preinjector it is about 1.58 A. That means the instability develops in the first main linac.
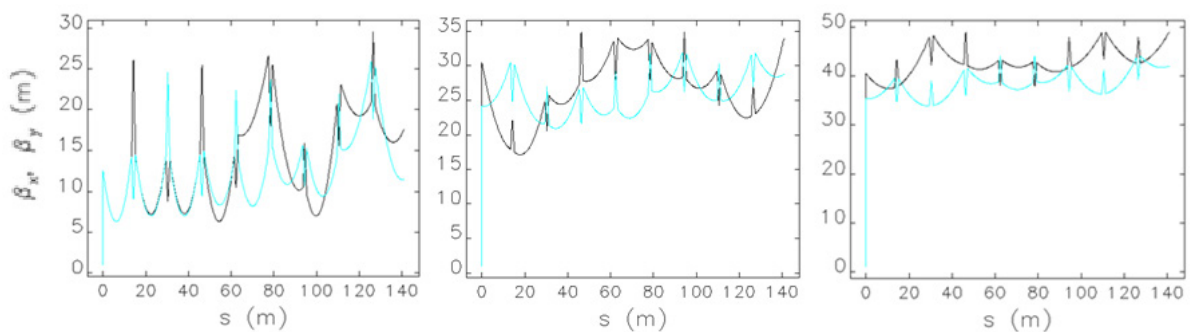
Figure 3.19: Optics design of the second 0.96 GeV linac of scalable scheme of FSF. 3 passes on acceleration are presented from left to right.

3.3.4. Summary of the results for the different schemes of FSF

In this paragraph the results of the estimations of the threshold currents from the 3 previous paragraphs are summarized.

Table 3.1: Threshold currents for different schemes of FSF

Linac scheme	I_{th}, A		
	Preinjector	1st Linac	2nd Linac
0.100 + 2x1GeV	1.26	0.88	3.73
250 + 666 + 1334MeV	1.64	1.46	3.58
Scalable scheme 230+2x960 MeV	1.58	0.73	2.34

It should be noted that the values in Table 3.1 are just the estimations of the threshold currents. These estimations were made assuming that there is only one mode in a linac. In principle this is the comparison of the square roots in the denominator of Eq. 2.53 for the different cavities and different injection schemes. Such problems as coupling and overlapping of the different modes are not taken into account. These problems will decrease the threshold current and, therefore, should be taken into account later.

4. Costs analysis

In this chapter the project construction costs for the direct injection scheme and for the scheme proposed for FSF are discussed. The analysis will include several parts of accelerator construction such as costs for infrastructure (costs of a land, buildings construction, accelerators tunnel), SRF (cryogenic plant, cryomodules, RF generators), warm machine (magnets, undulators, vacuum system, diagnostics, control systems, power supplies) and users (stations, beamline scientists). For the cost estimations a unit cost for each sub element of accelerator structure were assumed, and then the cost for two different designs were evaluated. In Table 4.1 the used unit costs are presented.

Table 4.1: Unit costs of different accelerator parts

Component	Unit cost
Land	0.16 k€/m^2
Tunnel	10 k€/m
Cryomodule	5 M€/m^2
RF generators	1.5 M€ for injector (200kW), 0.4 M€ for linacs (each of 10 kW)
Magnets	10 k€
Undulators	Short – 1 M€, Long – 5 M€
Vacuum system, diagnostics, control systems	10 k€/m
Power supplies	~ cost of magnets
Staff/Beamline scientists	50/100 k€/year
Users stations	200 M€

In the next chapters the costs of different parts of a facility for different schemes are separately compared. For comparison to be fair, it was assumed to have the same amount, as in FSF, of beamlines and insertion devices for direct injection scheme. So, its turn was made to be 3 times longer, but there are no available beamlines at lower than 6 GeV energies.

4.1. Infrastructure/tunnel

Let's the cost analysis with an estimation of the size of the area required to build the facility, excavation of the tunnel and construction of required buildings.
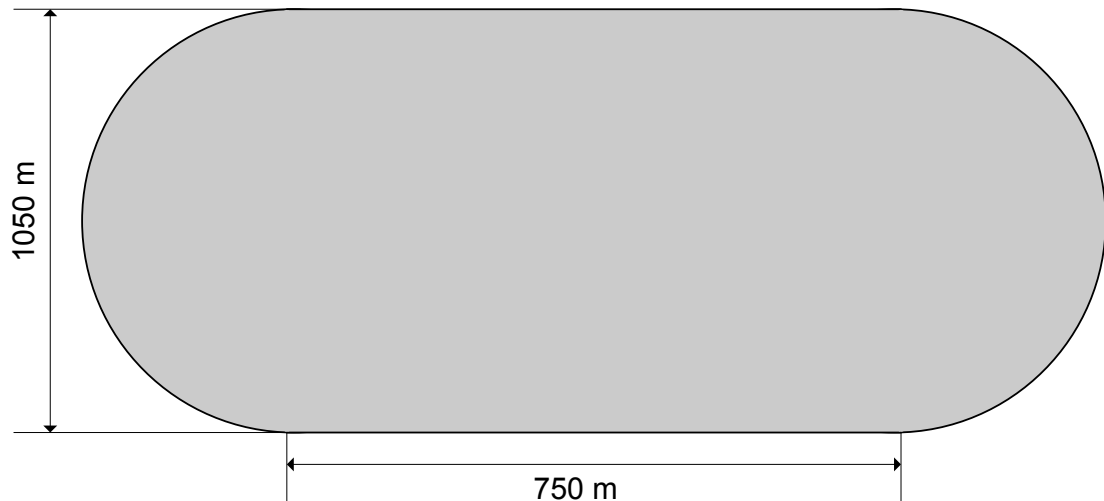
Figure 4.1: Land area, required to build a 6 GeV light source based on the direct injection scheme with one pass on acceleration.

In Fig. 4.1 with a grey colour marked the area required to build a 6 GeV light source with direct injection scheme and single turn. Size of this area and perimeter can be easily found and equal to about 1.65 km^2 and 4.8 km. It should be noted that we exclude the area outside of the arcs and make the facility with a "football stadium" like shape. The excluded area is about 0.24 km^2.

For the scheme of FSF (presented in Fig. 1.6) with 3 passes on acceleration and with a preinjection linac the area outside of the arcs can be neglected and the size of the land is estimated as just for a bar: 350x550 m^2. And the length of the tunnel is about 1.5 km.

For the construction of the buildings the costs assumed to be the same and about 50 M€ for the users buildings and about 10 M€ for the technical buildings.

Now one can use the unit costs from Table 4.1. The prices compared in Table 4.2.

Table 4.2: Costs of the infrastructure/tunnel for different schemes of 6 GeV light source

Component	Direct injection scheme cost, M€	3 turn FSF cost, M€
Land	265	31
Tunnel	48	15
Buildings	60	60
Total	373	106

As you can see from the table, the cost of the infrastructure/tunnel for the direct injection scheme is by the factor of about 3.5 higher than for the scheme with 3 turns on acceleration and with a split main linac. Nevertheless, the land cost for the direct injection scheme can be reduced, by excluding some area from the middle part of the facility.

4.2. Warm machine

There we would like to analyze the warm part of a 6 GeV light source based on two different schemes – the scheme with direct injection, one turn and the scheme of FSF with 3 turns and a split linac. In a warm part of the facility included:

a) All types of required magnets;

b) Undulators;

c) Power supplies;

d) Vacuum system;

e) Beam diagnostics and control systems.

Now let's count the number of magnets required for different schemes. We start with the scheme of FSF.

So the preinjector has the same amount of magnets as BERLinPro about 100. Each arc consist of 6 30^0 - bends with 46 magnets in each bend. So it has 12 arcs x 6 bends x 46 magnets what equals to 3312 magnets required to turn and transfer the beam through the FSF arcs. It requires 240 magnets for the spreaders/recombiners and 600 for the focusing in the undulators. Plus there are additional 50 more focusing triplet quadrupoles in the linacs. In total there are 4300 magnets needed for the realisation of the scheme proposed for FSF.

The direct injection scheme requires 3 times less magnets for the arcs and only 15 quadrupole magnets for the focusing in the linac. It has no spreaders and recombiners and no preinjector as well. The number of undulators assumed to be the same as for the scheme of FSF, therefore it needs the same number of magnets. So in total there are 1719 magnets required for the direct injection scheme.

The price for the power supplies for the magnets is about of the price of the magnets but can be reduced if the magnets are connected is series.

The total number of short undulators with 1000 periods for both schemes is 60 and there is additional long undulator in each scheme.

The price for the vacuum system, plus the beam diagnostics, plus control systems is proportional to the perimeter of the facility. Which for the direct injection scheme is about the length of the required tunnel ~ 4800 m. For the scheme of FSF it's a sum of 2 x 150m linacs, 4 spreaders and recombiners x 25 m plus arcs, what is about 7500 m of the transfer lines required for FSF. So one can use the unit costs from Table 4.1 and summarize the prices in Table 4.3.

Table 4.3: Costs of the warm machine part for different schemes of 6 GeV light source

Component	Direct injection scheme cost, M€	3 turn FSF cost, M€
Magnets	17.2	43
Undulators	65	65
Vacuum system + diagnostics/control systems	48	75
Power supplies	17.2	43
Total	147.4	226

The total cost for the warm part of the facility for the direct injection scheme is about 1.5 times cheaper than for the scheme of FSF. The main difference is coming from the number of magnets required for beam transportation through the facility and the power supplies for them.

4.3. SRF

In this part we would like to estimate the SRF costs for two schemes. In the SRF costs we include:

a) Cryogenic plant;

b) Cryomodules;

c) RF generators.

The cryogenic plant is assumed to be the same for both schemes and there we assume only its cost to be about 20 M€.

It requires 20 cryomodules for the scheme of FSF and 56 for the direct injection scheme.

The RF generators for the injector require 20mA x 10 MeV = 200 kW of power, assumed to be the same for both schemes. And 10 kW generator per cavity will be used in the linacs. What requires about 4.48 MW of generators power for the direct injection scheme and about 1.6 MW for the scheme of FSF. The SRF costs for both schemes summarized in Table 4.4.

Table 4.4: Costs of the SRF part for different schemes of 6 GeV light source

Component	Direct injection scheme cost, M€	3 turn FSF cost, M€
Cryogenic plant	20	20
Cryomodules	280	100
RF generators	180.7	65.5
Total	480.7	185.5

As you can see from the Table 4.4 the SRF part of the direct injection scheme is about 2.6 times (or about 300 M€) more expensive than the scheme of FSF.

4.4. Total cost

Here the results of comparison of two different schemes of 6 GeV light source are summarized. The results are presented in Table 4.5.

Table 4.5: Total costs of different parts for two schemes of 6 GeV light source

Component	Direct injection scheme cost, M€	3 turn FSF cost, M€
Infrastructure/tunnel	375	110
SRF	485	190
Warm machine	150	230
User stations	200	200
People for 10 years and beamline scientists	100	100
Total	1310	830

So a 6 GeV light source based on the direct injection scheme cost about 1.6 times (or about 480 M€) more than the scheme of FSF with 3 turns on acceleration and a split linac.

5. Conclusion

In this work an introduction to energy recovery based light sources was presented. Two ERLs are under development at Helmholtz Zentrum Berlin. One with 6 GeV beam energy is in the design phase, it is a multi-turn ERL based light source (Femto-Science Factory). The second with 50 MeV beam energy (B*ERL*inPro) funded since January 2011, is a test facility to demonstrate the feasibility of high current ERL operation using CW SRF linac technology.

One of the critical issues of ERL based machines is Beam Break Up instability. This instability was investigated during this work. The threshold currents of the instability were compared for the 100 MeV B*ERL*inPro based on two different types of cavities: 9-cell TESLA and 5-cell CEBAF. The comparison of the results shows that the threshold currents for two different types of the cavities approximately differ as the ratio of the impedances of the strongest dipole modes of these cavities.

Methods of suppression of BBU instability were discussed and applied for B*ERL*inPro. These methods include:

1. Adjusting the betatron phase advances of the recirculation turn. It seems to be a suitable method for small scale facilities (with low number of cavities). In the case when the number of cavities increases this method becomes less effective, because the optimum value of the phase cannot be achieved for all the cavities;

2. Variation of the time of the recirculation pass. For example, the 100 MeV B*ERL*inPro based on TESLA-type cavities, a variation of the pass length of two wavelengths of the main acceleration mode can change the threshold current by about 30% (Fig. 2.13). This method seems hard to be used in practice because it is required to know the parameters of the HOMs before assembling the facility. Alternatively, one can construct a turn with a variable path length of at least two wavelengths.

3. Usage of an element which couples the x and y planes of beams motion. This can be a pseudo-reflector or solenoid. Such an element can vary the threshold current by about 30-50% (Fig. 2.14).

The philosophies of linac optic design to achieve the maximum threshold currents of the instability were discussed. Optic of the linac for different layouts was calculated using these ideas. For example, the 50 MeV BERLinPro, in comparison with a standard optic, for the optic, optimized for BBU, the threshold current is higher by 30% and 75% for the first and middle cavities correspondingly (see §2.5.6).

Three different schemes of the ERL based light source were compared. These schemes are:

1. Direct injection scheme;

2. Two-stage injection scheme;

3. A scheme with two stage injection, a split linac and with 3 acceleration turns.

The main comparison criterions of the schemes were the threshold currents of the BBU instability and the construction costs. The results of the threshold currents for different schemes are summarized in Table 5.1.

Table 5.1: Estimations of the threshold currents

Scheme	I_{th}, A
Direct injection	0.4
Two stage injection	1.64
Scalable FSF	0.73

As one can see from the Table 5.1 the highest threshold current is achieved for the scheme with two stage injection and one turn. In this scheme the instability develops in the preinjecton linac. For the scheme of FSF the threshold current is about factor 2 lower and the instability develops in the first main linac due to the multiple turns in it. But in the FSF scheme the main linac is 3 times shorter which makes it more cost effective by about 500 M€ and the area required for it is smaller. The total cost of a multi-turn scheme of FSF is about 830 M€ this includes construction of the facility, user stations and staff for 10 years.

6. Appendix. Elegant files

There summarized the inputs for Elegant. To simplify the process of copying from one program to another, all the values were copied with accuracy given by program (a lot of digits after comma).

6.1. for §3.3.1

Initial energies for .ele file:

1-st pass 1-st Linac

p_central =200,

2-nd pass 1-st Linac

p_central = 4113.32,

3-rd pass 1-st Linac

p_central =8026.64,

1-st pass 2-nd Linac

p_central =2156.66,

2-nd pass 2-nd Linac

p_central = 6069.976,

3-rd pass 2-nd Linac

p_central = 9983.296,

.lte file:

LbCa: drif, L=0.3459

w1: watch, filename= "%s-%ld.w1"

cav7cellAcc: rfca, L=0.807133541, VOLT=13.9e6, PHASE=90, FREQ=1.3e9, CHANGE_P0=1, &

        END1_FOCUS=1, END2_FOCUS=1, BODY_FOCUS_MODEL="SRS"

cav7cellDec: rfca, L=0.807133541, VOLT=13.9e6, PHASE=-90, FREQ=1.3e9, CHANGE_P0=1, &

        END1_FOCUS=1, END2_FOCUS=1, BODY_FOCUS_MODEL="SRS"

L1m : drif, L = 1.037743124

L02m: drif, L = 0.230609583

LbC2.5l: drif, L= 0.576523958

LbQ: drif, L=0.752285

RTWI2_3: TWISS,BETAX=50.31521006416193,BETAY=41.44177326977371,&
 ALPHAX=0.8025508134866888,ALPHAY=-0.1677964656769029
"RTWI2_2": TWISS,BETAX=47.55973273161754,BETAY=23.64270319730079,&
 ALPHAX=0.4699610398358916,ALPHAY=0.1517001384110356
"RTWI2_1": TWISS,BETAX=1.17E+01,BETAY=1.17E+01,&
 ALPHAX=7.57E-01,ALPHAY=7.57E-01
"RTWI1_1": TWISS,BETAX=1.17E+01,BETAY=1.17E+01,&
 ALPHAX=7.57E-01,ALPHAY=7.57E-01
"RTWI1_2": TWISS,BETAX=68.71814074437405,BETAY=64.70852220398153,&
 ALPHAX=0.4452506268238382,ALPHAY=0.2251795836592895
"RTWI1_3": TWISS,BETAX=102.6510979747729,BETAY=108.7066590264029,&
 ALPHAX=0.3744069167384435,ALPHAY=0.4493636664948003
!cryomodule
cryo_4_1gev: Line=(L1m,7*(cav7cellAcc,LbC2.5l),cav7cellAcc,L1m,w1)
!!!!!!!!!!!!triplets 1st 1 GeV Linac
"TQ12_1N": KQUAD,L=0.15,BORE=0.035,B=0.05103126537734493
"TQ12_2N": KQUAD,L=0.15,BORE=0.035,B=-0.0957177090363464
"TQ23_1N": KQUAD,L=0.15,BORE=0.035,B=-0.07463940957710209
"TQ23_2N": KQUAD,L=0.15,BORE=0.035,B=0.1407306779283681
"TQ34_1N": KQUAD,L=0.15,BORE=0.035,B=-0.1012667811259562
"TQ34_2N": KQUAD,L=0.15,BORE=0.035,B=0.1907000296943905
"TQ45_1N": KQUAD,L=0.15,BORE=0.035,B=0.1273410061696678
"TQ45_2N": KQUAD,L=0.15,BORE=0.035,B=-0.2397624421754908
TrCr12n: LINE = (1*(LbQ,tq12_1n,LbQ,tq12_2n,LbQ,tq12_1n,LbQ))
TrCr23n: LINE = (1*(LbQ,tq23_1n,LbQ,tq23_2n,LbQ,tq23_1n,LbQ))
TrCr34n: LINE = (1*(LbQ,tq34_1n,LbQ,tq34_2n,LbQ,tq34_1n,LbQ))
TrCr45n: LINE = (1*(LbQ,tq45_1n,LbQ,tq45_2n,LbQ,tq45_1n,LbQ))
!!!!!!!!!!!!triplets 2nd 1 GeV Linac
"TQ12_1N2": KQUAD,L=0.15,BORE=0.035,B=-0.2876097238096304
"TQ12_2N2": KQUAD,L=0.15,BORE=0.035,B=0.5405106235505173
"TQ23_1N2": KQUAD,L=0.15,BORE=0.035,B=0.2952399743989904
"TQ23_2N2": KQUAD,L=0.15,BORE=0.035,B=-0.5584210683332118
"TQ34_1N2": KQUAD,L=0.15,BORE=0.035,B=-0.3206870667015269
"TQ34_2N2": KQUAD,L=0.15,BORE=0.035,B=0.6068173527581688

"TQ45_1N2": KQUAD,L=0.15,BORE=0.035,B=0.345238690152169

"TQ45_2N2": KQUAD,L=0.15,BORE=0.035,B=-0.6530381643371113

TrCr12n2: LINE = (1*(LbQ,tq12_1n2,LbQ,tq12_2n2,LbQ,tq12_1n2,LbQ))

TrCr23n2: LINE = (1*(LbQ,tq23_1n2,LbQ,tq23_2n2,LbQ,tq23_1n2,LbQ))

TrCr34n2: LINE = (1*(LbQ,tq34_1n2,LbQ,tq34_2n2,LbQ,tq34_1n2,LbQ))

TrCr45n2: LINE = (1*(LbQ,tq45_1n2,LbQ,tq45_2n2,LbQ,tq45_1n2,LbQ))

Linac1Gev:

Line=(w1,cryo_4_1gev,TrCr12n,cryo_4_1gev,TrCr23n,cryo_4_1gev,TrCr34n,cryo_4_1gev,
TrCr45n,cryo_4_1gev,TrCr45n,cryo_4_1gev,TrCr34n,cryo_4_1gev,TrCr23n,cryo_4_1gev,Tr
Cr12n,cryo_4_1gev)

Linac1Gev2nd:

Line=(w1,cryo_4_1gev,TrCr12n2,cryo_4_1gev,TrCr23n2,cryo_4_1gev,TrCr34n2,cryo_4_1g
ev,TrCr45n2,cryo_4_1gev,TrCr45n2,cryo_4_1gev,TrCr34n2,cryo_4_1gev,TrCr23n2,cryo_4
_1gev,TrCr12n2,cryo_4_1gev)

!RECIRCnew:

LINE=(rtwi1_1,w1,cryo_4_1gev,TrCr12n,cryo_4_1gev,TrCr23n,cryo_4_1gev,TrCr34n,cryo
_4_1gev,TrCr45n,cryo_4_1gev,TrCr45n,cryo_4_1gev,TrCr34n,cryo_4_1gev,TrCr23n,cryo_
4_1gev,TrCr12n,cryo_4_1gev)

RECIRCnew:

LINE=(rtwi2_3,w1,cryo_4_1gev,TrCr12n2,cryo_4_1gev,TrCr23n2,cryo_4_1gev,TrCr34n2,c
ryo_4_1gev,TrCr45n2,cryo_4_1gev,TrCr45n2,cryo_4_1gev,TrCr34n2,cryo_4_1gev,TrCr23n
2,cryo_4_1gev,TrCr12n2,cryo_4_1gev)

6.2. for §3.3.2

Initial energies for .ele file

!!!!!!!250+0.5mev

!!! 1st pass

!!!! 1st linac

!   p_central = 4.801432e+002,

!!!! 2nd linac

!   p_central = 1.784582e+003,

!!!!!2nd pass

!!! 1-st linac

!   p_central = 4.393456e+003,

!!! 2-nd Linac

!   p_central = 5.697893e+003,

!!!3rd pass

!!! 1-st Linac

         p_central = 8.306768e+003,

!!! 2nd Linac

!   p_central = 9.611205e+003,

!preinjector

         p_central = 19.569,

.lte file:

LbCa: drif, L=0.3459

w1: watch, filename= "%s-%ld.w1"

cav7cellAcc: rfca,   L=0.807133541,   VOLT=13.9e6,   PHASE=90,   FREQ=1.3e9, CHANGE_P0=1, &

         END1_FOCUS=1, END2_FOCUS=1, BODY_FOCUS_MODEL="SRS"

cav7cellDec: rfca,   L=0.807133541,   VOLT=13.9e6,   PHASE=-90,   FREQ=1.3e9, CHANGE_P0=1, &

         END1_FOCUS=1, END2_FOCUS=1, BODY_FOCUS_MODEL="SRS"

cav7cellAccpreinj: rfca,   L=0.807133541,   VOLT=14.9e6,   PHASE=90,   FREQ=1.3e9, CHANGE_P0=1, &

         END1_FOCUS=1, END2_FOCUS=1, BODY_FOCUS_MODEL="SRS"

cav7cellDecpreinj: rfca,   L=0.807133541,   VOLT=14.9e6,   PHASE=-90,   FREQ=1.3e9, CHANGE_P0=1, &

         END1_FOCUS=1, END2_FOCUS=1, BODY_FOCUS_MODEL="SRS"

L1m : drif, L = 1.037743124

L02m: drif, L = 0.230609583

LbC2.5l: drif, L= 0.576523958

LbQ: drif, L=0.752285

"RTWI2_3": TWISS,BETAX=39.062899434972,BETAY=78.67293977081414,&
 ALPHAX=0.1248919114427072,ALPHAY=0.08404964921807287

"RTWI2_2": TWISS,BETAX=45.2706123117699,BETAY=19.28654492405109,&
 ALPHAX=1.126190453628662,ALPHAY=-0.08862225381944949

"RTWI2_1":

TWISS,BETAX=12.53938228097638,BETAY=12.53938228097638,ALPHAX=0.99359338
16894664,&

 ALPHAY=0.9935933816894664

"RTWI1_1":

TWISS,BETAX=12.33057750489,BETAY=12.33057750489,ALPHAX=0.94329549639047
05,&

 ALPHAY=0.9432954963904705

"RTWI1_2": TWISS,BETAX=66.93511831651682,BETAY=55.76240671410563,&

 ALPHAX=0.1122112037437773,ALPHAY=0.3803515829423828

"RTWI1_3": TWISS,BETAX=85.73947184174607,BETAY=77.71992979757982,&

 ALPHAX=0.6906267352767432,ALPHAY=0.6947999074102813

RTWIpreinj: TWISS,BETAX=0.9870793398598936,ALPHAX=-0.2845486622653862,&

 BETAY=0.9870167259276019,ALPHAY=-0.2845212208591367

cryo_4_1gev: Line=(L1m,7*(cav7cellAcc,LbC2.5l),cav7cellAcc,L1m,w1)

cryo_preinj: Line=(L1m,7*(cav7cellAccpreinj,LbC2.5l),cav7cellAccpreinj,L1m,w1)

!!!triplet, preinjector

"TQpreinj_1N": KQUAD,L=0.15,BORE=0.035,B=0.02928778007419976

"TQpreinj_2N": KQUAD,L=0.15,BORE=0.035,B=-0.0553079711852654

TrCrpreinjn: LINE = (1*(LbQ,tqpreinj_1n,LbQ,tqpreinj_2n,LbQ,tqpreinj_1n,LbQ))

!!!!!!!!!!1st linac

"TQ12_1N": KQUAD,L=0.15,BORE=0.035,B=0.089428106784173

"TQ12_2N": KQUAD,L=0.15,BORE=0.035,B=-0.1663099894242368

"TQ23_1N": KQUAD,L=0.15,BORE=0.035,B=-0.1137101568541555

"TQ23_2N": KQUAD,L=0.15,BORE=0.035,B=0.2131929860515743

"TQ34_1N": KQUAD,L=0.15,BORE=0.035,B=0.05350521216790047

"TQ34_2N": KQUAD,L=0.15,BORE=0.035,B=-0.1899687815255773

"TQ34_3N": KQUAD,L=0.15,BORE=0.035,B=0.1415947149548661

TrCr12n: LINE = (1*(LbQ,tq12_1n,LbQ,tq12_2n,LbQ,tq12_1n,LbQ))

TrCr23n: LINE = (1*(LbQ,tq23_1n,LbQ,tq23_2n,LbQ,tq23_1n,LbQ))

TrCr34n: LINE = (1*(LbQ,tq34_1n,LbQ,tq34_2n,LbQ,tq34_3n,LbQ))

!!!!!!!!!!!!!2nd linac

"TQ12_1N2": KQUAD,L=0.15,BORE=0.035,B=-0.2614736347667703

"TQ12_2N2": KQUAD,L=0.15,BORE=0.035,B=0.4858989488151449

"TQ23_1N2": KQUAD,L=0.15,BORE=0.035,B=0.2871774743989846

"TQ23_2N2": KQUAD,L=0.15,BORE=0.035,B=-0.5347856516665404

"TQ34_1N2": KQUAD,L=0.15,BORE=0.035,B=-0.3143583652583663

"TQ34_2N2": KQUAD,L=0.15,BORE=0.035,B=0.5839039006096893

"TQ45_1N2": KQUAD,L=0.15,BORE=0.035,B=0.3387974021577785

"TQ45_2N2": KQUAD,L=0.15,BORE=0.035,B=-0.632006856480879

"TQ56_1N2": KQUAD,L=0.15,BORE=0.035,B=-0.3623043628175857

"TQ56_2N2": KQUAD,L=0.15,BORE=0.035,B=0.6758742570601005

"TQ67_1N2": KQUAD,L=0.15,BORE=0.035,B=-0.421742747118782

"TQ67_2N2": KQUAD,L=0.15,BORE=0.035,B=0.65273922567697

"TQ67_3N2": KQUAD,L=0.15,BORE=0.035,B=-0.2818707777396136

TrCr12n2: LINE = (1*(LbQ,tq12_1n2,LbQ,tq12_2n2,LbQ,tq12_1n2,LbQ))

TrCr23n2: LINE = (1*(LbQ,tq23_1n2,LbQ,tq23_2n2,LbQ,tq23_1n2,LbQ))

TrCr34n2: LINE = (1*(LbQ,tq34_1n2,LbQ,tq34_2n2,LbQ,tq34_1n2,LbQ))

TrCr45n2: LINE = (1*(LbQ,tq45_1n2,LbQ,tq45_2n2,LbQ,tq45_1n2,LbQ))

TrCr56n2: LINE = (1*(LbQ,tq56_1n2,LbQ,tq56_2n2,LbQ,tq56_1n2,LbQ))

TrCr67n2: LINE = (1*(LbQ,tq67_1n2,LbQ,tq67_2n2,LbQ,tq67_3n2,LbQ))

!Linacpreinj: Line=(RTWIpreinj,w1,cryo_preinj,TrCrpreinjn,cryo_preinj)

!RECIRCnew: LINE=(Linacpreinj)

RECIRCnew:
LINE=(rtwi1_3,w1,cryo_4_1gev,TrCr12n,cryo_4_1gev,TrCr23n,cryo_4_1gev,TrCr34n,cryo_4_1gev,TrCr23n,cryo_4_1gev,TrCr12n,cryo_4_1gev)

!RECIRCnew:
LINE=(rtwi2_1,w1,cryo_4_1gev,TrCr12n2,cryo_4_1gev,TrCr23n2,cryo_4_1gev,TrCr34n2,cryo_4_1gev,TrCr45n2,cryo_4_1gev,TrCr56n2,cryo_4_1gev,TrCr67n2,cryo_4_1gev,TrCr56n2,cryo_4_1gev,TrCr45n2,cryo_4_1gev,TrCr34n2,cryo_4_1gev,TrCr23n2,cryo_4_1gev,TrCr12n2,cryo_4_1gev)

6.3. for §3.3.3

Initial energies for .ele file

!!!!!!230+960mev

!!! 1st pass

!!!! 1st linac

!   p_central = 4.692700e+002,

!!!! 2nd linac

!   p_central = 2.346160e+003,

!!!!!2nd pass

!!! 1-st linac

!   p_central = 4.223049e+003,

!!! 2-nd Linac

!   p_central = 6.099936e+003,

!!!3rd pass

!!! 1-st Linac

!   p_central = 7.976824e+003,

!!! 2nd Linac

!   p_central = 9.853712e+003,

!preinjector

        p_central = 19.569,

.lte file

LbCa: drif, L=0.3459

w1: watch, filename= "%s-%ld.w1"

cav7cellAcc: rfca, L=0.807133541, VOLT=13.33333333e6, PHASE=90, FREQ=1.3e9, CHANGE_P0=1, &

        END1_FOCUS=1, END2_FOCUS=1, BODY_FOCUS_MODEL="SRS"

cav7cellDec: rfca, L=0.807133541, VOLT=13.33333333e6, PHASE=-90, FREQ=1.3e9, CHANGE_P0=1, &

        END1_FOCUS=1, END2_FOCUS=1, BODY_FOCUS_MODEL="SRS"

cav7cellAcc230MeV: rfca, L=0.807133541, VOLT=14.375e6, PHASE=90, FREQ=1.3e9, CHANGE_P0=1, &

END1_FOCUS=1, END2_FOCUS=1, BODY_FOCUS_MODEL="SRS"

cav7cellDec230MeV: rfca, L=0.807133541, VOLT=14.375e6, PHASE=-90, FREQ=1.3e9, CHANGE_P0=1, &

END1_FOCUS=1, END2_FOCUS=1, BODY_FOCUS_MODEL="SRS"

L1m : drif, L = 1.037743124

L02m: drif, L = 0.230609583

LbC2.5l: drif, L= 0.576523958

LbQ: drif, L=0.752285

"RTWI2_3": TWISS,BETAX=40.55751056124187,ALPHAX=0.2863301610686658,&
 BETAY=35.43609946424201,ALPHAY=0.03280936912136122

"RTWI2_2": TWISS,BETAX=30.49206255220344,ALPHAX=0.8431763699662878,&
 BETAY=24.14863766763482,ALPHAY=0.04018115252579833

"RTWI2_1":
TWISS,BETAX=12.53938228097638,BETAY=12.53938228097638,ALPHAX=0.99359338
16894664,&
 ALPHAY=0.9935933816894664

"RTWI1_1":
TWISS,BETAX=12.33057750489,BETAY=12.33057750489,ALPHAX=0.94329549639047
05,&
 ALPHAY=0.9432954963904705

RTWI230MEV: TWISS,BETAX=1.091733507761062,ALPHAX=-0.3231848354868172,&
 BETAY=1.091733507761062,ALPHAY=-0.3231848354868172

RTWIafter200MEV: TWISS,BETAX=6.045791e+000,BETAY= 6.045791e+000,&
ALPHAX=-6.754319e-001,ALPHAY=-6.754319e-001

cryo_4_1gev: Line=(L1m,7*(cav7cellAcc,LbC2.5l),cav7cellAcc,L1m)

cryo_230_MeV: Line=(L1m,7*(cav7cellAcc230MeV,LbC2.5l),cav7cellAcc230MeV,L1m)

cryo_4_1gevdec: Line=(L1m,7*(cav7cellDec,LbC2.5l),cav7cellDec,L1m)

cryo_230_MeVdec:
Line=(L1m,7*(cav7cellDec230MeV,LbC2.5l),cav7cellDec230MeV,L1m)

!!! preinjector, triplet

"TQ230MEV_1NN": KQUAD,L=0.15,BORE=0.035,B=0.02678693223571664

"TQ230MEV_2NN": KQUAD,L=0.15,BORE=0.035,B=-0.05075521155205445

TrCr230mevnn: LINE =

(1*(LbQ,tq230mev_1nn,LbQ,tq230mev_2nn,LbQ,tq230mev_1nn,LbQ))

!!!!!!!!!triplets first linac

"TQ12_1N": KQUAD,L=0.15,BORE=0.035,B=0.08728498875574105

"TQ12_2N": KQUAD,L=0.15,BORE=0.035,B=-0.1622941386689107

"TQ23_1N": KQUAD,L=0.15,BORE=0.035,B=-0.1107520012229698

"TQ23_2N": KQUAD,L=0.15,BORE=0.035,B=0.2074420800891823

"TQ34_1N": KQUAD,L=0.15,BORE=0.035,B=-0.1347149654818188

"TQ34_2N": KQUAD,L=0.15,BORE=0.035,B=0.2529515956030026

"TQ45_1N": KQUAD,L=0.15,BORE=0.035,B=0.1551762585414628

"TQ45_2N": KQUAD,L=0.15,BORE=0.035,B=-0.2905894577622814

!!!!!!!!!

TrCr12n: LINE = (1*(LbQ,tq12_1n,LbQ,tq12_2n,LbQ,tq12_1n,LbQ))

TrCr23n: LINE = (1*(LbQ,tq23_1n,LbQ,tq23_2n,LbQ,tq23_1n,LbQ))

TrCr34n: LINE = (1*(LbQ,tq34_1n,LbQ,tq34_2n,LbQ,tq34_1n,LbQ))

TrCr45n: LINE = (1*(LbQ,tq45_1n,LbQ,tq45_2n,LbQ,tq45_1n,LbQ))

!!!!!!!!!!!!!2nd 1 GeV Linac

"TQ12_1N2": KQUAD,L=0.15,BORE=0.035,B=-0.3263145756056179

"TQ12_2N2": KQUAD,L=0.15,BORE=0.035,B=0.6072974084892324

"TQ23_1N2": KQUAD,L=0.15,BORE=0.035,B=0.3415935690899017

"TQ23_2N2": KQUAD,L=0.15,BORE=0.035,B=-0.6407908451652209

"TQ34_1N2": KQUAD,L=0.15,BORE=0.035,B=-0.3605390978091807

"TQ34_2N2": KQUAD,L=0.15,BORE=0.035,B=0.6843628782583894

"TQ45_1N2": KQUAD,L=0.15,BORE=0.035,B=0.3183704903204688

"TQ45_2N2": KQUAD,L=0.15,BORE=0.035,B=-0.6302305737410014

!!!!!!!!!!!!!!!!

TrCr12n2: LINE = (1*(LbQ,tq12_1n2,LbQ,tq12_2n2,LbQ,tq12_1n2,LbQ))

TrCr23n2: LINE = (1*(LbQ,tq23_1n2,LbQ,tq23_2n2,LbQ,tq23_1n2,LbQ))

TrCr34n2: LINE = (1*(LbQ,tq34_1n2,LbQ,tq34_2n2,LbQ,tq34_1n2,LbQ))

TrCr45n2: LINE = (1*(LbQ,tq45_1n2,LbQ,tq45_2n2,LbQ,tq45_1n2,LbQ))

Linac230MeV: Line=(RTWI230mev,w1,cryo_230_mev,TrCr230mevnn,cryo_230_mev)

Linac230MeVdec: Line=(cryo_230_mevdec,TrCr230mevnn,cryo_230_mevdec)

!RECIRCnew:

LINE=(rtwi1_3,w1,cryo_4_1gev,TrCr12n,cryo_4_1gev,TrCr23n,cryo_4_1gev,TrCr34n,cryo

_4_1gev,TrCr45n,cryo_4_1gev,TrCr45n,cryo_4_1gev,TrCr34n,cryo_4_1gev,TrCr23n,cryo_
4_1gev,TrCr12n,cryo_4_1gev,w1)

!RECIRCnew:

LINE=(rtwi2_3,w1,cryo_4_1gev,TrCr12n2,cryo_4_1gev,TrCr23n2,cryo_4_1gev,TrCr34n2,c
ryo_4_1gev,TrCr45n2,cryo_4_1gev,TrCr45n2,cryo_4_1gev,TrCr34n2,cryo_4_1gev,TrCr23n
2,cryo_4_1gev,TrCr12n2,cryo_4_1gev,w1)

6.4. for BERLinPro

!p_central=15,

!!!!! berlin pro
 CAV1:

RFCA,L=0.8077,VOLT=15341000,PHASE=90,FREQ=1300000000,CHANGE_P0=1,&
 END1_FOCUS=1,END2_FOCUS=1,BODY_FOCUS_MODEL="SRS"
 CAV1/2:   RFCA,L="0.8077   2   /",VOLT="15341000   2
/",PHASE=90,FREQ=1300000000,CHANGE_P0=1,&
 END1_FOCUS=1,END2_FOCUS=1,BODY_FOCUS_MODEL="SRS"
rtwitestmid: twiss,betax = 2.225163431, alphax = 0.484281969, betay = 2.225163431, alphay
= 0.484281969
RTWITESTMID0: TWISS,BETAX=2.357120458542974,ALPHAX=-0.4226331466336725,
BETAY=2.357120l458542974,ALPHAY=-0.4226331466336725
L_CAV: DRIFT,L=0.4615
RECIRC50MeV:
LINE=(rtwitestmid0,cav1/2,w1,cav1/2,w1,L_CAV,CAV1/2,w1,cav1/2,L_CAV,CAV1/2,w1,
cav1/2,w1)
cavTESLA: rfca,   L=1.037743124,   VOLT=1.6e7,   PHASE=90,   FREQ=1.3e9,
CHANGE_P0=1, &
      END1_FOCUS=1, END2_FOCUS=1, BODY_FOCUS_MODEL="SRS"
Lacryo: drif, L=0.691828749
LbCr: drif, L=3.45914
LbQ: drif, L=0.752285
"TQ100MEV_1NN": KQUAD,L=0.15,BORE=0.035,B=0.02324777063085312
"TQ100MEV_2NN": KQUAD,L=0.15,BORE=0.035,B=-0.03917631448536403

TrCr100mevnn:LINE=

(1*(LbQ,tq100mev_1nn,LbQ,tq100mev_2nn,LbQ,tq100mev_1nn,LbQ))

rtwitestmid: twiss,betax = 1.841, alphax = -0.44, betay = 1.841, alphay = -0.44

RECIRC100MeV:

LINE=(rtwitestmid0,Lacryo,cavTESLA,LbCa,cavTESLA,LbCa,cavTESLA,Lacryo,TrCr100

mevnn,Lacryo,cavTESLA,LbCa,cavTESLA,LbCa,cavTESLA,w1)

6.5. for two stage injection scheme

Initial energies for .ele file

!initial energy for preinjector

      p_central = 19.569,

!for main linac

      p_central = 480,

.lte file

!!!!

LbCa: drif, L=0.3459

w1: watch, filename= "%s-%ld.w1"

cav7cellAcc: rfca, L=0.807133541, VOLT=12.931e6, PHASE=90, FREQ=1.3e9, CHANGE_P0=1, &

      END1_FOCUS=1, END2_FOCUS=1, BODY_FOCUS_MODEL="SRS"

cav7cellDec: rfca, L=0.807133541, VOLT=13.9e6, PHASE=-90, FREQ=1.3e9, CHANGE_P0=1, &

      END1_FOCUS=1, END2_FOCUS=1, BODY_FOCUS_MODEL="SRS"

L1m : drif, L = 1.037743124

L02m: drif, L = 0.230609583

LbC2.5l: drif, L= 0.576523958

LbQ: drif, L=0.752285

"RTWI1_1": TWISS,BETAX=12.5,ALPHAX=0.922560617440601,&

 BETAY=12.5,ALPHAY=0.922560617440601

cryo_4_1gev: Line=(L1m,7*(cav7cellAcc,LbC2.5l),cav7cellAcc,L1m)

!!!! Triplets

"TQ12_1N": KQUAD,L=0.15,BORE=0.035,B=   0.0850174319220445

"TQ12_2N": KQUAD,L=0.15,BORE=0.035,B=   -0.159925623403322

"TQ12_3N": KQUAD,L=0.15,BORE=0.035,B=   0.0859866615134687

"TQ23_1N": KQUAD,L=0.15,BORE=0.035,B=   -0.105597977022281

"TQ23_2N": KQUAD,L=0.15,BORE=0.035,B=   0.200370019713899

"TQ23_3N": KQUAD,L=0.15,BORE=0.035,B=   -0.107735585072339

"TQ34_1N": KQUAD,L=0.15,BORE=0.035,B=   -0.128954001680251

"TQ34_2N": KQUAD,L=0.15,BORE=0.035,B=   0.24227870666847

"TQ45_1N": KQUAD,L=0.15,BORE=0.035,B=   0.15293787560544

"TQ45_2N": KQUAD,L=0.15,BORE=0.035,B=   -0.287382687062942

"TQ56_1N": KQUAD,L=0.15,BORE=0.035,B=   0.177084879544713

"TQ56_2N": KQUAD,L=0.15,BORE=0.035,B=   -0.332691179073278

"TQ67_1N": KQUAD,L=0.15,BORE=0.035,B=   0.201032306334129

"TQ67_2N": KQUAD,L=0.15,BORE=0.035,B=   -0.37774369897825

"TQ78_1N": KQUAD,L=0.15,BORE=0.035,B=   -0.225211266457728

"TQ78_2N": KQUAD,L=0.15,BORE=0.035,B=   0.423094510231011

"TQ89_1N": KQUAD,L=0.15,BORE=0.035,B=   -0.249121911208668

"TQ89_2N": KQUAD,L=0.15,BORE=0.035,B=   0.468096089542393

"TQ910_1N": KQUAD,L=0.15,BORE=0.035,B=   -0.273295907914379

"TQ910_2N": KQUAD,L=0.15,BORE=0.035,B=   0.513427785513868

"TQ1011_1N": KQUAD,L=0.15,BORE=0.035,B=   0.2971173132630133

"TQ1011_2N": KQUAD,L=0.15,BORE=0.035,B=   -0.558383640978021

"TQ1112_1N": KQUAD,L=0.15,BORE=0.035,B=   -0.321404623018398

"TQ1112_2N": KQUAD,L=0.15,BORE=0.035,B=   0.603800792473566

"TQ1213_1N": KQUAD,L=0.15,BORE=0.035,B=   0.345300796981443

"TQ1213_2N": KQUAD,L=0.15,BORE=0.035,B=   -0.648798365619162

"TQ1314_1N": KQUAD,L=0.15,BORE=0.035,B=   -0.36956120480922

"TQ1314_2N": KQUAD,L=0.15,BORE=0.035,B=   0.694253287909629

"TQ1415_1N": KQUAD,L=0.15,BORE=0.035,B=   0.39339012303195

"TQ1415_2N": KQUAD,L=0.15,BORE=0.035,B=   -0.739149627107297

"TQ1516_1N": KQUAD,L=0.15,BORE=0.035,B=   -0.41766797284088

"TQ1516_2N": KQUAD,L=0.15,BORE=0.035,B=   0.784623169317841

"TQ1617_1N": KQUAD,L=0.15,BORE=0.035,B=   0.441512474869972

"TQ1617_2N": KQUAD,L=0.15,BORE=0.035,B=   -0.829555800833351

"TQ1718_1N": KQUAD,L=0.15,BORE=0.035,B=   -0.465840853389526

"TQ1718_2N": KQUAD,L=0.15,BORE=0.035,B=   0.875103188409603

"TQ1819_1N": KQUAD,L=0.15,BORE=0.035,B=   0.489646069440325

"TQ1819_2N": KQUAD,L=0.15,BORE=0.035,B=   -0.91998085940768

"TQ1920_1N": KQUAD,L=0.15,BORE=0.035,B=   -0.514011692649169

"TQ1920_2N": KQUAD,L=0.15,BORE=0.035,B=   0.9655797645922388

"TQ2021_1N": KQUAD,L=0.15,BORE=0.035,B=   0.537822402557419

"TQ2021_2N": KQUAD,L=0.15,BORE=0.035,B=   -1.01047656920617

"TQ2122_1N": KQUAD,L=0.15,BORE=0.035,B=   0.562194442511363

"TQ2122_2N": KQUAD,L=0.15,BORE=0.035,B=   -1.05607588437628

"TQ2223_1N": KQUAD,L=0.15,BORE=0.035,B=   -0.585901298867217

"TQ2223_2N": KQUAD,L=0.15,BORE=0.035,B=   1.10081052110663

"TQ2324_1N": KQUAD,L=0.15,BORE=0.035,B=   0.610263243843481

"TQ2324_2N": KQUAD,L=0.15,BORE=0.035,B=   -1.14638189246896

"TQ2425_1N": KQUAD,L=0.15,BORE=0.035,B=   -0.633962358008034

"TQ2425_2N": KQUAD,L=0.15,BORE=0.035,B=   1.19111321539437

"TQ2526_1N": KQUAD,L=0.15,BORE=0.035,B=   -0.658345293339037

"TQ2526_2N": KQUAD,L=0.15,BORE=0.035,B=   1.2367095303599

"TQ2627_1N": KQUAD,L=0.15,BORE=0.035,B=   0.681988421822958

"TQ2627_2N": KQUAD,L=0.15,BORE=0.035,B=   -1.28135877138116

"TQ2728_1N": KQUAD,L=0.15,BORE=0.035,B=   -0.706385901300609

"TQ2728_2N": KQUAD,L=0.15,BORE=0.035,B=   1.3269678573053

"TQ_1N": KQUAD,L=0.15,BORE=0.035,B=0.6603390500805135

"TQ_2N": KQUAD,L=0.15,BORE=0.035,B=-1.224755613734276

TrCr12n: LINE = (1*(LbQ,tq12_1n,LbQ,tq12_2n,LbQ,tq12_3n,LbQ))

TrCr23n: LINE = (1*(LbQ,tq23_1n,LbQ,tq23_2n,LbQ,tq23_3n,LbQ))

TrCr12s: LINE = (1*(LbQ,tq12_3n,LbQ,tq12_2n,LbQ,tq12_1n,LbQ))

TrCr23s: LINE = (1*(LbQ,tq23_3n,LbQ,tq23_2n,LbQ,tq23_1n,LbQ))

TrCr34n: LINE = (1*(LbQ,tq34_1n,LbQ,tq34_2n,LbQ,tq34_1n,LbQ))

TrCr45n: LINE = (1*(LbQ,tq45_1n,LbQ,tq45_2n,LbQ,tq45_1n,LbQ))

TrCr56n: LINE = (1*(LbQ,tq56_1n,LbQ,tq56_2n,LbQ,tq56_1n,LbQ))

TrCr67n: LINE = (1*(LbQ,tq67_1n,LbQ,tq67_2n,LbQ,tq67_1n,LbQ))

TrCr78n: LINE = (1*(LbQ,tq78_1n,LbQ,tq78_2n,LbQ,tq78_1n,LbQ))

TrCr89n: LINE = (1*(LbQ,tq89_1n,LbQ,tq89_2n,LbQ,tq89_1n,LbQ))

TrCr910n: LINE = (1*(LbQ,tq910_1n,LbQ,tq910_2n,LbQ,tq910_1n,LbQ))

TrCr1011n: LINE = (1*(LbQ,tq1011_1n,LbQ,tq1011_2n,LbQ,tq1011_1n,LbQ))

TrCr1112n: LINE = (1*(LbQ,tq1112_1n,LbQ,tq1112_2n,LbQ,tq1112_1n,LbQ))

TrCr1213n: LINE = (1*(LbQ,tq1213_1n,LbQ,tq1213_2n,LbQ,tq1213_1n,LbQ))

TrCr1314n: LINE = (1*(LbQ,tq1314_1n,LbQ,tq1314_2n,LbQ,tq1314_1n,LbQ))

TrCr1415n: LINE = (1*(LbQ,tq1415_1n,LbQ,tq1415_2n,LbQ,tq1415_1n,LbQ))

TrCr1516n: LINE = (1*(LbQ,tq1516_1n,LbQ,tq1516_2n,LbQ,tq1516_1n,LbQ))

TrCr1617n: LINE = (1*(LbQ,tq1617_1n,LbQ,tq1617_2n,LbQ,tq1617_1n,LbQ))

TrCr1718n: LINE = (1*(LbQ,tq1718_1n,LbQ,tq1718_2n,LbQ,tq1718_1n,LbQ))

TrCr1819n: LINE = (1*(LbQ,tq1819_1n,LbQ,tq1819_2n,LbQ,tq1819_1n,LbQ))

TrCr1920n: LINE = (1*(LbQ,tq1920_1n,LbQ,tq1920_2n,LbQ,tq1920_1n,LbQ))

TrCr2021n: LINE = (1*(LbQ,tq2021_1n,LbQ,tq2021_2n,LbQ,tq2021_1n,LbQ))

TrCr2122n: LINE = (1*(LbQ,tq2122_1n,LbQ,tq2122_2n,LbQ,tq2122_1n,LbQ))

TrCr2223n: LINE = (1*(LbQ,tq2223_1n,LbQ,tq2223_2n,LbQ,tq2223_1n,LbQ))

TrCr2324n: LINE = (1*(LbQ,tq2324_1n,LbQ,tq2324_2n,LbQ,tq2324_1n,LbQ))

TrCr2425n: LINE = (1*(LbQ,tq2425_1n,LbQ,tq2425_2n,LbQ,tq2425_1n,LbQ))

TrCr2526n: LINE = (1*(LbQ,tq2526_1n,LbQ,tq2526_2n,LbQ,tq2526_1n,LbQ))

TrCr2627n: LINE = (1*(LbQ,tq2627_1n,LbQ,tq2627_2n,LbQ,tq2627_1n,LbQ))

TrCr2728n: LINE = (1*(LbQ,tq2728_1n,LbQ,tq2728_2n,LbQ,tq2728_1n,LbQ))

TrCrCn: LINE = (1*(LbQ,tq_1n,LbQ,tq_2n,LbQ,tq_1n,LbQ))

RECIRCnew29:

LINE=(rtwi1_1,w1,cryo_4_1gev,TrCr12n,cryo_4_1gev,TrCr23n,cryo_4_1gev,TrCr34n,cryo_4_1gev,TrCr45n,cryo_4_1gev,TrCr56n,cryo_4_1gev,TrCr67n,cryo_4_1gev,TrCr78n,cryo_4_1gev,TrCr89n,cryo_4_1gev,TrCr910n,cryo_4_1gev,TrCr1011n,cryo_4_1gev,TrCr1112n,cryo_4_1gev,TrCr1213n,cryo_4_1gev,TrCr1314n,cryo_4_1gev,TrCr1415n,cryo_4_1gev,TrCr1516n,cryo_4_1gev,TrCr1617n,cryo_4_1gev,TrCr1718n,cryo_4_1gev,TrCr1819n,cryo_4_1gev,TrCr1920n,cryo_4_1gev,TrCr2021n,cryo_4_1gev,TrCr2122n,cryo_4_1gev,TrCr2223n,cryo_4_1gev,TrCr2324n,cryo_4_1gev,TrCr2425n,cryo_4_1gev,TrCr2526n,cryo_4_1gev,TrCr2627n,cryo_4_1gev,TrCr2728n,cryo_4_1gev,TrCrCn,cryo_4_1gev,TrCr2728n,cryo_4_1gev,TrCr2627n,cryo_4_1gev,TrCr2526n,cryo_4_1gev,TrCr2425n,cryo_4_1gev,TrCr2324n,cryo_4_1gev,TrCr2223n,cryo_4_1gev,TrCr2122n,cryo_4_1gev,TrCr2021n,cryo_4_1gev,TrCr1920n,cryo_4_1gev,TrCr1819n,cryo_4_1gev,TrCr1718n,cryo_4_1gev,TrCr1617n,cryo_4_1gev,

TrCr1516n,cryo_4_1gev,TrCr1415n,cryo_4_1gev,TrCr1314n,cryo_4_1gev,TrCr1213n,cryo_4_1gev,TrCr1112n,cryo_4_1gev,TrCr1011n,cryo_4_1gev,TrCr910n,cryo_4_1gev,TrCr89n,cryo_4_1gev,TrCr78n,cryo_4_1gev,TrCr67n,cryo_4_1gev,TrCr56n,cryo_4_1gev,TrCr45n,cryo_4_1gev,TrCr34n,cryo_4_1gev,TrCr23s,cryo_4_1gev,TrCr12s,cryo_4_1gev,w1)

!!!!!!!!!!!!!!!!!!!!!!!!!!!!!!!!!!!!!!preinjector for 2 stage scheme

CAVpi:

RFCA,L=0.8077,VOLT=14706175,PHASE=90,FREQ=1300000000,CHANGE_P0=1,&
 END1_FOCUS=1,END2_FOCUS=1,BODY_FOCUS_MODEL="SRS"

RTWIPI0: TWISS,BETAX=1.036055784612445,ALPHAX=-0.3044354381189601,&
 BETAY=1.036055784612445,ALPHAY=-0.3044354381189601

rtwipi: twiss,betax = 2.8036764209, alphax = -1.3988962787 , betay = 2.8036764209, alphay = -1.3988962787

TQ1PI: KQUAD,L=0.15,BORE=0.035,B=0.027268127221368

TQ2PI: KQUAD,L=0.15,BORE=0.035,B=-0.05168204896609516

TrCrpi: LINE = (1*(LbQ,tq1pi,LbQ,tq2pi,LbQ,tq1pi,LbQ))

cryo_pi: Line=(L1m,7*(cavpi,LbC2.5l),cavpi,L1m,w1)

Linac245MeV: Line=(7*(cavpi,LbC2.5l),cavpi,7*(cavpi,LbC2.5l),cavpi)

!RECIRCnew:

LINE=(rtwipi0,L1m,7*(cavpi,LbC2.5l),cavpi,L1m,TrCrpi,L1m,7*(cavpi,LbC2.5l),cavpi,L1m)

7. References

1. E. M. Rowe and F. E. Mills, Tantalus I, A Dedicated Storage Ring Synchrotron Radiation Source, Particle Accelerators, Vol. 4 (1973), pp. 211-227.

2. M. Vogt et al, The Free-Electron Laser FLASH at Desy, Proceedings of IPAC2013, Shanghai, China, pp. 1167-1169.

3. https://portal.slac.stanford.edu/sites/lcls_public/Pages/Default.aspx.

4. M. Tigner, A Possible Apparatus for Electron Clashing-Beam Experiments, Il Nuovo Cimento Vol. 37, No. 3 (1965).

5. V.P. Bolotin et al, Status of the Novosibirsk Terahertz FEL, 2004 FEL Conference Proceedings, pp. 226-228.

6. R. Hajima et al, Recent results of the JAERI Energy-Recovery Linac FEL, 2004 FEL Conference Proceedings, pp. 301-303.

7. S. Benson et al, High power lasing in the IR upgrade at Jefferson Lab , 2004 FEL Conference Proceedings, pp. 229-232.

8. F. Jackson et al, The status of the Alice R&D facility at STFC Daresbury laboratory, 2011 IPAC Conference Proceedings, pp. 934-936.

9. A.Richter, S-DALINAC: Project Status and Physics, Nuclear Physics News, Volume 1, Issue 1, 1990.

10. H. Abe et al, Energy Recovery Linac Conceptual Design Report, KEK report 2012-4, October 2012.

11. V. Litvinenko, Status of R&D ERL at BNL, PAC 2007.

12. R. Calaga, A proposal for an ERL test facility at CERN, IPAC 2013 Conference Proceedings, pp. 2414-2416.

13. S.H. Wang et al, Design studies on the ERL test facility at IHEP-BEIJING, proceedings of ERL2011, pp. 52-55.

14. S.L. Huang et al, Optics layout for the ERL test facility at Peking university, proceedings of ERL2011, pp. 49-51.

15. M. Abo-Bakr et al, Conceptual design report BERLinPro, 2012.

16. A. Bartnik et al, Cornell Energy Recovery Linac Science Case and Project Definition Design Report, 2013.

17. H. Abe et at, Energy Recovery Linac Conceptual Design Report, KEK Report 2012-4, http://pfwww.kek.jp/ERLoffice/detabase/ERL_CDR_full_text.pdf.

18. G.N. Kulipanov et al, ERL11 Conference proceedings, pp. 60-63.

19. Y. Petenev et al., Feasibility Study of an ERL-based GeV scale Multi-turn Light Source, IPAC12 Conference Proceedings, USA, pp. 604-606.

20. I Ben-Zvi, Ya. Derbenev, V.N. Litvinenko and L. Merminga, Energy recovery linacs in high-energy and nuclear physics, Nucl. Instr. and Meth. A 557 (2006).

21. V.N.Litvinenko, LHeC and eRHIC, In the Proc.of the 2009 Europhysics Conference on High Energy Physics, Poland, http://www.bnl.gov/isd/documents/70608.pdf.

22. S. Ahmed et al, Conceptual design of a polarized Medium Energy Electron-Ion Collider at JLab, IPAC11 Conference Proceedings, pp. 2306-2308.

23. V.N. Litvinenko, Y.S. Derbenev, Coherent Electron Cooling, Physical Review Letters 102 (2009) 114801.

24. V. Litvinenko, ERLs in the High Energy and Nuclear Physics, ERL'11 Workshop.

25. R. Heine et al., MESA – sketch of an Energy Recovery Linac for Nuclear Physics experiments at Mainz, IPAC 12 Conference Proceedings, USA, pp. 1993-1995.

26. K. Aulenbacher et al, Status of the MESA accelerator, Proceedings of ERL2013, Russia, PLT01, pp. 1-5.

27. W. Anders et al, BERLinPro: a Prototype ERL for Future Synchrotron Light Sources, SRF2009, Berlin, 2009.

28. M. Abo-Bakr, B. Kuske, A. Matveenko, Magnet Optics and Beam Dynamics of BERLinPro, Proc. of IPAC'10, pp. 2135-2137.

29. T. Kamps et al, Journal of Physics: Conference Series, 298 (2011) 012009.

30. A.N. Matveenko et al, Status of the BERLinPro optics design, Proc. of IPAC'11, pp.1500-1502.

31. A.W. Chao and M. Tigner, eds., Handbook of Accelerator Physics and Engineering, World Scientific, 1999.

32. H. Wiedemann, Particle Accelerator Physics, 3rd Edition, Springer, 2007.

33. The European X-Ray Free-Electron Laser, Technical design report, DESY 2006-097, 2007.

34. J.Wu at al, Coherent Synchrotron Radiation Analysis for the Photoinjected ERL and UVFEL Projects at NSLS, Proc. of 2001 Pacticle Accelerator Conf., pp. 2866-2868.

35. M. Sands, The physics of electron storage rings. An introduction, Proc. of the International School of Physics "Enrico Fermi", ed. B. Touschek, Academic Press, 1971.

36. S.Y. Lee, Accelerator Physics, 2nd Edition, World Scientific Pub. 2004.

37. H. Padamsee, J. Knobloch, and T. Hays, RF Superconductivity for Accelerators, 2nd Edition, Wiley-VCH 2008.

38. A.W. Chao, Physics of collective beam instabilities in high energy accelerators, Wiley series in beam physics and accelerator technology 1993.

39. T.P. Wangler, RF Linear Accelerators, 2nd completely revised and enlarged edition, Wiley-VCH, 2008.

40. Claude M. Lyneis, Michael S. McAshan, Roy E. Rand, H. Alan Schwettman, Todd I. Smith and John P. Turneaure, The Stanford Superconducting Recyclotron, IEEE Transactions on Nuclear Science, Vol. NS-26, No. 3, June 1979.

41. P.Axel, L.S.Cardman, H.D.Graef, A.O.Hanson, R.A.Hoffswell, D.Jamnik, D.C.Sutton, R.H.Taylor, and L.M.Young, Operating Experience with MUSL-2, IEEE Transactions on Nuclear Science, Vol. NS-26, No. 3, June 1979.

42. R.E. Rand and T.I. Smith, Beam optical control of beam breakup in a recirculating electron accelerator, Particle accelerators, Vol. 11, pp. 1-13 (1980).

43. J.J. Bisognano, R.L. Gluckstern, in Proceedings of the 1987 Particle Accelerator Conference, Washington, DC (IEEE Catalog No. 87CH2387-9), pp. 1078-1080.

44. G.A. Krafft, J.J. Bisognano, in Proceedings of the 1987 Particle Accelerator Conference, Washington, DC (IEEE Catalog No. 87CH2387-9), pp. 1356-1358.

45. G.H. Hoffstaetter, I.V. Bazarov, Beam-breakup instability theory for the energy recovery linacs, Phys. Rev. ST AB 7, 054401 (2004).

46. E. Pozdeyev et al, Multipass beam breakup in energy recovery linacs, NIM A 557 (2006) 176-188.

47. N.A. Vinokurov et al., Proc. of SPIE Vol. 2988, p. 221 (1997).

48. E. Pozdeyev, Regenerative multipass beam breakup in two dimensions, PRST AB 8, 2005.

49. G.A. Krafft, J.J. Bisognano, Two dimensional simulations of Multipass Beam Break up, SLAC-121 (1987).

50. K .B. Beard, L. Merminga, B.Yunn, Jlab Tech. Note JLAB-TN-02-044, 2002.

51. The tracking code "bi", http://www.lepp.cornell.edu/~ib38/bbucode/doc/bbudoc.pdf.

52. Generic Beam BreakUp (GBBU) by E. Pozdeyev.

53. B. Riemann et al, Alternative Approaches for HOM-Damped Cavities, Proceedings of LINAC12, pp. 330-332.

54. A. Neumann et al, Results and Performance Simulations of the Main Linac Design for B*ERL*inPro, Proceedings of LINAC12, pp.333-335.

55. http://tesla.desy.de/oracle/6i/CavityDB/GUI/ view?config=app_hom_meas

56. F. Marhauser et al., "JLAB high current cryomodule development" Proc. ERL Workshop 2009, Cornell University, U.S.

57. J. Rosenzweig, L. Serafini. "Transverse particle motion in radio-frequency linear accelerators". Phys. Rev. E, vol. 49, number 2 (2004).

58. M. Borland, "Elegant: A Flexible SDDS-Compliant Code for Accelerator Simulation," APS LS-287, 2000.

59. CST Microwave Studio, User Guide, CST GmbH, Buedinger Str. 2a, D-64289 Darmstadt, Germany.

60. The MAFIA Collaboration, CST GmbH, Buedinger Str. 2a, D-64289 Darmstadt, Germany.

61. A.N. Matveenko, private communication.

62. L.Xiao et al., "Modelling imperfection effects on dipole modes in TESLA cavity", Proceedings of PAC07, pp. 2454-2456.

63. В.И. Лотов, Теория вероятностей и математическая статистика, конспект лекций для студентов физического факультета, Новосибирск, НГУ, 2003. - 116 с. (in Russian).

64. G.E.P. Box and M.E. Muller, A note on the generation of random normal deviates, The Annals of Mathematical Statistics 29 (1958), no. 2, pp. 610-611.

65. K. Wille, Physic der Teilchenbeschleuniger und Synchrotronstrahlungsquellen, B.G. Teubner Stuttgart, 1992. (in German).

66. A.N. Matveenko et al., Feasibility Study of Multi-turn ERL-based Synchrotron Light Facility, ERL'13 Workshop, Novosibirsk, Russia, pp. 80-84.

Acknowledgement

First of all I would like to emphasize my gratitude for the support to all colleagues at Helmholtz-Zentrum Berlin without whom the completion of this thesis couldn't be possible. Special thank is owed to:

Prof. Dr. Aleksandr Matveenko for his supervision in a very friendly way, for a huge number of advices which were given to me during this work, for being available all the time for discussions,

Prof. Dr. Andreas Jankowiak for all advices given to me in a very friendly way,

Alexey Bondarenko for ongoing support during last years and for productive discussions,

Terry Atkinson for collaboration and for the unlimited number of English corrections,

Dr. Axel Neumann for friendly collaboration and for providing me information about HOMs I needed,

Dr. Jörg Feikes, Dr. Michael Abo-Bakr, Dr. Atoosa Meseck, Dr. Wolfgang Anders for the support during the last years,

Yaroslav Getmanov for collaboration and useful discussions,

Jens Rehanek and Markus Ries for helpful advices on various tasks.

And, finally, I would like to thank my family and my friends for their unlimited support and understanding during my life.

Selbständigkeitserklärung

Ich erkläre, dass ich die vorliegende Arbeit selbständig und nur unter Verwendung der angegebenen Literatur und Hilfsmittel angefertigt habe.

Berlin, den 30.01.2014   Yuriy Petenev